CHALMERS

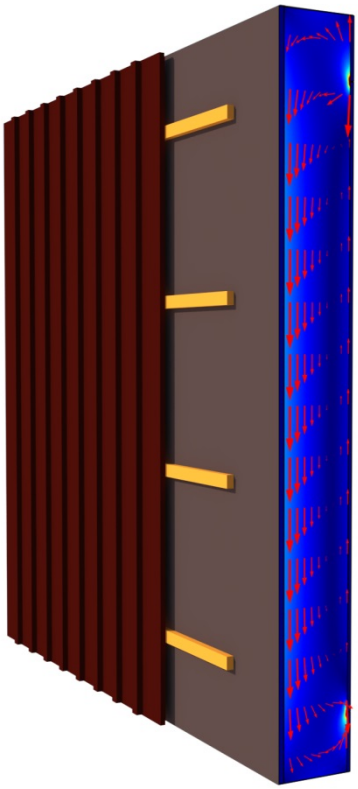

Hygrothermal Performance of a Light Weight Timber Wall Assembly with an Exterior Air Barrier

Master of Science Thesis in the Master's Programme Structural Engineering and Building Technology

DUNCAN WATT & STAFFAN SJÖBERG

Department of Civil and Environmental Engineering
Division of Building Technology

Building Physics Research Group

CHALMERS UNIVERSITY OF TECHNOLOGY
Göteborg, Sweden 2014

Master's Thesis 2014:16

MASTER'S THESIS 2014:16

Hygrothermal Performance of a Light Weight Timber Wall Assembly with an Exterior Air Barrier

Master of Science Thesis in the Master's Programme *Structural Engineering and Building Technology*

DUNCAN WATT & STAFFAN SJÖBERG

Department of Civil and Environmental Engineering
Division of Building Technology
Building Physics Research Group
CHALMERS UNIVERSITY OF TECHNOLOGY
Göteborg, Sweden 2014

Hygrothermal Performance of a Light Weight Timber Wall Assembly with an Exterior Air Barrier

Master of Science Thesis in the Master's Programme Structural Engineering and Building Technology
DUNCAN WATT & STAFFAN SJÖBERG

Examensarbete / Institutionen för bygg- och miljöteknik,
Chalmers tekniska högskola 2014:16

Department of Civil and Environmental Engineering
Division of Building Technology
Building Physics Research Group
Chalmers University of Technology
SE-412 96 Göteborg
Sweden
Telephone: + 46 (0)31-772 1000

Cover:
The influence of gaps introduced in the interior vapour retarder layer on the velocity profile over the cross section of a light-weight timber framed wall cavity.

Chalmers Reproservice / Department of Civil and Environmental Engineering
Göteborg, Sweden 2014

Hygrothermal Performance of a Light Weight Timber Wall Assembly with an Exterior Air Barrier

Master of Science Thesis in the Master's Programme Structural Engineering and Building Technology

DUNCAN WATT & STAFFAN SJÖBERG
Department of Civil and Environmental Engineering
Division of Building Technology
Building Physics Research Group
Chalmers University of Technology

ABSTRACT

In Norway, an emerging method in ensuring the air and vapour tightness of light weight timber framed walls, positions a sealed wind barrier at the exterior and a sealed vapour barrier to the interior. It has been found that the exterior layer alone is often sufficient in ensuring an acceptable level of air tightness. In terms of the overall airtightness requirements set on the building, it is thought that the interior vapour barrier could be left unsealed as the wall possesses a certain degree of redundancy. It is then important to assess whether the durability of the envelope is compromised due to moisture ingress from the interior driven by convection and diffusion.

This project investigates the effect of convection on moisture accumulation, and mould growth potential, in a light-weight timber frame wall system where the air barrier is situated at the exterior and the unsealed vapour retarder at the interior.

A two dimensional numerical HAM (Heat, Air and Moisture) model is used. The model is constructed and verified in COMSOL Multiphysics to evaluate the hygrothermal behaviour of a light-weight timber frame wall system with the previously described attributes. The studied wall is subject to climate conditions representative of the Gothenburg region of Sweden over one year. The light-weight timber wall system assessed is comprised of bitumen impregnated soft fibreboard with a treated exterior surface as the exterior air barrier, mineral wool as the cavity insulation and orientated strand board type 3 (OSB/3) as the interior vapour retarder. The unsealed nature of the interior vapour retarder is represented by the introduction of two 1 mm gaps in the layer. As means of comparison a wall assembly possessing a sealed interior OSB layer is simulated separately (no gaps). The mould growth potential of the wall system is assessed and compared utilizing the data output from the numerical model simulations and a material specific mould growth index.

The results suggest that the joints of the interior vapour retarder need not be sealed considering the exterior air barrier, wall geometry, material properties and imposed boundary conditions. While the degree of moisture accumulation is comparatively larger behind the exterior air-tight layer of the simulated wall assembly possessing an unsealed interior OSB layer, especially at the top of the wall section, the influence on mould growth potential is limited. This is because the disparities in moisture accumulation between the two wall assemblies is only apparent during the winter months when low exterior temperatures prevent any kind of mould growth regardless of critical humidity values.

Keywords: Numerical HAM model, hygrothermal performance, natural convection, light-weight timber frame building, mould growth potential, exterior air barrier.

Fuktsäkerhet hos en träregelvägg med ett yttre lufttätt skikt

Master of Science Thesis in the Master's Programme Structural Engineering and Building Technology

DUNCAN WATT & STAFFAN SJÖBERG
Institutionen för bygg- och miljöteknik
Avdelningen för byggnadsteknologi
Byggnadsfysik
Chalmers tekniska högskola

SAMMANFATTNING

I Sverige är det gängse praxis att byggnader med träregelkonstruktion konstrueras med ett enkelt lager omsorgsfullt tätad polyetenfolie placerad på klimatskalets insida för att tillgodose kraven på fuktsäkerhet och lufttäthet. Detta skikt benämns vanligen ångspärr (eller ångbroms om det utgörs av ett material med högre ångpermeabilitet än polyetenfolie) och fungerar när det är tillräckligt tätat även som lufttätt skikt. Denna metod är relativt arbetssam. Monteringen av ångspärren är besvärlig och noggrant arbetsutförande är av största vikt. Det är också lätt att i efterhand oavsiktligt punktera skiktet. En metod som kommit att bli allt vanligare i Norge är att komplettera det ovan nämnda interiöra skiktet med en exteriör vindspärr som till skillnad från i Sverige också har noggrant tätade fogar. Den får därmed det dubbla syftet att skydda mot regn och vind under byggnadens uppförande och under dess brukarfas, samt att bidra till klimatskalets totala lufttäthet. Det har emellertid påvisats att detta exteriöra skikt på egen hand kan tillgodose klimatskalets krav på lufttäthet. Frågan är då om det är nödvändigt att i detta fall täta även den interiöra ångspärren för att säkerställa dess funktion som lufttätt skikt. För att svara på denna frågeställning är det nödvändigt att undersöka om fuktsäkerheten hos klimatskalet äventyras på grund av konvektiv fukttransport från inomhusluften, då vindspärren är tätad men ångspärren otätad.

Syftet med detta exjobb är att undersöka luftkonvektionens inverkan på fuktsäkerheten och risken för mögelpåväxt i en träregelvägg med ett exteriört lufttätt skikt när den interiöra ångbromsen ej är tätad. En modell har konstruerats i COMSOL Multiphysics för simulering av kombinerad värme- luft- och fukttransport. Modellen har, efter att ha verifierats, applicerats på ovan beskrivna väggelement och simuleringarna har utförts där väggen exponerats för ett klimat representativt för göteborgsregionen. Det simulerade väggelementet består av ytbehandlad asfaltsimpregnerad träfiberskiva med tätade skarvar som exteriört lufttätt skikt, isolering i form av mineralull, och OSB/3 som interiör ångbroms. Simuleringar har gjorts både med tätade och otätade skarvar mellan OSB-skivorna. Resultaten har sedan jämförts för att utvärdera det konvektiva fuktflödet och risken för mögelpåväxt.

Resultaten tyder på att det, för den väggeometri och med de materialparametrar och randvillkor som använts i simuleringen, inte finns behov av att täta skarvarna mellan OSB-skivorna. Även om en ökad fuktnivå kan observeras innanför den exteriöra träfiberskivan i fallet med otätade OSB-skivor, särskilt i den övre regionen av väggen, så har detta ingen signifikant inverkan på risken för mögelpåväxt.

Nyckelord: Värme, luft och fukttransport, naturlig konvektion, träregelvägg, mögelpåväxt, exteriört lufttätt skikt.

Contents

Preface

This study was inspired by the involvement of Staffan Sjöberg and Duncan Watt in the HALO project for the Solar Decathlon Competition 2013 in China. The ongoing dialogue regarding the moisture safety system of the home during design and construction was the primary stimulus in the formulation of the thesis topic, Staffan as lead building physics engineer and Duncan as construction manager. Under the guidance of Paula Wahlgren, both the supervisor and examiner of the thesis, the topic was solidified and focused into a region most suitable for the progression of research at the division of building technology at Chalmers University of Technology. The majority of modelling work was done between September and December 2013; the thesis was then completed and presented in February of 2014.

There are many people that deserve acknowledgement on the successful completion of this thesis as without them it would most likely have not been possible:

Paula Wahlgren for her continual support and guidance in all aspects of the work involved with the thesis. Especially as the area of study presented by the authors was unintelligibly vague and extremely broad at the outset.

Angela Sasic Kalagasidis for the sharing of her fantastic knowledge on numerical heat, air and moisture modelling with regard to building physics problems.

Natalie Leonor Williams Portal for her guidance on the use of COMSOL and also the sharing of her previously constructed numerical models on the subject.

Silje Korsnes for her knowledge and work on the subject of OSB board type 3 as an effective and efficient vapour retarder in light-weight timber framed buildings.

COMSOL support staff, specifically Daniel Ericsson for his continued support regarding the functionality and interface of the software.

Tommie Månsson for his collaboration in the initial stages of the HAM model development

Carlos Mora for formatting knowledge and moral support while we both occupied room 3004.

Hanna Modin for her objective advice and opposition.

Rickard Ekdahl for his assistance in acquiring some hardware that was fit for purpose.

Johan Claesson for his tutorage and guidance on partial differential equations.

Additional acknowledgements must be made for those who offered guidance and experience with regard to the area of research:

Mia Bondelind, Carl-Eric Hagentoft, Ernst Jan de Place Hansen, Jelle Langmans, Stephen Burke, Hans Wetterlund, Tormod Aurlien.

Finally the authors would like to thank their families for their continued trust and support in this endeavor and all future aspirations.

Notations

Note: Benchmark notations are distinct and described in the benchmark chapters.

Roman upper case letters

A	Gap area	(m^2)
D_l	Liquid conductivity	(s)
D_p	Vapour permeability of air, for partial vapour pressure gradient	(s)
H_0	Elevation of neutral pressure plane	(m)
L	Length of air channel	(m)
M_w	Molar mass of water	(kg/mol)
P	Air pressure	(Pa)
P_{atm}	Standard atmospheric air pressure	(Pa)
P_b	Air pressure at the boundary	(Pa)
P_d	Dry air pressure	(Pa)
P_s	Suction pressure	(Pa)
P_{sat}	Saturated vapour pressure	(Pa)
P_{tot}	Total air pressure	(Pa)
P_v	Partial vapour pressure	(Pa)
$\dot{Q}_s$	Heat source	(W/m^3)
R	Universal gas constant	(J/(kg·mol))
R_a	Volumetric air flow rate	(m^3/s)
R_d	Specific gas constant of dry air	(J/(kg·K))
R_e	Reynolds number	(-)
RH	Relative humidity	(- or %)
RH_{cr12w}	Critical relative humidity after 12 weeks incubation	(- or %)
Sd	Equivalent air layer thickness	(m)
S'_e	Gap entrance air flow resistance factor	($Pa/(m^3/s)^2$)
S_g	Air flow resistance for the inner of a gap	($Pa/(m^3/s)$)
T	Temperature	(K)
T_b	Boundary temperature	(K)
T_{ref}	Reference temperature	(K)
T_s	Surface temperature	(K)
T_∞	Surrounding temperature	(K)
$\boldsymbol{V_a}$	Velocity of fluid particles within a pore space	(m/s)
Y_l	Mass fraction of liquid water	(kg/kg)
Z_v	Vapour resistance of layer	(s/m)

Roman lower case letters

b	Width of gap	(m)
$c_{p,a}$	Specific heat capacity of dry air	(J/(kg·K))
$c_{p,eff}$	Effective heat capacity of material	(J/(kg·K))
$c_{p,l}$	Specific heat capacity of liquid water	(J/(kg·K))
$c_{p,m}$	Specific heat capacity of dry material	(J/(kg·K))
$c_{p,v}$	Specific heat capacity of vapour	(J/(kg·K))
d	Material layer thickness	(m)
g	Gravity acceleration constant	(m/s^2)
$\boldsymbol{g}$	Gravity acceleration vector	(m/s^2)
g_b	Inwards moisture flux across the boundary	(kg/(m^2·s))
h_{evap}	Latent heat of condensation/evaporation	(J/kg)
$\dot{m}_c$	Condensation/evaporation rate	(kg/s)
q_b	Inwards heat flux across boundary	(W/m^2)
t	Time	(s)
v_a	Darcy's air velocity magnitude	(m/s)
$\boldsymbol{v_a}$	Darcy's air velocity vector	(m/s)
v_{gap}	Mean air velocity across gap boundary	(m/s)
y	Elevation of point of evaluation	(m)
w	Moisture content	(kg/m^3)

Greek upper case letters

ϕ	Relative humidity	(- or %)
ϕ_s	Surface relative humidity	(- or %)
ϕ_∞	Surrounding relative humidity	(- or %)

Greek lower case letters

α	Surface heat transfer coefficient	(W/(m^2·K))
β_p	Surface vapour transfer coefficient	(s/m)
δ_p	Vapour permeability for partial vapour pressure gradient	(s)
δ_v	Vapour permeability for humidity by volume gradient	(m^2/s)
ε	Porosity	(-)
κ	Air permeability	(m^2)
λ	Thermal conductivity	(W/(m·K))
μ	Dynamic viscosity of air	(Pa s)
μ_{vrf}	Water vapour resistance factor	(-)
ξ	Moisture capacity	(kg/m^3)
ρ_a	Air density	(kg/m^3)
ρ_m	Material density	(kg/m^3)
ρ_w	Water density	(kg/m^3)
ν	Kinetic viscosity of air	(m^2/s)
ω	Absolute humidity	(kg/kg)
ω_b	Boundary absolute humidity	(kg/kg)
ω_s	Surface absolute humidity	(kg/kg)
ω_∞	Surrounding absolute humidity	(kg/kg)

COMSOL parameters

Ω	Domain
$\partial\Omega$	Boundary
e_a	Mass coefficient
$\boldsymbol{u}$	Dependent variable field
t	Time
d_a	Damping or mass coefficient
c	Diffusion coefficient
α	Conservative flux convection coefficient
γ	Conservative flux source
β	Convection coefficient
a	Absorption coefficient
f	Source term
n	Outward unit normal vector
g	Boundary flux/source
q	Boundary absorption/impedance term
r	Prescribed boundary value

1 Introduction

Moisture safety and the potential for mould growth in light-weight timber framed building envelopes are of considerable interest to the building authorities in Sweden. Recent investigations have shown that up to 30 % of single family houses and 15 % of other building types exhibit moisture-related damage (Boverket, 2009). Damage which is associated with significant repair costs.

Moisture safety is generally ensured in Swedish light-weight timber framed building envelopes through use of a vapour resistant polyethylene sheeting which lines the interior (Wahlgren & Sikander, 2010). The polyethylene material is essentially vapour impermeable which inhibits diffusive moisture transfer through the envelope. This affirms its function as a vapour barrier. The polyethylene material is also virtually air impermeable and when the joints between sheets are sealed air infiltration/exfiltration through the building envelope is greatly restricted, therefore moisture transfer due to convection is also inhibited. This means that the interior polyethylene layer functions not only as the vapour barrier but also as the air barrier in the envelope system. The dual functionality of the polyethylene layer reduces its flexibility. Any damage to the layer or inadequate sealing of the joints can induce localised air leakages through the envelope which increases the risk of moisture accumulation and so mould growth in the building envelope. This is especially pertinent for the polyethylene material as it is prone to perforation (Hansen, 2010), the material is difficult to handle/seal, and improper installation due to poor workmanship is common (Zou, 2010).

A new method for ensuring moisture safety in light weight timber framed buildings, originating from Norway, supplements the air/vapour barrier at the interior with a carefully sealed (as opposed to unsealed in Sweden) wind and rain resistant layer on the exterior (Relander, 2011). While inhibiting the wind washing of cavity insulation and rain infiltration, the sealed wind resistant layer also contributes to the airtightness of the envelope, effectively creating an additional exterior air barrier. In fact, this exterior air barrier alone is often sufficient in meeting airtightness requirements (Relander, et al., 2011). This introduces a certain level of redundancy with regard to the airtightness of the light-weight timber framed building envelope. The interior air/vapour barrier now holds less significance regarding the overall airtightness of the building which affords the layer a greater degree of flexibility. Considering the time and labour invested in the process of sealing, the need to seal the interior vapour barrier to ensure its credentials as an air barrier can be questioned as convective moisture transfer through infiltration/exfiltration is now restricted by the presence of the exterior air barrier.

The emergence of OSB board type 3 (OSB/3) as a multipurpose sheathing option which exhibits a distinctly low vapour permeance (Korsnes, 2013), offers a new and sustainable material for use as a vapour retarder at the interior (vapour ‘barrier’ denotes materials possessing a constant vapour resistance of a magnitude similar to polyethylene). Additionally the recent introduction of bitumen impregnated fibreboard as an effective, autonomous, wind and rain resistant material which also possesses a low air permeance (Langmans, et al., 2011), presents a viable opportunity to incorporate this material as the exterior air barrier.

Finite element analysis is a method which can and has been used to evaluate the hygrothermal performance of such building envelope systems. The works of Langman (2012), Tariku (2008) and van Schijndel (2007) are examples of this approach. Field and laboratory testing of full-scale envelope systems are also viable methods of assessment but due to time constraints and limited access to facilities with regard to this investigation, finite element analysis was deemed the most suitable evaluation method.

1.1 Objectives

The objective of the thesis is to investigate moisture accumulation, and so potential risk of degradation through mould propagation, within a light-weight timber wall system where the air barrier is located on the exterior and the vapour retarder is located on the interior but considered discontinuous (joints are unsealed). The hygrothermal behaviour of the wall assembly is documented with regard to a climate pertaining to the Gothenburg region of Sweden. The wall assessed comprises of bituminous impregnated soft fibreboard with a treated exterior surface as the exterior air barrier, mineral wool as the cavity insulation and orientated strand board type 3 (OSB/3) as the interior vapour retarder.

1.2 Methodology

A literature review is initiated regarding the feasibility of utilizing bitumen impregnated fibreboard and OSB board type 3 as the exterior air barrier and the interior vapour retarder respectively, in a light-weight timber wall assembly subject to a northern European temperate climate.

The investigation of the proposed wall assembly is based on a numerical model constructed in the COMSOL Multiphysics software package which accurately replicates transient heat, moisture and air movements within porous building materials in two dimensions. In this case the numerical model is constructed first in one dimension then verified with the European Provisional Standard prEN 15026 heat and moisture (HM), and heat, air and moisture (HAM) model benchmark tests (specifically benchmarks 2, 5 and 3). Once verified the model can then be expanded to encompass two dimensional geometries and physics for the testing of the proposed wall assembly. Ultimately, the two dimensional model is considered verified by extension, however its validity is also discussed in greater detail within the body of the thesis.

The test wall assembly shall be configured in three different simulation types for means of comparison and so evaluation.

- Simulation 1: HM model where the interior vapour retarder is continuous
- Simulation 2: HAM model where the interior vapour retarder is continuous
- Simulation 3: HAM model where the interior vapour retarder is discontinuous

These simulation types are then subject to two differing boundary condition cases.

Initially, the simulations are subject to a controlled climatic case to assess the responsiveness of the model and also to compare and evaluate the predominant moisture transport mechanisms in all simulations.

Secondly, the simulations are subject to commonly occurring western Sweden (Landvetter) climatic conditions at the exterior over a typical reference year. The simulations are evaluated and comparisons drawn in terms of moisture accumulation and mould growth potential over the full year.

1.3 Limitations

In the HM and HAM evaluation of the three simulations, the hygrothermal performance of the light-weight timber framed wall assembly is based solely on the two dimensional modelled geometry. The absence of a three dimensional analysis means that any lateral hygrothermal behaviour in relation to the wall is neglected. The wall assembly geometry is also isolated from the rest of the building, therefore no flux is considered across the top and bottom wall boundaries.

Additionally factors such as sub-standard workmanship in construction (for example perforations in the bitumen impregnated fibreboard layer) or naturally occurring faults during operation (displacement of cavity insulation) are not considered.

The wall assembly in the three simulations is designed and modelled for use in a northern European temperate climate, specifically western Sweden. The wall assembly may not be applicable for all climate types as differing regions bring differing requirements on building envelopes. It follows that the interior moisture load profile utilized in the simulations is representative of a small residential building situated in the previously described regional climate, and remains constant for all simulations.

Finally, the material parameters and model geometry remain constant in all simulations except for the introduction of gaps in the interior vapour retarder for certain simulations. Gap orientation and size remains constant for all simulations where they are included.

This limits the scope of the investigation and offers a reduced data set from which to form comparative conclusions.

To see specific limitations on the numerical HAM model and simulation types, see Chapter 5.2.1.

2 Air tightness and moisture safety

In building applications airtightness is defined as the ability of a building envelope or a building component to prevent air leakage caused by a pressure difference between interior and exterior. In this aspect the term air leakage is referred to as unwanted air transport trough the building envelope, thereby not including air transport through intentionally placed vents.

The overall airtightness of a building envelope is an important issue when considering the specific standards that have been introduced in many international and national building codes concerning the energy efficiency of new builds and renovations. In temperate climates the buildings energy consumption can be significantly reduced if there are efforts made to minimise air leakage through the building envelope.

Additionally, localized airtightness has a strong influence on the moisture safety of the envelope. It is this relationship between airtightness and moisture safety that will form the base of the proposed investigation.

2.1.1 Air convection theory

In a general sense convection is the phenomena of movements and circulations in fluids due to a gradient in pressure. In building physics, heat and moisture transfer caused by convection of air is an important phenomenon with regards to the energy efficiency and moisture safety of the building envelope.

Convection is caused by differences in air pressure and is usually split into forced convection and natural convection depending on what is causing the pressure difference.

Forced convection is the result of air movements caused by an external source such as a fan or the wind. Wind induced convection is dependent on many factors such as local weather conditions, surrounding terrain, shape and height of the building. Generally the windward side of the building will experience an overpressure on the exterior while the leeward side will have an exterior under pressure. Forced convection can also be generated by the mechanical ventilation system. In the case of extract ventilation the fans will create an under pressure on the interior causing an air flow in through vents in the building envelope. Also a ventilation system with mechanical exhaust and supply air might be intentionally designed with an interior under pressure preventing exfiltration of moist air out through the building envelope. Additionally there might exist an unintended imbalance in the ventilation, causing an interior/exterior pressure difference, for example due to faulty design or refurbishments.

Natural convection is the air movements resulting from differences in the air density due to a difference in temperature (air density is also dependent on the vapour content in the air, but that influence is minor in comparison with the temperature part, and is not included in this thesis). Natural convection might occur within a room or for example a wall cavity due to differences in the surface temperatures. The temperature difference is also what is causing the so called stack effect. This means that there is a difference in the slope of the vertical air pressure gradient between the interior and the exterior due to the difference in air temperature. This is causing a driving potential for air flow through the building envelope (se Figure 2.1). At a certain height the pressure is equal on the interior and the exterior side. This is known as the neutral pressure plane. The height of the neutral pressure plane is dependent on the characteristics of the leakages of the envelope. If the building envelope is leakier at the upper part then the neutral pressure plane tend to move to a higher level.

If the air temperature on the interior is higher than on the exterior then the stack effect will create a driving force for air flow inwards through the lower part of the building envelope and outwards through the upper part of the envelope.

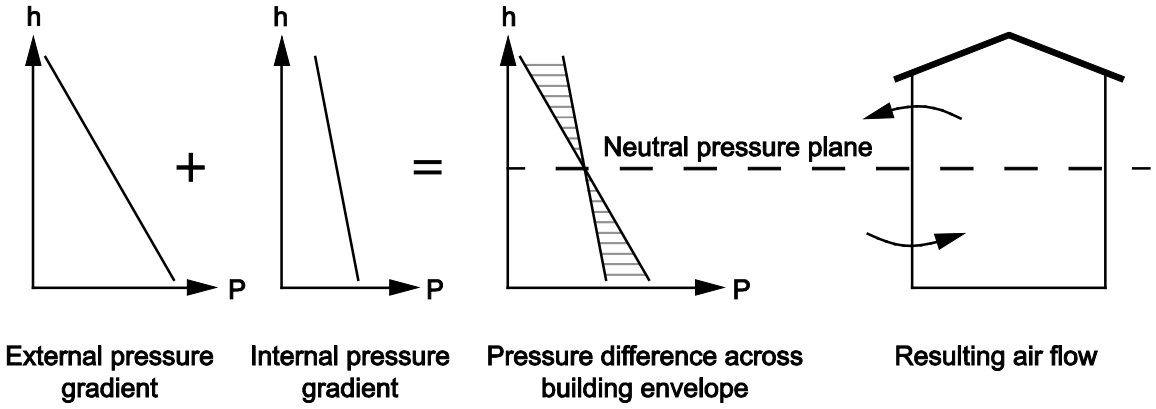

Figure 2.1 Illustration of the concepts of stack effect and neutral pressure plane.

Finally, the total driving force for air leakage through the building envelope is decided by the overall pressure situation which is a combination of the pressure difference induced by wind, mechanical ventilation and temperature differences.

2.1.2 Airtightness regulations

Due to the energy crisis of the 1970's, regulations on the minimum level of airtightness regarding light-weight timber framed building envelopes has been a fairly constant feature in the Swedish building codes for the most part of the last 40 years (Mattsson, 2004). So the need of an air-tight building envelope for both moisture safety and energy efficiency is common knowledge in the construction industry. Therefore this demand is catered for in all new builds and renovations with a multitude of techniques, all with varying degrees of success.

In 2006, the minimum level of airtightness requirement, previously 0.8 l/sm^2, was dropped from Boverkets Byggregler (BBR) and combined in the overall energy efficiency demand and moisture safety requirements for the building. So while there remains a specific value on the minimum level of airtightness required in attaining the status of 'Passive house' (0.3 l/sm^2 according to Swedish regulations for passive houses by FEBY) there is no specific guidance values proposed for the majority of building types. This may be due to the difficulties in the accurate appraisal of the airtightness of a particular buildings envelope, as the only accepted method is a technique known as the 'blower door test'. The blower door test is a technique where a fan is inserted into one of the buildings openings to the exterior while all others are sealed. The fan then creates an overpressure within the building to a degree of 50 Pascal. The air leakage rate through the envelope then approximately corresponds to the flow across the fan which is usually given in litres per second metre squared (l/sm^2).

While there is no specific minimum value of airtightness cited in the BBR regarding light-weight timber framed buildings, it is in the interests of all involved in the construction process that the new build or renovation in question, is as air-tight as possible.

2.2 Moisture safety

Moisture safety and the potential for mould growth in light-weight timber framed building envelopes are of considerable interest to the building authorities in Sweden. Recent investigations have shown that up to 30 % of single family houses and 15 % of other building types exhibit moisture-related damage (Boverket, 2009). Damage which is associated with significant repair costs.

Excluding heavy wetting due to rain and defective or improperly installed exterior sheathing layers and guttering or internal water leaks (which will not be covered within the scope of this investigation), moisture accumulation and associated moisture damage within light-weight timber framed envelopes is closely tied to moisture exfiltration from the interior and is mitigated by the moisture control system of the particular building envelope (Karagiozis, 2002). In the majority of cases related to moisture damage within light-weight timber framed envelopes in temperate climates, it is convection that is the integral transport mechanism by which moisture infiltrates the envelope from the interior (Kalamees & Kurnitski, 2009). Diffusion plays a comparatively minor role in the transfer of moisture from the interior into the envelope when considering the presence of a general purpose interior sheathing layer (gypsum board, timber panelling etc) with unsealed joints or minor perforations (Quirouette, 1985). Therefore in constructing an effective moisture control system regarding a light-weight timber framed building, both moisture safety and airtightness must be considered simultaneously.

2.3 Swedish wood frame walls today

Figure 2.2 shows the typical layout of a traditional Swedish light-weight timber framed wall. The figure also highlights the typical moisture control system present within such building envelopes in Sweden.

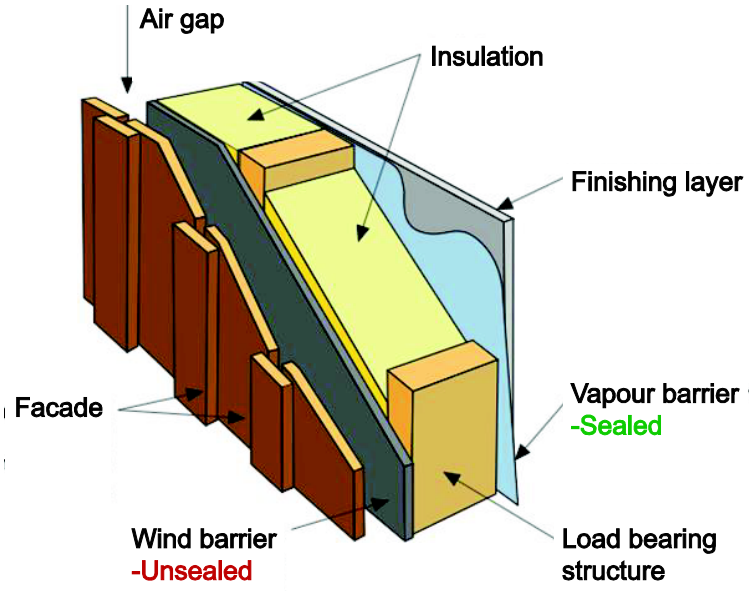

Figure 2.2 Illustration of typical Swedish wood frame wall layout (Bankvall, 2013).

As previously described, diffusive moisture transfer from the interior to the building envelope is inhibited by the presence of the interior vapour barrier. When sealed, the vapour barrier also functions as an air barrier, restricting infiltration/exfiltration through the building envelope and so limiting moisture transfer from the interior to the building envelope through convection. To achieve this, the vapour barrier needs to possess a low air permeability and low vapour permeability. Typically for a Swedish climate, the vapour barrier needs to be positioned close to the interior to stop vapour from being transported out to the colder region of the wall, which might result in critical relative humidity levels with regards to mould growth, or even condensation. The vapour barrier is usually made out of polyethylene and often positioned at a small buffer distance from the interior layer to avoid penetrations from nails and screws when mounting objects on the interior wall. Detailed advice on preferable sealing solutions can be found in Wahlgren (2010).

The wind barrier in a typical Swedish wall assembly has a slightly different purpose than that of the vapour barrier. It has to prevent for so called “wind washing” of the insulation which means that cold exterior air blowing through the insulation and so exacerbating heat losses through the building envelope. The wind barrier also needs to protect the wall from ingress of liquid water that has entered through the exterior cladding. At the same time the wind barrier has to allow for moisture within the construction to be able to dry out to the exterior. To fulfil all these requirements the wind barrier material should possess a low air permeability, a low water permeability, but a comparatively high vapour permeability. Typically no effort is put into sealing all the joints in the wind barrier. Because of the lack of sealing, the wind barrier cannot completely restrict air infiltration/exfiltration through the wall, thus cannot be considered as an air barrier.

2.4 Norwegian approach- double air barrier

In Norway, the demands on light-weight timber framed building envelope performance is similar to that in Sweden. However, in some cases there has been an increased focus on carefully sealing not only the interior vapour barrier but also the exterior wind barrier (Solvang & Handal Bjelland, 2011).

In this case the wind barrier then becomes an important factor in the overall airtightness of the building envelope (Blom & Uvsløkk, 2012) which can now be said to possess both an exterior and an interior air barrier. The wind barrier often constitutes of a sealed water and wind resistant board or a sealed water and wind resistant rolled textile. A method which is becoming increasingly popular is the so called double wind barrier, meaning that both rolled textile and board are used simultaneously (Relander, et al., 2011).

Defining the wind barrier as air tight allows for airtightness measurements to be made at an earlier stage of the construction process as the exterior wind barrier is mounted immediately after the completion of the structural framing. Such preliminary measurements of airtightness have become increasingly common in Norway. It has been proven possible to meet the building code requirements on airtightness with only the wind barrier mounted (Holøs & Relander, 2010). However, it cannot automatically be assumed that the final measuered airtightness of the finished building (after the installation of the interior air/vapour barrier) will be improved over the preliminary measurements since additional penetrations may be introduced either intentionally or accidently (Holøs & Relander, 2010). Additionally, the practise of carefully sealing the exterior wind barrier is beneficial as this layer provides effective weather protection during the construction phase.

2.5 Exterior air barrier

The subsequent investigation is made with close regard to a series of studies made by Jelle Langman and Staf Roels from the Katholieke Universiteit Leuven, Belgium.

This series presents field (Langmans, et al., 2011), laboratory (Roels, et al., 2012) and computational (Langmans, et al., 2012) studies regarding moisture re-distribution due to natural and forced convection in light-weight timber framed wall cavities when considering an external air barrier and a discontinuous internal vapour retarder.

The test wall setup in the laboratory study is shown in Figure 2.3.

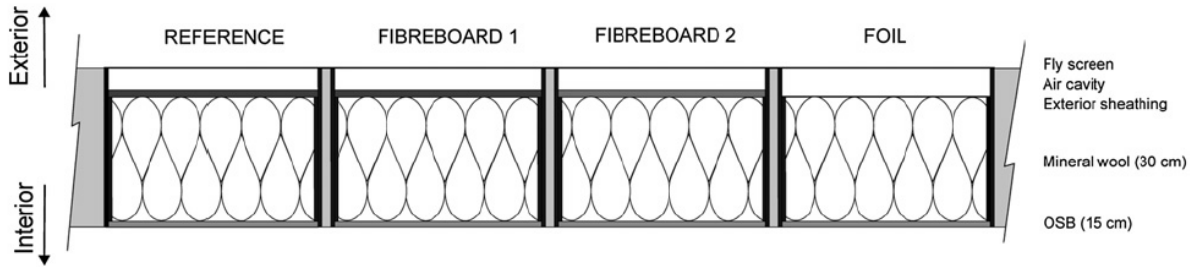

Figure 2.3 Test wall configuration (Roels, et al., 2012).

The materials used in the test wall are 18 mm bituminous impregnated soft fibreboard with a treated exterior surface (FIBREBOARD 1 and REFERENCE), 18 mm bituminous impregnated soft fibreboard without a treated exterior surface (FIBREBOARD 2) and spun bonded foil (FOIL), acting as the exterior air-tight layer. Cavities are 0.5 m wide and 2.3 m high. Discontinuity in the vapour retarder is achieved by the inclusion of 10 mm slots running the width of the test wall at 200 mm from the top and the bottom of the OSB layer. It is noted that the OSB board type is not specified. A reference case (REFERENCE) is also tested where the OSB layer is not perforated and considered continuous throughout the testing process.

To successfully register physical phenomena pertinent to the experiment a range of sensors were placed inside and at the boundaries of the test walls at three different heights (200 mm from the top and bottom and at mid-height). Three removable specimens were integrated in each test wall and positioned at the same heights as the sensors. To document moisture accumulation in the fibreboard exterior sheathing (not applicable for spun bond foil) these samples were then weighed intermittently to determine the moisture content (kg/m^3) of the fibreboard over time.

The wall is then inserted into vertical, highly insulated, calibrated hot/cold box where it is carefully positioned and sealed to minimise heat and moisture transmission through the box and around the test wall frame. Here the test wall is subject to a constant climate representative of a typical Belgian winter on the external 'cold' side, and a constant climate representative of a corresponding interior domestic condition on the internal 'hot' side.

A horizontal and vertical section of the hot/cold box used in the experiment including associated equipment is shown in Figure 2.4:

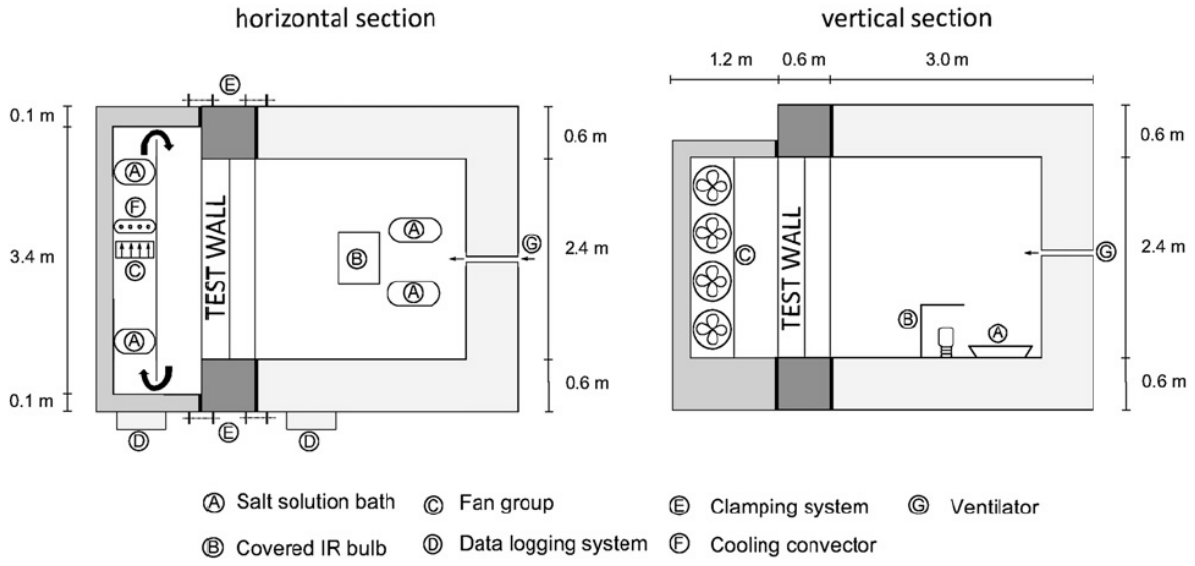

Figure 2.4 Horizontal and vertical section of hot box (right)/cold box (left) experiment including associated equipment (Roels, et al., 2012).

The boundary conditions produced in the hot/cold box were not precisely constant due to the nature of the experiment. Values representative of the conditions found within the hot/cold box are shown in Figure 2.5:

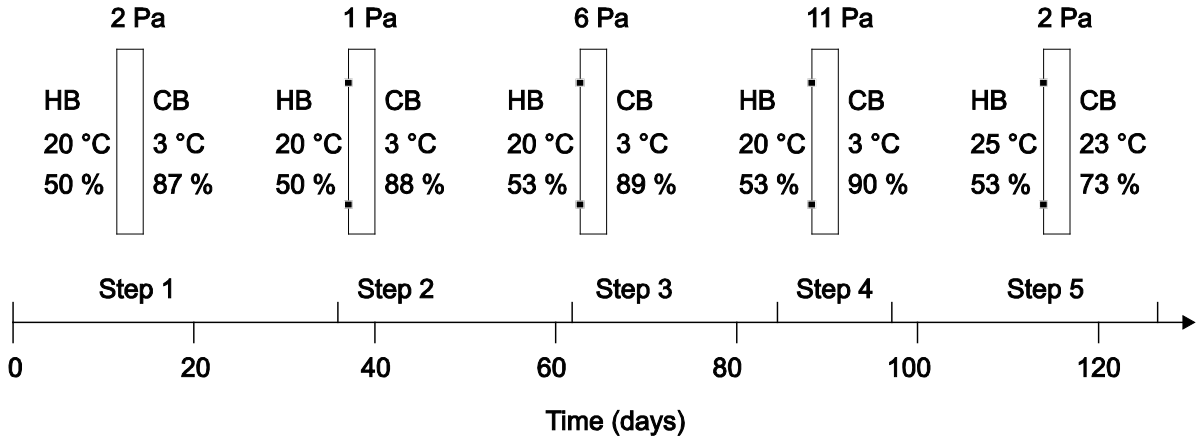

Figure 2.5 Prevailing boundary conditions in hot box (HB)/ cold box (CB) experiment (Langmans, et al., 2012).

The slots are introduced in the OSB layer between steps 1 and 2, the hot box is then pressurized to varying degrees in steps 3 and 4 and finally step 5 represents an arbitrary drying condition excluding mechanically induced pressurization.

It was found that moisture accumulation within the exterior sheathing (spun bon foil was not measured) was most pronounced at the upper part of the wall. This process was driven by buoyancy forces and was highly dependent on the air permeability of the exterior sheathing layer and the inclusion of slots in the OSB layer. Additionally, the study highlighted that the thermal resistance provided by the exterior fibreboard proved beneficial in the delay of condensation conditions behind the exterior sheathing layer as opposed to the spun bonded foil where 100% relative humidity was reached early in step 2.

Ultimately, the study proposed there was a risk of mould growth or degradation due to moisture accumulation in light-weight walls with an exterior air barrier although this was not quantified.

The laboratory exercise was initiated as a method to obtain tangible results for a representative test with realistic boundary conditions that would serve to validate a two dimensional numerical HAM model.

The numerical HAM model was constructed using the DELPHIN software from the Technical University of Dresden (TUD) as a base. DELPHIN was applied in two dimensions and supplemented with a decoupled air mass balance equation over the modelled geometry. A simulation was carried with the test case of FIBREBOARD 1 and was found to be in good agreement with the laboratory data.

Prior to these studies a field experiment was carried out on a full scale light-weight building envelope wall under real atmospheric boundary conditions. A test wall setup, similar to the test wall in the laboratory experiment, but with slightly different dimensions and interior sheathing materials, was installed in the north east side of a test building in the Belgian city of Leuven. The test wall was then monitored in-situ for approximately one year and a half. Here it was found that convection became the prevailing transport mechanism for moisture re-distribution when the interior sheathing surface was perforated. Additionally, it was stated that the moisture content of the exterior sheathing layer was directly proportional to the vapour permeability of the interior sheathing layer when continuous. Moisture accumulation

in the field study test walls was said to be limited in the winter months if the test walls were sufficiently air-tight. This accumulated moisture then dried out during the summer.

2.6 Materials

2.6.1 Orientated strand board, type 3

Orientated strand board (OSB) is a common building material used widely in the construction industry. It is often used as structural sheathing for wall and roof elements although its role in the overall moisture safety and hyrothermal performance of the envelope is often ignored.

OSB is manufactured in three different board types. For the purpose of light-weight timber frame structural sheathing in a temperate climate such as western Sweden, OSB board type 3 is applicable. The ability of OSB/3 to perform as a structural board in humid climates is ensured by the boards high vapour resistance, which for some brands of OSB/3 far exceeds those values outlined for OSB/3 in the European building codes (EN-13986/-ISO 10456) (Korsnes, 2013).

Figure 2.6 Orientated Strand Board of unknown board type (Wikipedia).

The significant vapour resistances exhibited by OSB/3 and highlighted by Korsnes (2013) in a dry cup/wet cup experiment (Figure 2.7) are a strong argument for its use as an interior vapour retarder, alongside its established structural sheathing role.

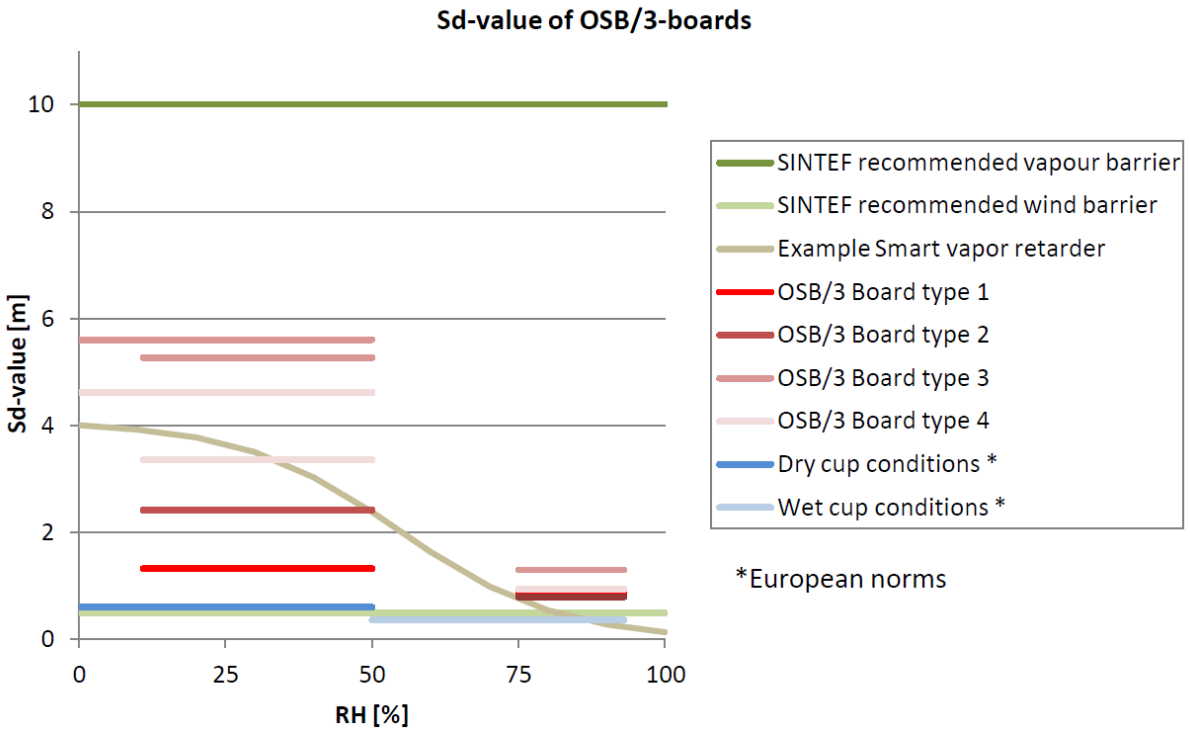

Figure 2.7 Sd-value (m) of various OSB/3 brands at a varying relative humidity (%) (Korsnes, 2013).

OSB/3 use as the interior vapour retarder in light-weight timber framed buildings is not a new concept. There are many examples in Europe and North America where a taped (or sealed in another manner) interior OSB/3 layer constitutes both the structural sheathing system and the vapour retarder. This is highlighted in the recent studies of Langman and Roels (2012).

2.6.2 Bitumen impregnated fibreboard

The potential of bitumen impregnated fibreboard as an effective exterior air barrier for light-weight timber framed buildings is gaining traction within the construction industry. Its high vapour permeance, comparatively low air permeance and non-capillary status (Roels, et al., 2012) makes the bitumen impregnated fibreboard a rain resistant, moisture breathable, air resistant material, which are all desirable qualities of an wind barrier. When the material is incorporated as an air barrier, where the joints between boards are taped or sealed in another manner, the entire layer can attain levels of airtightness which meet or exceed passive house standards (Langmans, et al., 2010).

Figure 2.8 Bitumen impregnated fibreboard exterior sheathing (Hunton Bitroc).

Additionally, bitumen impregnated fibreboard is also fairly mould growth resistant when compared to other common exterior sheathing materials (Holme, 2008) which increases its durability.

Finally, bitumen impregnated fibreboard is easier to manipulate and seal when considering common house wraps or wind and rain resistant textiles. The inherent stiffness of the material enables it to function in autonomy at the exterior with no additional support required. While the materials ability to resist shear during building operation is not fully certified, the shear strength that it does possess is sufficient during the temporary construction phase (Braathen, 2010). This allows flexibility in the construction procedure. Combined with an interior structural sheathing layer such as OSB/3 and mineral wool cavity insulation, the complete light weight timber wall assembly potentially provides a structurally sound, environmentally conscious, cost effective and hygrothermally efficient solution.

3 Modelling coupled heat, air and moisture transport

In the investigation of moisture infiltration due to convection in a light-weight timber framed wall assembly, a numerical model which takes into account the combined effect of air, heat and moisture transport shall be utilized. Such a model is commonly referred to as a HAM (Heat, Air and Moisture) model.

There is existing software intended for building physics applications, such as WUFI developed by Fraunhofer Institute, that are able to simulate heat and/or moisture transport through porous media. However, none of these software developed especially for building physics are able to also take into account the effect of air movements. In order to build such a model it is necessary to use a more flexible software environment which allows the user to state the governing partial differential equations (PDEs) for heat, air and moisture transport independently and then link them together in order to solve a coupled model. An example of such a modelling tool is HAMLab (van Schijndel, 2007) developed at the technical university of Eindhoven. HAMLab is a number of tools using Matlab, Simulink and COMSOL for simulating various heat air and moisture related problems.

In this thesis a simpler model is proposed through solely utilizing COMSOL Multiphysics. In COMSOL it is possible to add various physics to the model from a library of predefined modules such as “Heat transfer in porous media”, however it is also possible to define custom PDE (Partial Differential Equation) modules. These modules can then be coupled and solved simultaneously.

3.1 Numerical model description

To understand the numerical model implemented in this thesis it is necessary to have basic understanding of the physical transport mechanisms involved in the process. This aim of this section is to give a brief introduction to physics behind the model.

In porous building materials, moisture can exist both in the form of vapour and liquid. The model described in this thesis takes into account both vapour transport (through diffusion and convection) and liquid transport (through capillary suction and due to gravity). The vapour diffusion and capillary suction transport mechanisms are strongly dependent on relative humidity. Between these two transport mechanisms the slower vapour diffusion process dominates at a lower relative humidity while the comparatively rapid capillary suction dominates at a relative humidity level approaching 100 %. These processes are very much material dependent. From measurements it is possible to determine the sorption isotherm of a particular material which highlights the approximate amount of moisture contained within the material at any given relative humidity. For examples of such sorption isotherms see Appendix D. To accurately model the moisture transport it is also necessary to possess reliable data on vapour diffusion coefficients and liquid transport coefficients which can sometimes be difficult to find.

Moisture transport can be modelled with different driving potentials such as partial vapour pressure or moisture content. Here, relative humidity is chosen as the dependent variable and so the driving potential, which means all moisture transport processes are given in terms of relative humidity.

The heat transfer mechanisms included in this model are conduction and convection (including sensible heat transport both by dry air and vapour), as well as latent heat (heat released or absorbed due to a phase change between liquid water and vapour).

As described in Chapter 2.1.1, air flow is caused by a gradient in air pressure and can be referred to as either natural convection or forced convection depending on what is causing the pressure difference. There are a number of mathematical models, with a varying degree of complexity for describing an air flow though a porous medium. In this thesis, where slow and laminar air flows are to be expected, Darcy's law is applicable.

Heat, air and moisture transport mechanisms are highly interconnected and dependent on each other. Figure 3.1 gives a schematic description on how the governing equations for heat, air and moisture transport are coupled and what boundary conditions are being used. The dependant variables of the governing equations are given in parenthesis.

The heat and moisture equations are closely coupled in multiple ways. Heat is released or absorbed due to condensation or evaporation of moisture. Effective heat capacities of the material and moist air require an input of relative humidity. In the moisture equation, the vapour diffusion and capillary suction parts have terms which are dependent on the temperature or the gradient of temperature. Also saturated vapour pressure is dependent on the temperature.

Heat and moisture equations are coupled to the air flow equation through convective heat and moisture transport which are dependent on air velocity. The air flow is also connected to the heat equation by the air density, which is dependent on temperature.

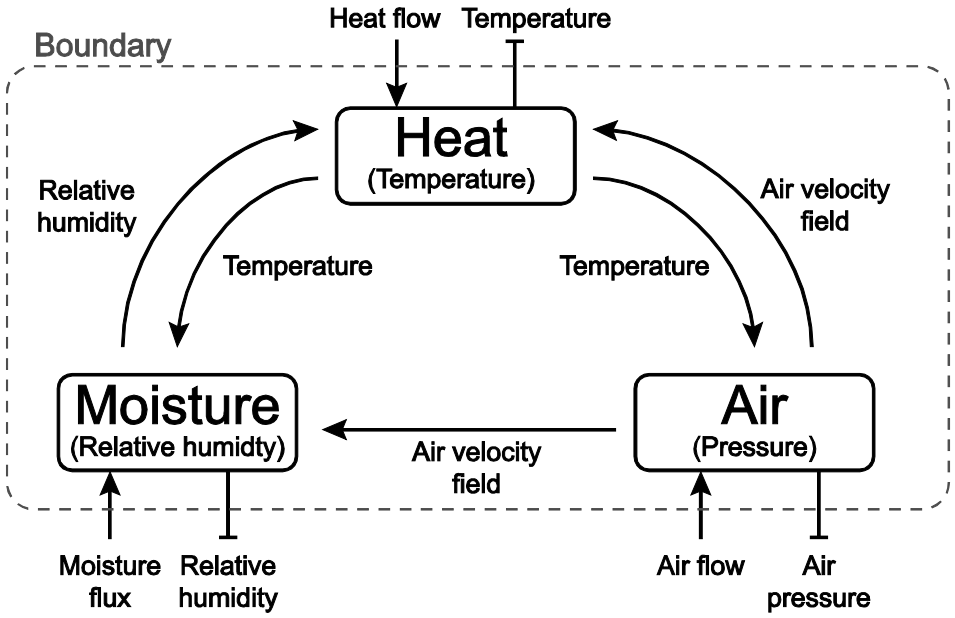

Figure 3.1 Flowchart describing model coupling between heat, moisture and air transport. Dependent variables in parenthesis.

The numerical model implemented in this thesis has a set of limitations regarding the involved physics and boundary condition cases etc. All of the general model limitations are further discussed in Chapter 5.2.1 together with more specific limitations regarding the actual setup of the simulations.

3.2 Heat transfer

The heat balance implemented in this thesis is given by Equation 3.1 (Tariku, et al., 2009):

$$\underbrace{\rho_m c_{p,eff} \frac{\partial T}{\partial t}}_{I} = \nabla \cdot \left(\underbrace{\lambda \nabla T}_{II} - \underbrace{\rho_a \boldsymbol{v_a} \left(c_{p,a} + \omega\, c_{p,v}\right) T}_{III} \right) + \underbrace{\dot{m}_c \left(h_{evap} + T\left(c_{p,v} - c_{p,l}\right)\right)}_{IV} + \underbrace{\dot{Q}_s}_{V} \tag{3.1}$$

The equation is divided into five parts that are described separately. The first term (*I*) is the transient term where T (K) is the temperature, ρ_m(kg/m^3) is the density of the material and $c_{p,eff}$ (J/(kg·K)) is the effective heat capacity of the material which is also changing with moisture content (Tariku, 2008):

$$c_{p,eff} = c_{p,m} + Y_l c_{p,l} \tag{3.2}$$

Here $c_{p,m}$ and $c_{p,l}$ are the specific heat capacities (J/(kg·K)) of the dry material and liquid water respectively and Y_l (kg/kg) is the mass fraction of liquid water.

The two terms inside the divergence (*II* and *III*) of Equation 3.1 are the heat conduction and convection fluxes respectively. Here λ (W/(m·K)) is the thermal conductivity, $\boldsymbol{v_a}$(m/s) represents air velocity, ω (kg/kg) is the absolute humidity according to Equation 3.7, ρ_a(kg/m^3) is the air density and $c_{p,a}$ and $c_{p,v}$ are the specific heat capacities (J/(kg·K)) of dry air and vapour respectively.

The fifth term (*V*) in Equation 3.1 is the heat source term where $\dot{Q}_s$ (W/m^3) is a heat source and the forth term (*IV)* is the heat released by condensation where h_{evap} (J/kg) is the latent heat of condensation/evaporation and $\dot{m}_c$ (kg/s) is the amount of water condensed or evaporated according to Equation 3.3.

$$\dot{m}_c = \nabla \cdot \left(\left(\delta_p \nabla (P_{sat} \phi) - \rho_a \boldsymbol{v_a} \omega\right) \right) \tag{3.3}$$

Here δ_p (s) is the vapour permeability, P_{sat} (Pa) is the saturated vapour pressure and ϕ (-) is the relative humidity

For a detailed derivation of Equation 3.1 to 3.3 it is referred to Tariku (2008).

The attempt to implement Equation 3.1 in COMSOL by setting term *IV* as a source term proved to pose certain difficulties and this seemed to give less accurate results. It is believed that this is due to the way that boundary conditions are coupled to the domain equations within COMSOL. Therefore T in term *IV* is replaced with reference temperature (T_{ref}), which is constant across the domain, so that also this term can be included within the divergence as shown in Equation 3.4. A varying temperature in term *IV* only influences the heat from condensation/evaporation by a few percent which means setting it to a constant reference temperature does not significantly influence the results.

Therefore, the equation implemented in COMSOL for heat transfer is Equation 3.4.

$$\underbrace{\rho_m c_{p,eff}\frac{\partial T}{\partial t}}_{I} = \nabla\cdot\left(\underbrace{\lambda\nabla T}_{II} - \underbrace{\rho_a \boldsymbol{v_a}\left(c_{p,a}+\omega\, c_{p,v}\right)T}_{III} + \underbrace{\left(h_{evap}+T_{ref}\left(c_{p,v}-c_{p,l}\right)\right)\left(\delta_p\nabla(P_{sat}\phi)-\rho_a\boldsymbol{v_a}\omega\right)}_{IV}\right)+\underbrace{\dot{Q}_s}_{V} \tag{3.4}$$

3.3 Moisture transport

The model for moisture transport presented in this thesis is based on Tariku, et al. (2009). More in depth derivations of Equation 3.5 and 3.6 are also given in Tariku (2008). Equation 3.5 gives a basic moisture balance equation for both liquid and vapour.

$$\underbrace{\frac{\partial w}{\partial t}}_{I} = \nabla\cdot\left(\underbrace{\delta_p\nabla P_v}_{II} - \underbrace{\rho_a\boldsymbol{v_a}\omega}_{III} + \underbrace{D_l\nabla P_s}_{IV} - \underbrace{D_l\rho_w\boldsymbol{g}}_{V}\right) \tag{3.5}$$

Here *I* is the transient term. Terms *II* and *III* are the vapour diffusion and convection fluxes respectively. Term *IV* represents capillary suction and term *V* represents liquid transport due to gravity. The letter δ_p (s) denotes vapour permeability, $\boldsymbol{v_a}$ (m/s) represents air velocity, ω (kg/kg) is the absolute humidity, D_l (s) is liquid conductivity, $\boldsymbol{g}$ (m/s^2) is the downwards gravity acceleration vector and ρ_w and ρ_a are the densities (kg/m^3) of water and air respectively.

Equation 3.5 is expressed with multiple dependent variables such as moisture content w (kg/m^3), vapour pressure P_v (Pa), absolute humidity ω (kg/kg) and suction pressure P_s (Pa). In order to solve the equation it must be transformed to be expressed in terms the dependent variables used in this numerical model, namely relative humidity ϕ (-) and temperature T (K). This results in the expression described by Equation 3.6.

$$\underbrace{\xi\frac{\partial\phi}{\partial t}}_{I} = \nabla\cdot\left(\underbrace{\delta_p\left(\phi\frac{dP_{sat}}{dT}\nabla T + P_{sat}\nabla\phi\right)}_{II} - \underbrace{\rho_a\boldsymbol{v_a}\omega}_{III} + \underbrace{D_l\frac{\rho_w R}{M_w}\left(\ln(\phi)\nabla T+\frac{T}{\phi}\nabla\phi\right)}_{IV} - \underbrace{D_l\rho_w\boldsymbol{g}}_{V}\right) \tag{3.6}$$

Here P_{sat} (Pa) is the saturated vapour pressure, R (J/(kg·mol)) represents the universal gas constant and M_w (kg/mol) is the molar mass of water.

The letter ω (kg/kg) denotes the absolute humidity and is expressed according to Equation 3.7 where P_{atm} (Pa) represents the standard atmospheric pressure

$$\omega = \frac{0.622\, P_{sat}\phi}{P_{atm}} \tag{3.7}$$

The letter ξ (kg/m^3) in Equation 3.6 is the moisture capacity defined by:

$$\xi = \frac{\partial w}{\partial \phi} \tag{3.8}$$

In some of the calculations, vapour permeability δ_p is given in terms of the vapour resistance factor μ_{vrf} (-) since this is often what is found in material data. This factor describes the vapour permeability of the material in relation to the vapour permeability of air D_p (s):

$$\mu_{vrf} = \frac{D_p}{\delta_p} \tag{3.9}$$

3.4 Air transport

A slow viscous air flow through a porous medium can be modelled with Darcy's law according to Equations 3.10 and 3.11 (Nield & Bejan, 2006).

$$\varepsilon \frac{\partial \rho_a}{\partial t} + \nabla \cdot (\rho_a \boldsymbol{v_a}) = 0 \tag{3.10}$$

Here ρ_a (kg/m^3) is air density, ε (-) represents the porosity of the material (fraction of the total volume of the material that is occupied by a void space) and $\boldsymbol{v_a}$ (m/s) is a vector describing the Darcy air velocity according to Equation 3.11.

$$\boldsymbol{v_a} = -\frac{\kappa}{\mu}(\nabla P - \rho_a \boldsymbol{g}) \tag{3.11}$$

Here κ (m^2) is the air permeability of the material and μ (Pa s) is the dynamic viscosity of air. The driving potential for the air flow is the gradient in air pressure. The overall pressure gradient consist of two parts, where ∇P is the pressure gradient caused by wind and mechanical ventilation etc. and the product $\rho_a \boldsymbol{g}$ accounts for the addition due to gravity. The letter $\boldsymbol{g}$ (m/s^2) is the downwards gravity acceleration vector.

Note the Darcy velocity $\boldsymbol{v_a}$ is not equivalent to the actual velocity of the fluid particles within the pore space $\boldsymbol{V_a}$. The Darcy velocity represents the fluid flow per the entire cross section area. Since only part of the cross section area consists of pore space allowing for fluid flow, the Darcy velocity is related to the fluid particle velocity by porosity (Nield & Bejan, 2006):

$$\boldsymbol{v_a} = \boldsymbol{V_a}\varepsilon \tag{3.12}$$

For building physics applications the air density in Equation 3.11 can be calculated using a simplified model according to Equations 3.13 and 3.14 (Janssens, 1998).

First it is assumed that the metrological fluctuations in air pressure are negligible compared to total pressure meaning that total air pressure P_{tot} (Pa) (the sum of dry air pressure P_d and partial vapour pressure P_v) is equal to standard atmospheric pressure P_{atm}.

$$P_{tot} = P_d + P_v \cong P_{atm} \tag{3.13}$$

Second it can be assumed that density of air is varying with temperature alone and not with vapour pressure. The influence of a variation in vapour pressure with regard to building

physics applications is usually two to three orders of magnitude less than the influence from temperature variations (Janssens, 1998). This assumption together with the general gas law and Equation 3.13 gives the final expression for the air density, where R_d (J/(kg·K)) is the specific gas constant of dry air:

$$\rho_a \cong \frac{P_{atm}}{R_d T} \tag{3.14}$$

Darcy's law is valid for sufficiently slow flow, requiring that the air flow is clearly laminar. A criterion for the validity of the application of Darcy's law for flow calculations in a porous medium is given by Equation 3.15, stating that it is valid if the representative Reynolds number Re_k (-) is below one (Nield & Bejan, 2006). Here ν (m^2/s) is the kinetic viscosity of air.

$$Re_k = \frac{v_a\sqrt{\kappa}}{\nu} < 1 \tag{3.15}$$

This criterion is generally fulfilled in building physics applications (Janssens, 1998). However, for the simulations performed in this thesis, additional calculations have been done to check the Reynolds number at the most critical points with the highest velocities. They all proved to be far below the criterion. Thus, the Reynolds number for the air flow within the domain is not further discussed in this thesis.

3.5 Boundary conditions

The boundary conditions are given for each governing equation either by prescribing the dependant variable on the boundary (Dirichlet boundary condition) or by giving an expression for the flux across the boundary (Neumann boundary condition) or by saying that the flux across the boundary is zero. So for example, for the heat equation either temperature or heat flux could be given on a boundary, or the heat flux across the boundary could be set to zero (which for heat transfer is referred to as an adiabatic boundary condition). The flux boundary conditions in this thesis are based on Sasic Kalagasidis (2004).

The framework of the model was designed to incorporate additional boundary conditions including solar radiation, sky radiation, liquid transport due to rain as well as pressure differences caused by wind and mechanical ventilation. However, due to time constraints it was not possible to implement these additional boundary conditions. The framework of the model allows for these to be implemented at a later date if required by a need for further research.

3.5.1 Heat flux boundary condition

Equation 3.16 gives an expression for heat flux q_b (W/m^2) inwards (towards the domain) across the boundary, given that also the air flow is defined as positive inwards.

$$q_b = \underbrace{\alpha(T_\infty - T_s)}_{I} + \underbrace{g_b\left(h_{evap} + T_{ref}\left(c_{p,v} - c_{p,l}\right)\right)}_{II} + \underbrace{\rho_a v_a\left(c_{p,a} + \omega\, c_{p,v}\right)T_b}_{III} \quad (3.16)$$

Here boundary temperature T_b is equal to the surrounding temperature T_∞ if the air flow is positive (inward flow) and equal to the surface temperature T_s if the air flow is negative (outward flow or away from the domain). The letter g_b (kg/(m^2·s)) is the moisture flux across the boundary according to Equation 3.17 and α (W/(m^2·K)) is the surface heat transfer coefficient.

Term *I* is equal to the convective heat transfer, Term *II* represents the latent heat transfer and term *III* is the convective heat transfer. Note the similarity to the equation for the heat flow within the domain (3.4).

3.5.2 Moisture flux boundary condition

The expression for the inwards moisture flux across the boundary g_b (kg/(m^2·s)) can be given in a similar way as for the heat flux:

$$g_b = \underbrace{\beta_p(\phi_\infty P_{sat} - \phi_s P_{sat})}_{I} + \underbrace{\rho_a v_a \omega_b}_{II} \quad (3.17)$$

Here, boundary absolute humidity ω_b is equal to the surrounding absolute humidity ω_∞ if the air flow is positive (inward air flow) and equal to the surface absolute humidity ω_s if the air flow is negative (outward air flow). The letter β_p (s/m) is the surface vapour transfer coefficient and ϕ_∞ and ϕ_s are the surrounding relative humidity and the surface relative humidity respectively.

Term *I* represents the moisture flux due to diffusion and term *II* represents the convective moisture flux. Note the similarity to the moisture flow within the domain (Equation 3.6).

3.5.3 Air pressure boundary condition

When buoyancy is taken into account, the air pressure varies with height. This needs to be taken into account when prescribing the air pressure at the boundary with regard to the air pressure equation. The air pressure at the boundary P_b (Pa) is then given by Equation 3.18 (Langmans, et al., 2012).

$$P_b = \rho_a \, g(H_0 - y) \tag{3.18}$$

Here ρ_a is the temperature dependent air density, g (m/s^2) is the gravity acceleration constant, H_0 (m) the elevation of the neutral pressure plane and y (m) is the elevation of the boundary point being evaluated.

3.5.4 Air gap leakage boundary condition

The aim of this thesis is to build a model of a light-weight timer wall assembly subject to air leakage via gaps in the interior vapour retarder layer (specifically gaps between OSB boards). Hence there is a need for the numerical model to reflect the boundary conditions at those gaps. This is achieved by implementing the model for air flow through an air gap in an air tight building envelope component described in Hagentoft (2001). See Figure 3.2 for a description of the geometry.

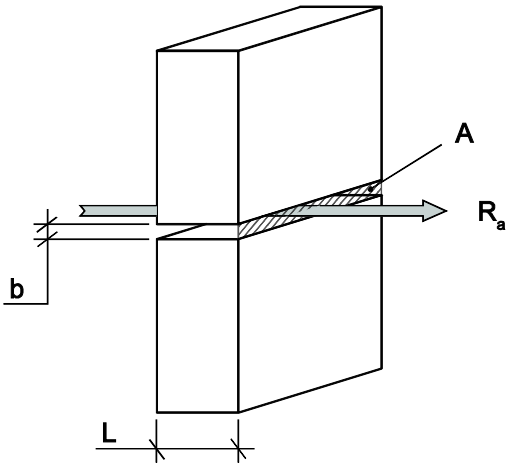

Figure 3.2 Air flow through an air gap (Hagentoft, 2001)

The volumetric air flow rate thorough the gap R_a (m^3/s) is then given by:

$$R_a = \frac{\Delta P}{S_g + S_e' \, R_a} \tag{3.19}$$

Here ΔP (Pa) is the total pressure loss over the gap, including the entrance pressure loss, S_g (Pa/(m^3/s)) is the air flow resistance of the inner of the gap and the product $S_e' \cdot R_a$ (Pa/(m^3/s)) is the flow resistance at the gap entrance. In Hagentoft (2001) the product $S_e' \cdot R_a$ is referred to as the combined resistance due to turbulence at the gap entrance and exit. However, in the particular case which is investigated in this thesis, where the space on each side of the air gap has a much larger flow area than within the gap itself, it can be shown that the product $S_e' \cdot R_a$ is actually equal to air flow resistance of the entrance alone (Kronvall, 1980). S_e' and S_g are defined by Equation 3.20 and 3.21 respectively.

$$S'_e = \frac{1.8\,\rho_a}{2A^2} \tag{3.20}$$

$$S_g = \frac{12\,\mu\,L}{b^2\,A} \tag{3.21}$$

Here, μ (Pa s) is the dynamic viscosity of air, ρ_a (kg/m^3) is the air density, L (m) is the length of the air channel, b (m) is the width of the gap and A (m^2) is the gap area (see Figure 3.2).

Concerning the case studied in this thesis, air leakage is permitted though gaps between interior OSB boards that are set flush to the insulation material. Hence, there is a porous material on one side of the gap. The air flow in the porous material is expected to be laminar. Therefore the gap entrance resistance, as the air is flowing from the insulation, can be neglected (see case *a* in Figure 3.3). In this case the product $S'_e \cdot R_a$ can be set to zero and the Equation 3.19 could then be reduced to a simplified expression for the air flow:

$$R_a = \frac{\Delta P}{S_g} \tag{3.22}$$

On the other hand, if the air flows from the open side through the gap, the entrance resistance needs to be taken into account (see case *b* in Figure 3.3. The air flow can then be calculated according to Equation 3.23, achieved by solving Equation 3.19 for R_a.

$$R_a = \frac{1}{2\,S'_e}\left(\sqrt{S_g^2 + 4\,\Delta P\,S'_e} - S_g\right) \tag{3.23}$$

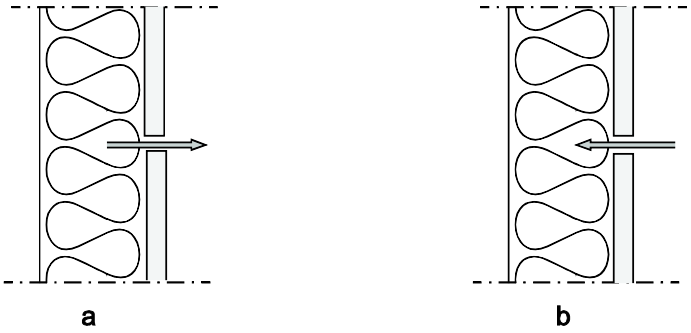

Figure 3.3 Illustration of case a where the air flow resistance of the gap entrance can be neglected and case b where it needs to be taken into account

The boundary condition implemented in COMSOL is the mean air velocity v_{gap} (m/s) across the gap boundary, which is given by dividing the air flow by the gap area:

$$v_{gap} = \frac{R_a}{A} \tag{3.24}$$

For the modelling of air flow through an air gap to be valid, the Reynolds number (-) must fulfil the criteria in Equation 3.25 meaning that the air flow within the gap is laminar.

$$\mathrm{R_e} = \frac{v_{\mathrm{gap}}\ 2\ b\ \rho_a}{\mu} < 2000 \tag{3.25}$$

3.6 COMSOL implementation

Within the COMSOL interface different physics can be added to the model either as a predefined physics module or as a custom module where the physics is defined manually.

For calculating the air transport there is a suitable predefined physics module available in COMSOL which utilizes Darcy's law as described previously in this chapter. This module can be set to use the temperature computed in another module as an input to calculate the air density and subsequently produce an air velocity field.

However, for the described mechanisms for heat and moisture transport, there are no appropriate predefined physics modules available. One way to implement these equations is by using a module called "Coefficient Form PDE", as described in Williams Portal (2011). The coefficient form PDE is described by Equation 3.26 on the computational domain Ω, with the unknown variables $\boldsymbol{u}$ (COMSOL AB, 2013). The boundary conditions on the boundary $\partial\Omega$ are given by Equations 3.27 and 3.28, where the former could be used to prescribe the flux across the boundary while the latter is used to prescribe the dependent variable at the boundary. The vector **n** is the outward (away from the domain) unit normal vector on the boundary $\partial\Omega$.

$$e_a \frac{\partial^2 \boldsymbol{u}}{\partial t^2} + d_a \frac{\partial \boldsymbol{u}}{\partial t} + \nabla \cdot (-c\nabla \boldsymbol{u} - \alpha \boldsymbol{u} + \gamma) + \beta \cdot \nabla \boldsymbol{u} + a\boldsymbol{u} = f \quad in\ \Omega \tag{3.26}$$

$$-\mathbf{n} \cdot (-c\nabla \boldsymbol{u} - \alpha \boldsymbol{u} + \gamma) = g - q\boldsymbol{u} \quad on\ \partial\Omega \tag{3.27}$$

$$\mathbf{u} = \mathrm{r} \quad on\ \partial\Omega \tag{3.28}$$

The heat and moisture equations can be coupled directly within the Coefficient Form PDE interface by expanding the equation to an equation system dependent on both temperature and relative humidity. This means that $\boldsymbol{u}$ should be given as a vector according to:

$$\boldsymbol{u} = \begin{bmatrix} T \\ RH \end{bmatrix} \tag{3.29}$$

Equations 3.26 to 3.28 are general expressions in which the desired physics could be implemented by giving expressions for the different coefficients. However, to implement the heat and moisture transport equations described in this chapter, not all those coefficients are used. Coefficients e_a, β, a and q could all be set to zero and Equations 3.26 and 3.27 could therefore be simplified to:

$$d_a \frac{\partial \boldsymbol{u}}{\partial t} + \nabla \cdot (-c\nabla \boldsymbol{u} - \alpha \boldsymbol{u} + \gamma) = f \quad in\ \Omega \tag{3.30}$$

$$-\mathbf{n} \cdot (-c\nabla \boldsymbol{u} - \alpha \boldsymbol{u} + \gamma) = g \quad on\ \partial\Omega \tag{3.31}$$

Since the dependent variable for the coefficient form PDE ($\boldsymbol{u}$), is given as a vector, the different coefficients need to be input as matrices. The Equations 3.32 to 3.35 show how the heat and moisture transfer equations, Equations 3.4 and 3.6 respectively, are implemented in the different coefficients for a one-dimensional case.

$$d_a = \begin{bmatrix} \rho_m c_{p,eff} & 0 \\ 0 & \xi \end{bmatrix} \tag{3.32}$$

$$c = \begin{bmatrix} \lambda & 0 \\ \delta_p \phi \frac{dP_{sat}}{dT} + D_l \frac{\rho_w R}{M_w} \ln(\phi) & \delta_p P_{sat} + D_l \frac{\rho_w R}{M_w} \frac{T}{\phi} \end{bmatrix} \tag{3.33}$$

$$\alpha = \begin{bmatrix} \rho_a v_a \left(c_{p,a} + \omega\, c_{p,v}\right) & 0 \\ 0 & \rho_a v_a \frac{0.622\ P_{sat}}{P_{atm}} \end{bmatrix} \tag{3.34}$$

$$\gamma = \begin{bmatrix} \left(h_{evap} + T_{ref}\left(c_{p,v} - c_{p,l}\right)\right)\left(\delta_p \nabla(P_{sat}\phi) - \rho_a v_a\, \omega\right) \\ 0 \end{bmatrix} \tag{3.35}$$

Note that $v_a$in the equations above is the air velocity calculated in the Darcy's law module.

Expanding the system to two or three dimensions is rather straightforward within the COMSOL interface, but this will mean that some of the PDE coefficients described above become multidimensional arrays that are difficult to visualize in a simple way. Within this thesis only 1D and 2D studies are performed. For a 2D study, material properties such as conductivity or air permeability can be anisotropic, meaning that they have directional properties. Also, for a 2D simulation, the air flow needs to be input in terms of the x and y components.

Figure 3.4 gives a simplified example of how the model described above can look in COMSOL. To the left in the figure is the Model Builder where nodes are added for the different physics, geometries, type of studies and results etc. Section *III* and *IV* indicates the Coefficient Form PDE and Darcy's Law modules respectively. Each one has several sub nodes for boundary conditions, initial values and domain expressions. Clicking on them opens an interface where the relevant expressions or material data can be entered. The middle part in Figure 3.4 shows such an interface for the domain expressions for the Coefficient Form PDE module. Here the PDE coefficients can be entered according to Equations 3.32 to 3.35 (the model in the figure is simplified and does not show the actual expressions since they would not fit within the window). Part *I* and *II* in the model builder, can include nodes for general constants, material constants and general model expression such as the expression for the saturated vapour pressure as well as material parameters that are functions of, for example, relative humidity. It could also be convenient to give other expressions, such as boundary conditions, here as separate nodes which are then called within the specific boundary condition interface. Material parameters that are functions of a dependent variable could be given as an analytical expression directly within COMSOL or imported as tabulated data by means of interpolation functions.

The two windows to the right in Figure 3.4 show the geometry (in this case a straight line) and the solver log (showing the status of the simulation process)

The simulation is solved using the time dependent solver named MUMPS using variable time stepping with a maximum step of one hour. Under the "Study" node several settings for the solver can be altered. One important setting that had to be adjusted was modifying the jacobian update from "minimal" to "on every iteration" as the governing balance equations are highly non-linear. This is highlighted as the heat and moisture transfer and storage coefficients are functions of their relevant driving potentials, rather than constants.

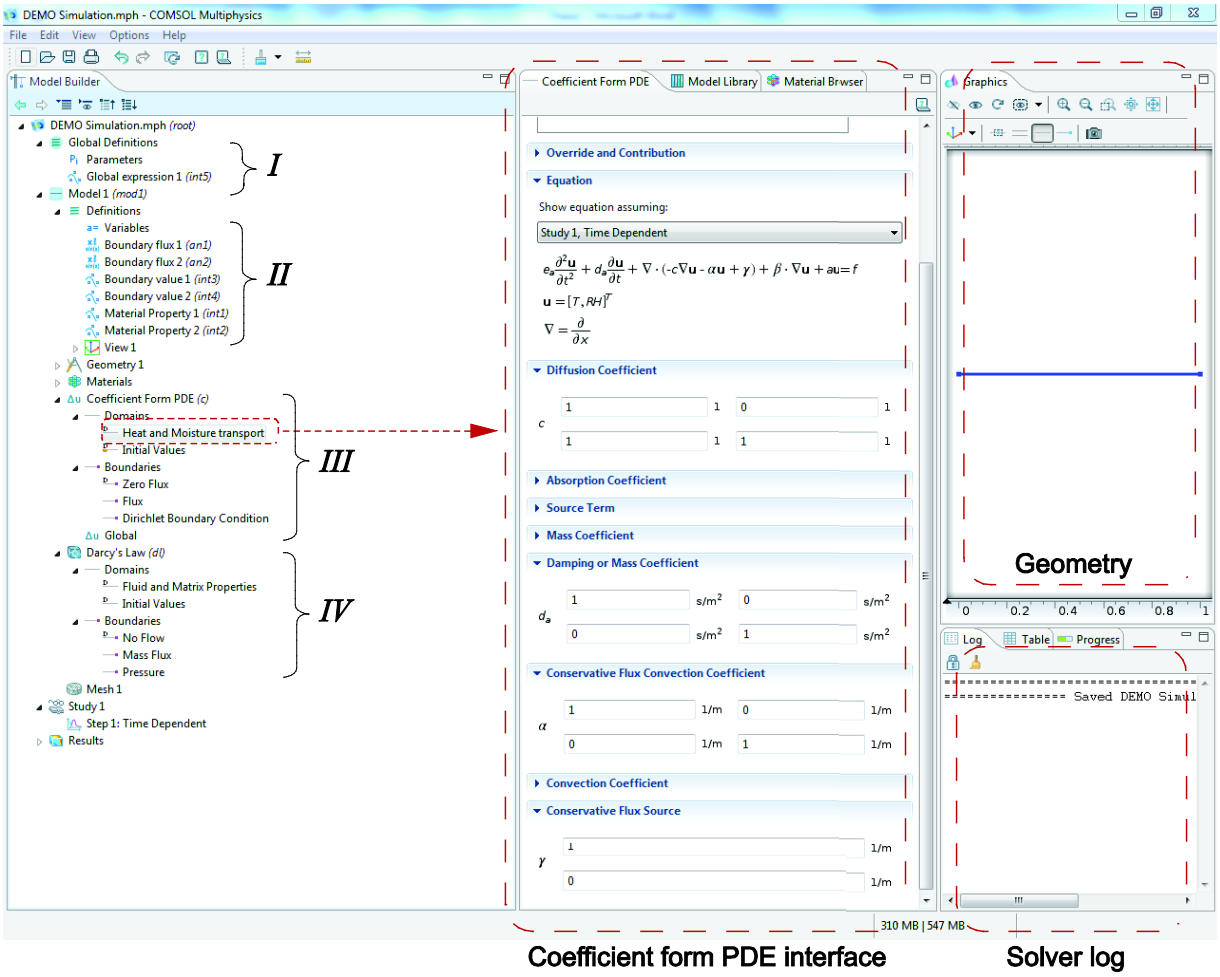

Figure 3.4 Screenshot of an example model in COMSOL

4 1D HAM Model

4.1 Verification

The validation of the model constructed in COMSOL was achieved through a series of verification processes. These processes were outlined by the normative benchmark tests of the European Provisional Standard prEN 15026.

The HAMSTAD project was an EU led initiative involving numerous universities and institutes from Europe, Israel and Canada. The goal of the project was to establish a standard for the evaluation of numerical Heat, Moisture and Air (HAM) transport models within the scope of building physics.

To establish this standard five benchmarks of varying complexity representing heat, moisture and air transport mechanisms in porous building material, have been set forth by the HAMSTAD group. These benchmarks have been separately evaluated by HAMSTAD participants and the resultant data pooled and tabulated. The various solutions then offer a comparative standard by which all future numerical models can be assessed.

It must be noted that the benchmarks outlined by the HAMSTAD group all represent HAM transport mechanisms in one dimension.

For this study a simple transient Heat and Moisture (HM) model was constructed in line with benchmark 2. This was then verified with respect to the analytical solution as defined by benchmark 2.

Secondly, a more complex transient HM model was constructed in line with benchmark 5. This was then verified with respect to the comparative solution as defined by benchmark 5.

Lastly, a simple transient HAM model was constructed in line with benchmark 3. This was then verified with respect to the comparative solution as defined by benchmark 3.

Benchmark 3 is documented within the body of the thesis, Benchmarks 2, 5 as well as the extended results of Benchmark 3 are found within Appendices A, C and B respectively.

Comparative solution data regarding benchmarks 5 and 3 is sourced from the following HAMSTAD participating institutes; NRC (National Research Council of Canada), CTH (Chalmers Tekniska Högskola), TUD (Technical University of Dresden) and Technion (Technion Isreal Istitute of Technology).

4.2 Benchmark 3

4.2.1 Introduction

Benchmark 3 is a 1D, HAM numerical model verification tool initiated by Chalmers University of Technology (CTH) for the HAMSTAD project. This benchmark provides comparative solutions from various universities involved in the HAMSTAD project, against which the numerical model can be assessed for conformity and so relative accuracy.

In this benchmark a single layer is analysed in one direction. The geometry is shown in Figure 4.1.

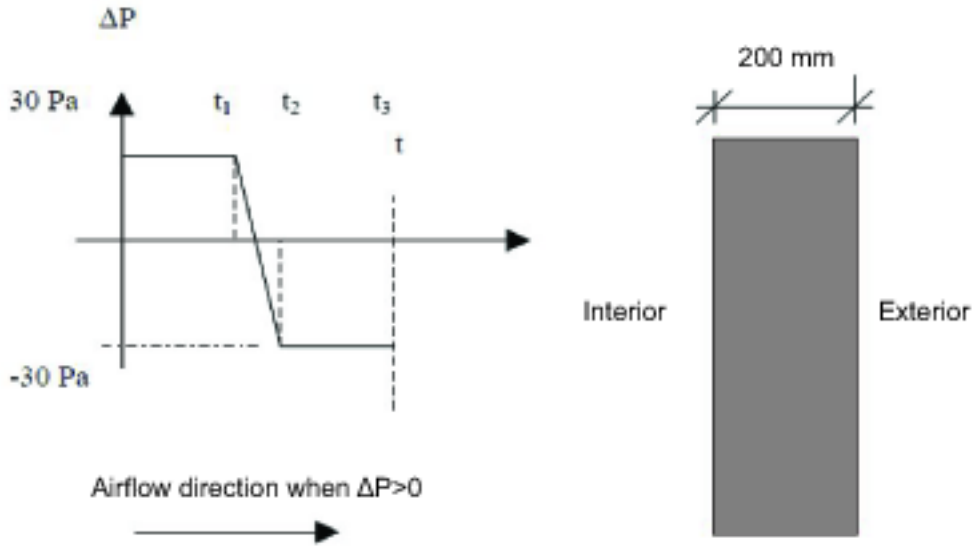

Figure 4.1 Geometry of single layer and pressure profile in HAMSTAD benchmark 3

The homogenous layer is considered in a steady-state condition with both boundaries (interior and exterior) exhibiting constant and equal relative humidity and temperature values of 95% and 20°C. This is until at a time zero where there is a step change in relative humidity and temperature values at each boundary, to 70% and 20°C on the interior and 80% and 2°C on the exterior. Here, heat and moisture transport mechanisms due to air movements must be modelled as the inclusion of a pressure profile implies an airflow.

4.2.2 Global parameters and material properties

The global parameters shown for this benchmark are valid for all benchmarks outlined by the HAMSTAD group.

Table 4.1 HAMSTAD Benchmark global parameters

Definition	**Term**	**Unit**	**Value**
Reference temperature	T_{Ref}	K	293.15
Liquid water density	ρ_w	kg/m^3	1000
General gas constant	R	J/(mol·K)	8.314
Molar water mass	M_w	kg/mol	0.018
Vapour gas constant	R_v	J/(kg·K)	R/ M_w
Heat of evap/cond	$\ell_{\ell v}$	J/kg	$2.5 \cdot 10^6$
Gravity acceleration	g	m/s^2	9.81
Capillary suction height	H	m	$P_{suc}/(\rho_w \cdot g)$
Kelvin relationship	P_{suc}	m	$- \rho_w \cdot R_v \cdot T \cdot \ln(\phi)$
Gravimetric liquid water content	W	kg/m^3	-
Volumetric liquid water content	θ_l	m^3/m^3	w/ ρ_w
Heat capacity of air	$\rho_a c_p$	$kJ/m^3 \cdot K$	1.25

The variation of air properties due to temperature change are neglected.

The material properties of the layer are represented by numerous equations which are implemented in the numerical model.

Sorption isotherm.

$$w(P_{suc}) = w_{sat} \cdot \sum_{i=1}^{N} \frac{k_i}{\left(1 + \left(a_i \cdot h(P_{suc})\right)^{n_i}\right)^{m_i}} \ (kg/m^3) \tag{4.1}$$

$$m_i = 1 - 1/n_i \tag{4.2}$$

Vapour diffusion.

$$\delta_p(w,T) = \frac{M_w}{RT} \cdot D_{vapour}(w); \tag{4.3}$$

$$D_{vapour}(w) = \frac{26.1 \cdot 10^{-6}}{\mu_{dry}} \cdot \frac{1 - \frac{w}{w_{sat}}}{(1-p)\left(1 - \frac{w}{w_{sat}}\right)^2 + p} \ (\mathrm{m^2/s}) \tag{4.4}$$

Liquid water conductivity.

$$K(w) = exp\left[\sum_{i=0}^{5} a_i \cdot (w/\rho_w)^i\right] \ (\mathrm{s}) \tag{4.5}$$

Thermal conductivity.

$$\lambda = \left(\lambda_{dry} + \lambda_{mst}\frac{w}{\rho_w}\right) \ (\mathrm{W/(m{\cdot}K)}) \tag{4.6}$$

Heat capacity for dry material.

$$\rho_0 c_0 \ (\mathrm{J/m^3{\cdot}K}) \tag{4.7}$$

Table 4.2 Benchmark 3 fitting parameters

	Single layer
Water retention	
w_{sat} (kg/m^3)	871.5
k_1 (-)	0.41
k_2 (-)	0.59
a_1 (-)	0.006
a_2 (-)	0.012
n_1 (-)	2.4883
n_2 (-)	2.3898
Vapour diffusion	
μ_{dry} (-)	5.6
p (-)	0.2
Liquid water conductivity	
a_0 (-)	-46.245
a_1 (-)	294.506
a_2 (-)	-1439
a_3 (-)	3249
a_4 (-)	-3370
a_5 (-)	1305
Thermal conduction	
λ_{dry} (-)	0.06
λ_{mst} (-)	0.056
Heat capacity	
ρ_0 (kg/m^3)	212
c_0 (kg/m^3)	1000

4.2.3 Boundary and initial conditions

Exterior boundary conditions.

$$RH_{ext} = 80\%\,,\ T_{ext} = 2℃ \text{ at } t > 0$$

$$\alpha_{ext} = 10\ (\mathrm{W/m^2{\cdot}K})\,,\ \beta_{ext} = 7.38 \cdot 10^{-12}\ (\mathrm{s/m})$$

Interior boundary conditions.

$$RH_{int} = 70\%\,,\ T_{int} = 20℃ \text{ at } t > 0$$

$$\alpha_{int} = 10\ (\mathrm{W/m^2{\cdot}K})\,,\ \beta_{int} = 2 \cdot 10^{-7}\ (\mathrm{s/m})$$

Initial conditions.

$$RH = 95\%\,, T = 20℃$$

$$r_a = C \cdot \Delta P^{\gamma}$$

$$C = 3.10^{-5}\ (\mathrm{m^3/m^2{\cdot}s{\cdot}Pa})$$

$$\gamma = 1$$

t_1 = 20 days, t_2 = 21 days, t_3 = 100 days

Here, r_a is air velocity in m/s.

4.2.4 Output requirements

The simulation time for the benchmark is 100 days. Moisture content, $w(x)$, and temperature, T(x), is output daily for the x-coordinates positions 0.05, 0.10, 0.15, 0.17 and 0.19 (m).

4.2.5 HAM model setup in COMSOL

Material properties are approximated in EXCEL before their implementation as interpolation curves in the COMSOL model definitions field. This was to minimise computation time and effort. Moisture capacity curves are calculated from the slope of the moisture content (sorption isotherm) curves for each material.

The implementation of the HAM model in the COMSOL PDE field is shown in Figure 4.2.

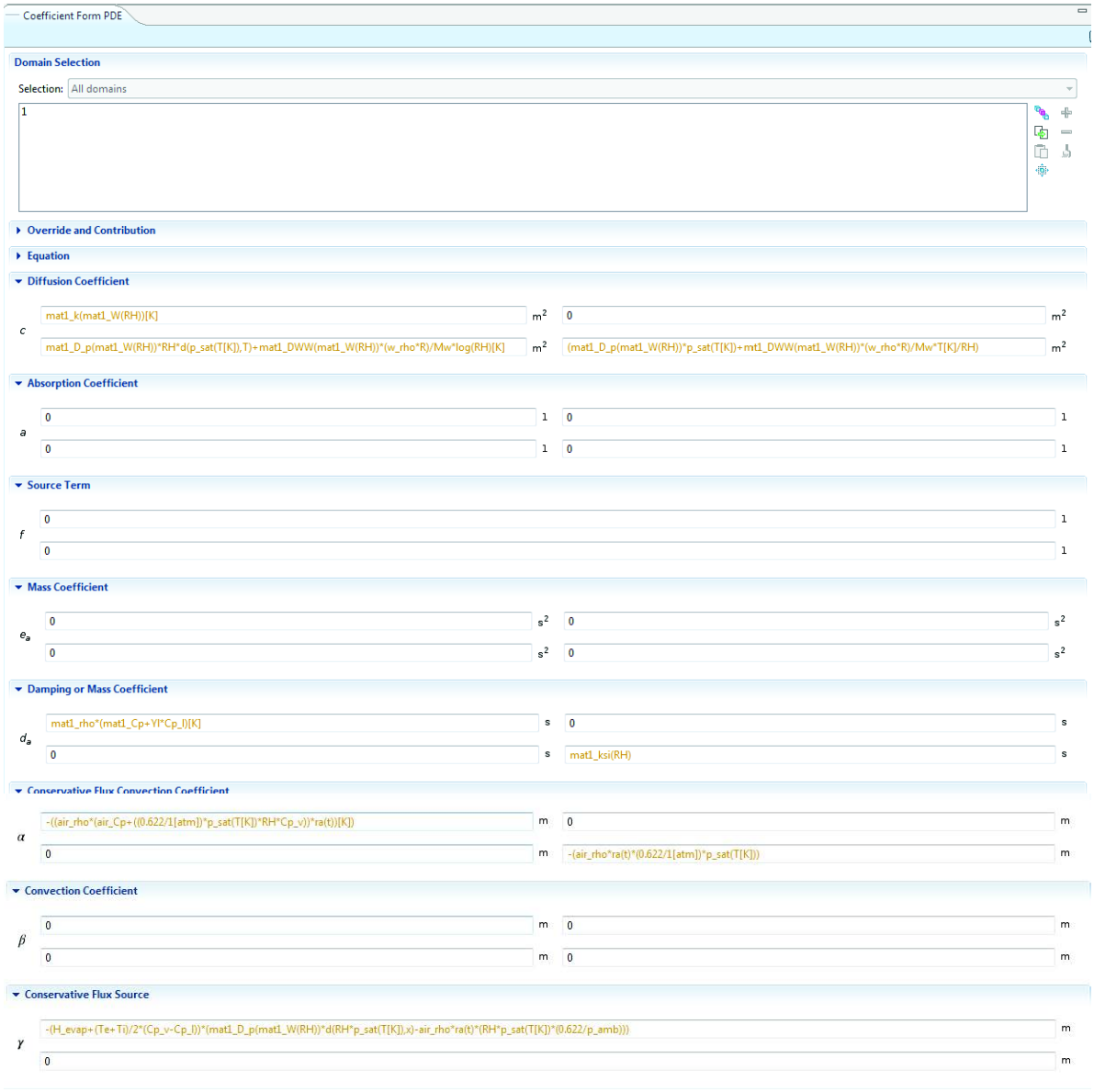

Figure 4.2 Benchmark 3 COMSOL model PDE layout

4.2.6 Results

Here, the solutions are shown for position x = 0.1 m, as well as the solutions from four participating HAMSTAD institutes. Solutions for all positions can be found in Appendix B. A comparatively 'good fit' is observed at all output positions for both moisture content and temperature over 100 days.

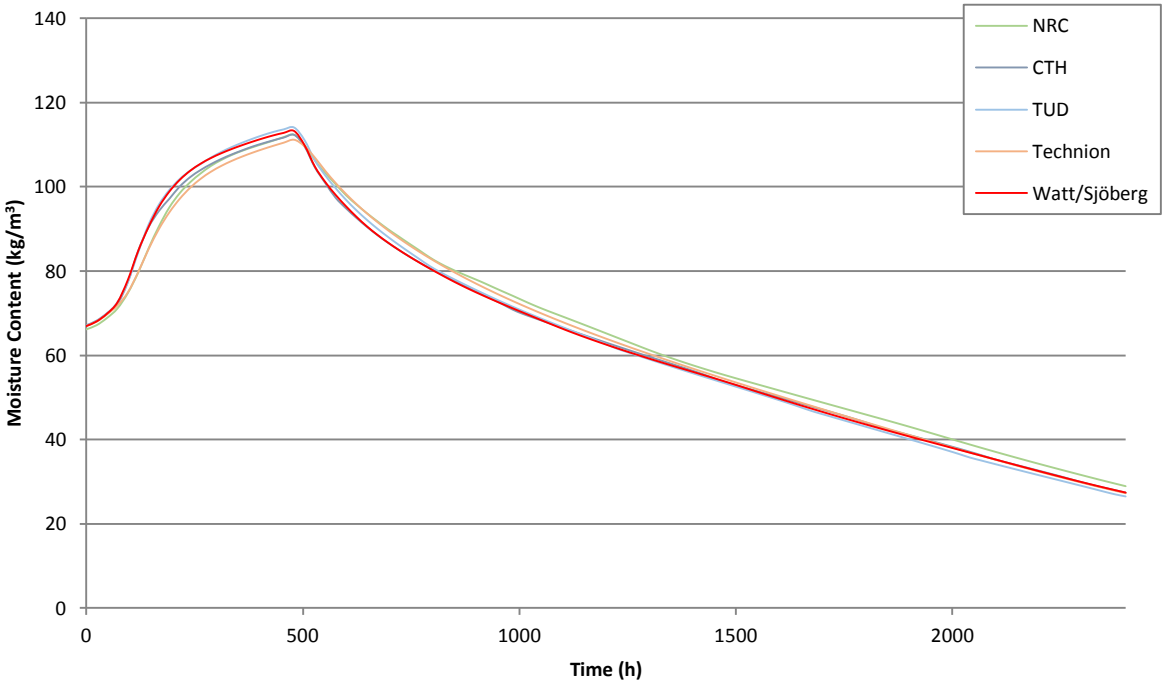

Figure 4.3 Benchmark 3: Moisture content at x = 0.1 m over 100 days

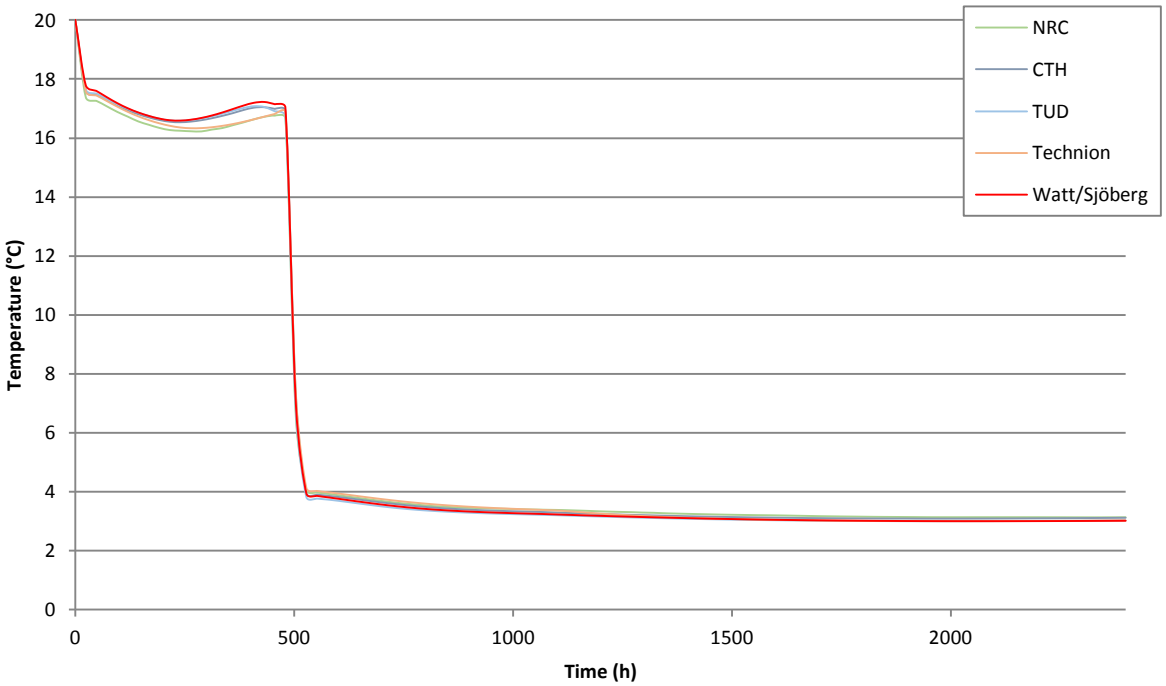

Figure 4.4 Benchmark 3: Temperature at x = 0.1 m over 100 days

4.3 Verification limitations

As stated previously, the benchmark outlined here validates the model in only one dimension. There is no benchmark documented by the HAMSTAD group to validate HAM transport mechanisms in two dimensions, which is a demand of this particular research proposal. With this in mind there is no provision within the HAMSTAD framework to evaluate the gravitational influence on HAM transport mechanisms as well as anisotropic materials.

Additionally, due to time constraints, the numerical model was only assessed for three of the five benchmarks. These benchmarks were selected as they were deemed most pertinent for a valuable assessment considering the aims of the research.

5 2D HAM Model

The two dimensional HAM model is introduced to facilitate the evaluation of the hygro-thermal behaviour of a light-weight timber framed wall assembly which possesses an exterior air barrier and an unsealed interior vapour retarder. The mould growth potential of the wall assembly is then assessed in comparison with a wall assembly where the interior vapour retarder is sealed. A third wall assembly incorporating simplified transport physics is utilized to offer further comparison.

The wall assembly types and associated physics are known as 'Simulation Types' and are numbered 1 to 3 (see Table 5.1). Simulations 1 and 2 both possess a completely sealed interior vapour retarder meaning there are no gaps allowing for air movement from the interior into the wall cavity. The difference is that simulation 1 is strictly a HM model, meaning that only heat and moisture transport mechanisms are modelled, while the simulation 2 is a HAM model which also includes air transport. The effect of natural convection on the hygrothermal behaviour of the wall assembly can be studied by comparing these two simulations. Similar to simulation 2, simulation 3 also includes air transport. However, the third simulation possesses gaps in the interior vapour retarder allowing for air transfer from the interior into the wall cavity. Introducing gaps in the interior vapour retarder influences the air movements within the wall assembly. The effect this has on the hygrothermal performance of the wall assembly is evaluated.

The three different simulation types been evaluated for two sets of boundary conditions cases, a control case and a climate case. The control case study is carried out over 60 days for each simulation. Boundary conditions are constant with a step change occurring at 30 days. The purpose of this control case is to visualize the difference between the simulations as they approach steady state conditions and also to assess the responsiveness of the model. The boundary conditions for the climate case study represent realistic climatic boundary conditions in western Sweden over a full year. The climate case is to assess the difference in mould growth potential between the simulations with and without gaps in the interior vapour retarder.

This gives a total of six different simulations according to Table 5.1. The boundary condition case and simulation type combinations are denoted by an alphanumeric system. For example a simulation that incorporates air transport but no gap geometry and is subject to climatic boundary conditions is referred to as B2. More simulations with additional complexity may be considered, but due to time constraints, the simulation efforts were limited to the six simulations described in the table.

Table 5.1 Overview of the simulation setup of the six different simulations.

Simulation type:	1	2	3
Air Transport	No	Yes	yes
Gaps	No	No	yes
A. Control Case	X	X	x
B. Climate Case	X	X	x

5.1 Test wall setup

The wall assembly to be investigated in this thesis consists of an exterior air barrier of 18 mm bitumen impregnated soft fibreboard with a treated exterior surface, a 240 mm mineral wool insulation layer and an interior vapour retarder of 12 mm OSB, board type 3. The geometry of the wall element is shown in Figure 5.1. The wall element has a height of 2.4 meters. In simulation 3 gaps with a width of 1 mm are introduced in the OSB at a height of 200 mm from the top and bottom of the wall. This is to simulate the gaps present between butted orientated strand boards when unsealed.

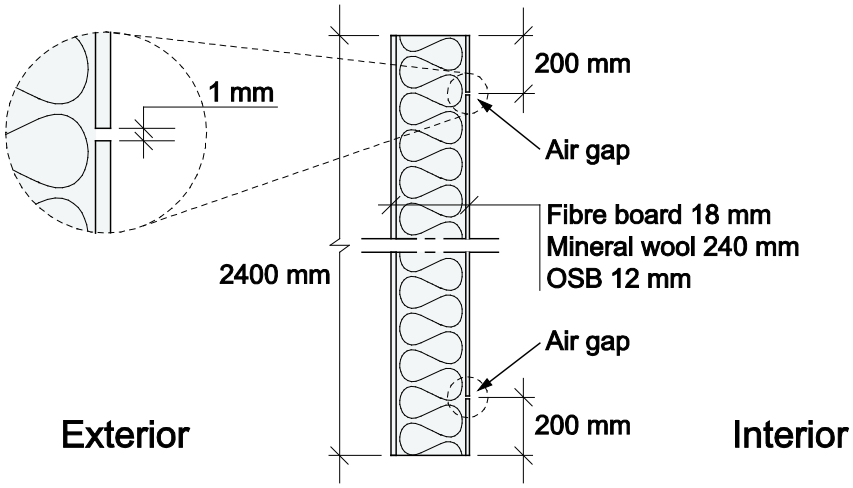

Figure 5.1 Simulated wall geometry with air gaps between interior OSB boards.

The test setup closely resembles that of Langmans et.al(2012) described in Chapter 2.5. However, the wall assembly simulated here has a slightly different setup based on a typical Nordic light-weight timber wall assembly design. In Langmans numerical and physical study he uses constant boundary conditions based on a severe Belgian winter condition. The intention of this study is to use dynamic boundary conditions representative of a typical climate in western Sweden to closer replicate the hygrothermal behaviour of a wall assembly in a realistic Swedish scenario. Another important difference to the study carried out by Langmans is the size of the gaps in the interior OSB layer, which in the study performed by Langmans was set to 10 mm.

The complexity of the geometry is simplified in order to reduce computational effort. Hence the simulated geometry does not include any of the load bearing structure or the exterior façade and interior finishing layers.

The simulated wall is assumed to be positioned at the top floor of a three storey residential building representative of the type of building where this type of wall assembly might be suitable. The top floor is where the overpressure at the interior compared to the exterior is at its highest and hence having the largest driving potential for air exfiltration out through the wall assembly. This is the most critical location with regards to moisture safety since air exfiltration means transport of humid air from the interior out through the wall cavity. The position of the wall in relation to the neutral pressure plane is detailed in Figure 5.2.

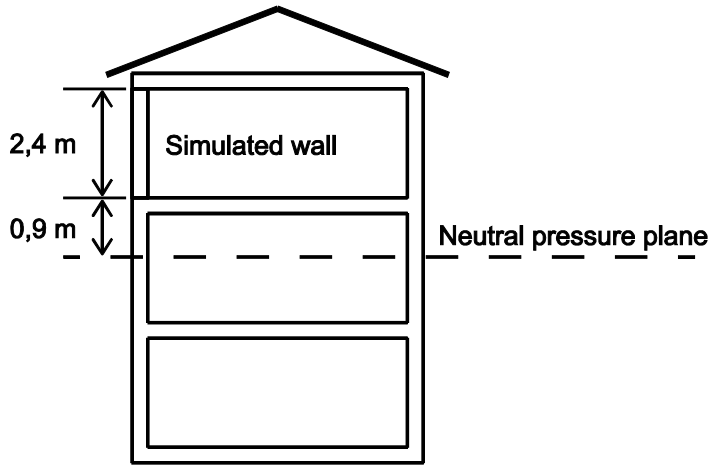

Figure 5.2 Drawing showing the position of the simulated wall in relation to the neutral pressure plane

5.1.1 Air gap properties

As described in Figure 5.1, the width of the gap between the interior OSB boards is set to 1 mm. In reality the size of gaps and consequently the flow through the joints between OSB boards would be highly dependent on the workmanship and is likely to vary significantly between different joints. The modelled gap size is set to take into account board swelling, possible interior finishing layers and that boards are fixed along all edges to a structural stud or sole/top plate. It is noted that typical sheathing patterns would not cause joints between boards to fall in the orientation outlined previously and in Figure 5.1. However, for means of comparison between simulation types and to avoid spurious results by placing the gaps too close to the top and bottom wall boundaries, the location of the gaps is deemed representative.

Figure 5.3 describes the air flow as a function of the pressure difference for the analytical solution of a 1 mm gap in the OSB compared to two relevant measured test cases. The first measured case describes air flow through an open 1 mm gap between two gypsum boards (Sandberg & Sikander, 2004). The second case describes the air flow through a joint between two gypsum boards that are screwed to a stud, as described by Figure 5.4, which closely resembles the kind of joint that would be considered for the type of construction analysed in this thesis (Sikander & Olsson Jonsson, 1997). It can be seen in the Figure 5.3 that the analytical solution gives a lower flow than the measured data for a gap of 1 mm when there is over pressure at the interior side of the wall. At under pressure the analytical solution gives a higher flow compared to the measured flow. This is due to the fact that the analytical solution takes into account the presence of an insulation layer on one side of the gap while the geometry of the experiments from which the measured data is sourced, do not. The presence of an insulation layer means that the entrance pressure loss of the gap could be neglected when air is flowing from the insulation out through the gap (see Chapter 3.5.4) which is the case when there is an under pressure at the interior. However, for both under pressure and overpressure the analytical solution gives a much larger flow than the measured data for two gypsum boards being joined at a stud. This discrepancy gives a certain safety margin regarding the imperfections in the joints, which is necessary since in reality when interior vapour retarder boards are installed less accurately, the air flow is likely to exceed that measured in laboratory.

Although air flow through gaps of this nature vary greatly depending on multiple variables, for the case of this investigation and the comparison outlined in Figure 5.3, the air flow model utilized here is deemed acceptable.

Additionally to give a reference value for the air tightness of the wall assembly, the air leakage of the wall with gaps in the interior OSB has been simulated at a pressure difference of 50 Pascal. For the complete wall assembly, the resulting flow (as a mean value between over pressure and under pressure) per wall area is 0.007 l/(m^2s) which is a low value since the exterior fibre board is considered perfectly sealed. For the case when the exterior fibre board is removed the equivalent flow is 1.6 l/(m^2s).

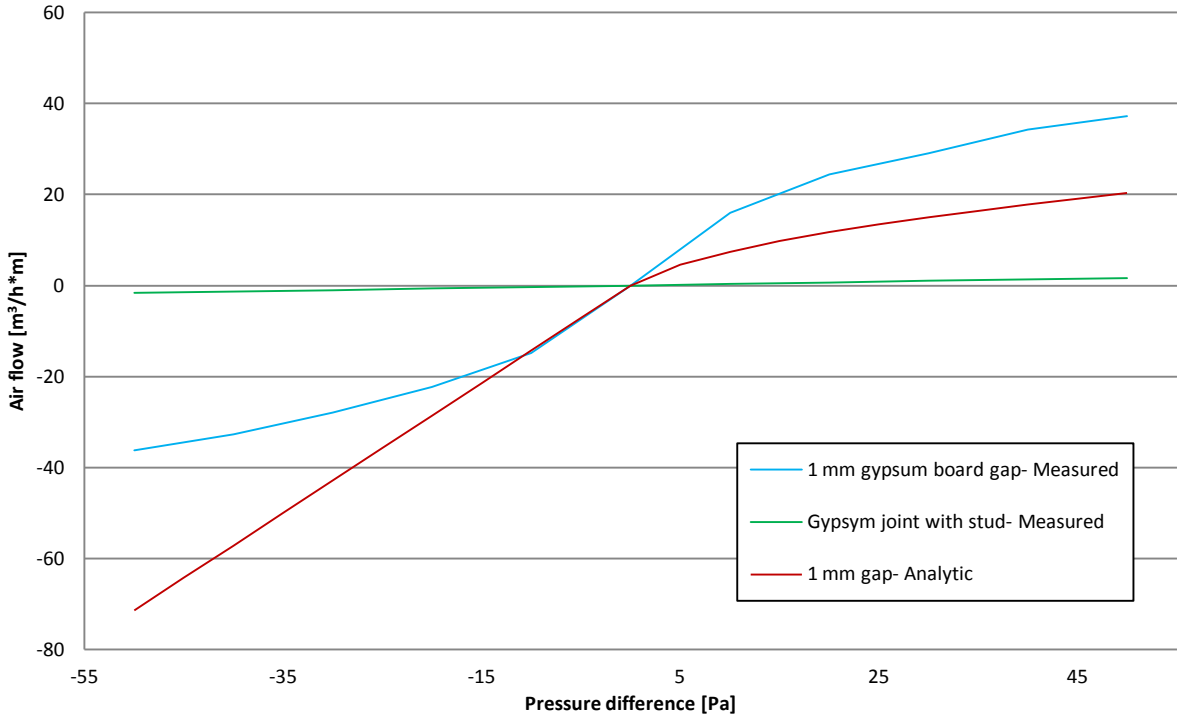

Figure 5.3 *Comparison between analytical solution for air flow through a gap in the OSB and two reference measured test cases.*

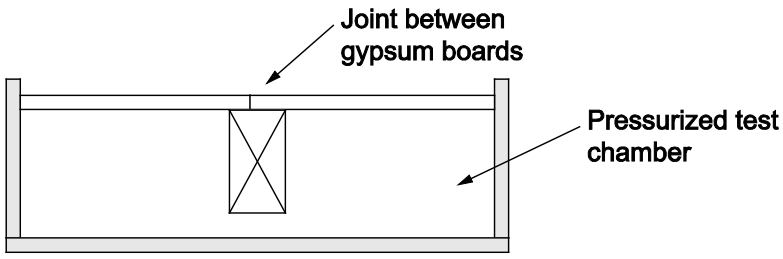

Figure 5.4 *Setup for test of air leakage in gypsum joint with stud (green line, Figure 5.3)(Sikander & Olsson Jonsson, 1997).*

5.1.2 Material properties

When simulating a specific model of this kind, a major challenge is to find suitable material data. The model is as accurate as the material data that is input and it is sometimes difficult to find all necessary data for a specific material. This means that data for a single material often needs to be collected from multiple sources. This is the case for all three wall materials in this model. However, each source material was thoroughly cross referenced with the others of the same type to ensure all material data was as similar as possible. Table 5.2 describes all the necessary material properties for the wall assembly materials. The sorption isotherm and the moisture buffering capacity are expressed in terms of relative humidity and are not given here but they can be found in Appendix D. The vapour diffusion resistance factor is also a function of the relative humidity, but is given in the table as the value for the dry material. The moisture dependent vapour diffusion resistance factor can also be found in Appendix D. The last four rows in Table 5.2 describe different ways to express the same physical parameter, but for comparison they are all given here.

Table 5.2 Wall material properties (material properties marked with an asterisk are given in the table for dry material, while the moisture dependent values can be found in Appendix D).

Notation	Description	Unit	Mineral wool	OSB	Fibre board
d	Material layer thickness	[m]	0.24 (1)	0.012 (6)	0.018 (1)
ρ_m	Density	[kg/m³]	20 (1)	615 (4)	274 (1)
ε	Porosity	[ ]	0.95 (3)	0.9 (4)	0.8 (5)
$c_{p,m}$	Specific heat capacity	[J/(kg·K)]	840 (1)	1500 (4)	2068 (1)
λ	Thermal conductivity	[W/(m·K)]	0.0347 (1)	0.13 (6)	0.0469 (1)
κ_{perp}	Air permeability perpendicular	[m²]	1.3E-09 (2)	8.2E-15 (2)	4.65E-14 (2)
κ_{par}	Air permeability parallel	[m²]	3.8E-09 (2)	8.2E-15 (2)	4.65E-14 (2)
w	Sorption isotherm	[kg/m³]	appendix (1)	appendix (4)	appendix (1)
ξ	Moisture capacity	[kg/m³]	appendix (1)	appendix (4)	appendix (1)
μ_{vrf}	Vapour diffusion resistance factor *	[ ]	1.5 (1)	467 (6)	7.8 (1)
δ_v	Vapour permeability *	[m²/s]	1.67E-05 (1)	5.35E-08 (6)	3.21E-06 (1)
Z_v	Vapour resistance of layer *	[s/m]	14400 (1)	224160 (6)	5616 (1)
S_d	Equivalent air layer thickness *	[m]	0.36 (1)	5.60 (6)	0.1404 (1)

Table 5.3 Sources for material properties.

Source number	Source	Material names in source
(1)	(Langmans, et al., 2011)	Fibreboard sheeting, Mineral wool
(2)	(Roels, et al., 2012)	Fibreboard 1, OSB, Mineral wool
(3)	(Fraunhofer Institut Bauphysik (IBP), 2010)	Roxul Plus
(4)	(Fraunhofer Institut Bauphysik (IBP), 2010)	Oriented Strand Board (density 615 kg/m³)
(5)	(Fraunhofer Institut Bauphysik (IBP), 2010)	Wood-Fibre Board
(6)	(Korsnes, 2013)	OSB/3 Board type 3

5.2 Numerical model assessment

5.2.1 Numerical model limitations

In the formulation of an effective and efficient HM or HAM model pertaining to building physics based problems, there must be certain simplifications of the modelled problem. These simplifications culminate in various model limitations that were initially set forth by Glaser(1958),(1959). These have since been refined, and the HM and HAM model framework utilized in this investigation has followed that which is outlined in the HAMSTAD final report (2002).

Additionally, in the evaluation of the three simulation types, further model limitations are imposed for the sake of clarity of output and/or computational simplicity. This was mostly due to time constraints but it is entirely feasible that, with more time, the simulations could be made to incorporate some of these excluded parameters.

These limitations can be sorted into three categories. Limitations set forth in the HAMSTAD report are marked with an asterisk.

Limitations on boundary condition:

- Temperature should be in the range of -30 °C to +80 °C*
- External temperature gains due to solar and sky radiation are neglected
- External pressure variations due to wind are omitted
- Internal pressure gains/losses due to HVAC equipment are not considered
- External moisture gains due to driven rain are neglected.

Transport physics considerations:

- Effects associated with the phase change, liquid to ice, are neglected*
- Sorption isotherm is temperature independent*
- No hysteresis accounted for*
- No chemical reactions are considered*
- Thermal conductivity is considered independent of moisture content
- Air density is considered independent of moisture content.
- Air permeability is considered independent of moisture content.
- Liquid transport is not considered.

Liquid transport is neglected in the wall assembly simulations as both the bitumen impregnated fibreboard and mineral wool is described as hygroscopic yet non-capillary (Roels, et al., 2012). Also the OSB/3 at the interior is never subject to a relative humidity exceeding approximately 60 % in both boundary condition cases. At these values of relative humidity liquid transport is considered negligible for OSB/3 (Orientated strand board of a density 615 kg/m^3, (Fraunhofer Institut Bauphysik (IBP), 2010))

Limits to the model geometry:

- Façade, ventilated cavity and finishing layers are not modelled.
- Ageing effects or changes in the geometrical dimensions are neglected*
- Structural timber framework is not modelled.

There is a strong possibility that if the structural timber framework were included in the wall assembly geometry (for example the top and sole plate), the framework would be of most concern regarding moisture accumulations and so mould growth potential. However, this would potentially be the case for any combination of exterior and interior sheathing materials. For this reason the timber framework geometry is not included.

5.2.2 Numerical model validity

The validity of the one dimensional HAM model as outlined in Chapter 4, gives a strong indication of the suitability of the HAM model in two dimensions, especially as liquid transport is omitted in the two dimensional model (highlighted in Chapter 5.2.1). This allows for the exclusion of the gravitational liquid transport term (term V in Equation 3.6) which could not be verified in the one dimensional HAMSTAD benchmarks.

The air mass balance equation, as outlined in Chapter 3.4, is implemented via the pre-defined 'Darcy's Law' module within COMSOL (Chapter 3.6). The validity of the Darcy Law module and the buoyancy effect is highlighted in multiple COMSOL library convection models.

The Darcy's Law module is coupled in conjunction with the custom PDE module, highlighted in Chapter 3.1, which represents the heat and moisture balance equations. The heat and moisture PDE module requires a domain velocity field to calculate heat and moisture transport through convection, while the Darcy's Law module requires a domain temperature field to take account of the buoyancy effect which drives natural convection (Tariku, 2008). As such, the two modules are fully coupled at every computational time step thus are solved simultaneously. Variable time stepping was utilized although the maximum time step was set at one hour, this was to correlate with the boundary conditions which are imposed every hour. This is deemed acceptable for common HAM model simulations (Langmans, et al., 2012).

5.3 Control case

A transient control case (denoted A in Figure 5.1) is introduced to visualise, evaluate and compare the behaviour of the HAM model for the three simulation types (denoted with 1, 2 and 3 in Figure 5.1) in two dimensions. A snapshot of a typical winter condition representative of Landvetter, Sweden is applied as a constant boundary condition at the exterior over 60 days with the exception of a drop in temperature and rise in relative humidity occurring at the 30 day mark with a duration of 1 day and a half day ramp up and ramp down period. The step change represents a brief drop in external temperature and rise in external relative humidity during the winter months. The interior temperature remains constant for the duration of the simulation while the interior relative humidity is determined from a vapour gain equation (Maier, 2012) which is tied to the relative humidity and temperature condition at the exterior (see Figure 5.7). Vapour gain is set to a maximum of 4 $g/m^3 \cdot s$ according to an internal moisture class representative of a residential building, referred to in the source as a building with low occupancy (Maier, 2012),

The step change is introduced to gauge the domains response to fluctuating boundary conditions over time. The control case is effectively a verification of the HAM model before its implementation in the climate case. Ultimately, the responsiveness of the HAM model was deemed acceptable, graphical depictions of the transient behaviour of the domain over the entire simulation time are not included in this thesis as they would be superfluous.

The step change also allows for a study on the effect of increased natural convection on moisture redistribution due to the presence of a greater driving potential. This is assessed in Appendix E where cross sectional data (cut lines) is extracted at three different heights over the domain (Figure 5.9) at 60 days (end of simulation time, close to steady state conditions) and at 31.5 days (end of step change duration, immediately before ramp down).

Here, a comparison shall be drawn between the three simulations types regarding moisture distribution and temperature. For means of effective comparison and ease of visualisation the data shall be sourced from the three cut lines outlined previously at 60 days, where the simulations have more or less reached steady state.

This data also identifies the general location within the wall domain where moisture accumulation and so mould growth potential is most critical.

5.3.1 Boundary conditions

The exterior boundary conditions are constant at 89 % relative humidity and 0 °C for 60 days with the exception of one step change occurring at 30 days where relative humidity rises to 97% and temperature drops to -10 °C. The step change conditions are constant for one day with a half day ramp up and ramp down period. The internal relative humidity, which is derived from a vapour gain equation, is approximately 35 % during the step and 48 % the remainder of the simulation time. The internal temperature is kept constant at 20°C. Heat, moisture and air flow over the top and bottom wall boundaries is set to zero.

The relative humidity and temperature conditions at the boundaries are shown in Figure 5.5 and Figure 5.6 respectively. The vapour gain profile is outlined in Figure 5.7.

The static pressure at the exterior and interior boundaries relative to the neutral pressure plane when the exterior boundary temperature is -10 °C, is shown in Figure 5.8.

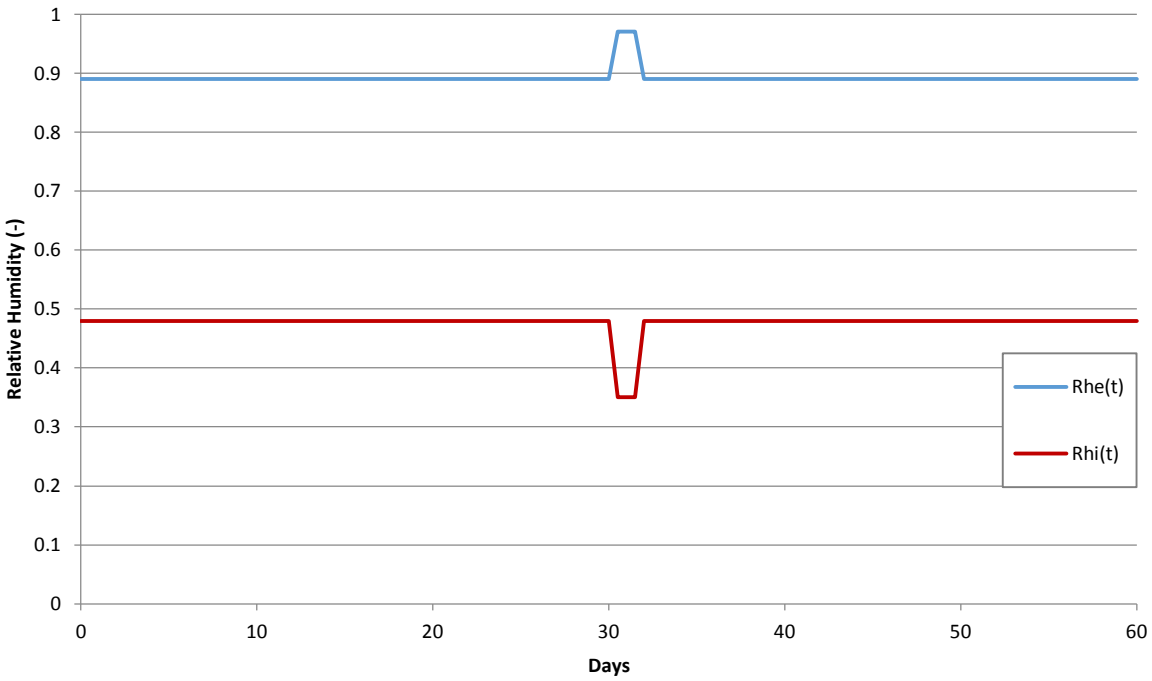

Figure 5.5 Relative humidity (-) boundary conditions for control case

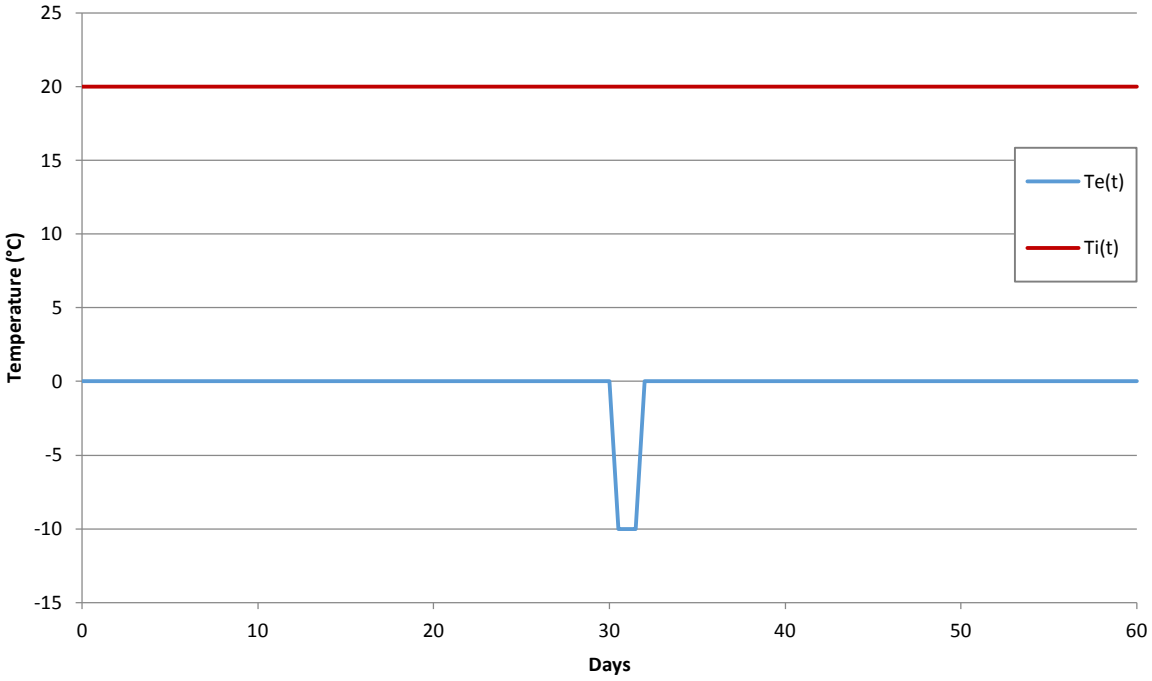

Figure 5.6 Temperature (°C) boundary conditions for control case

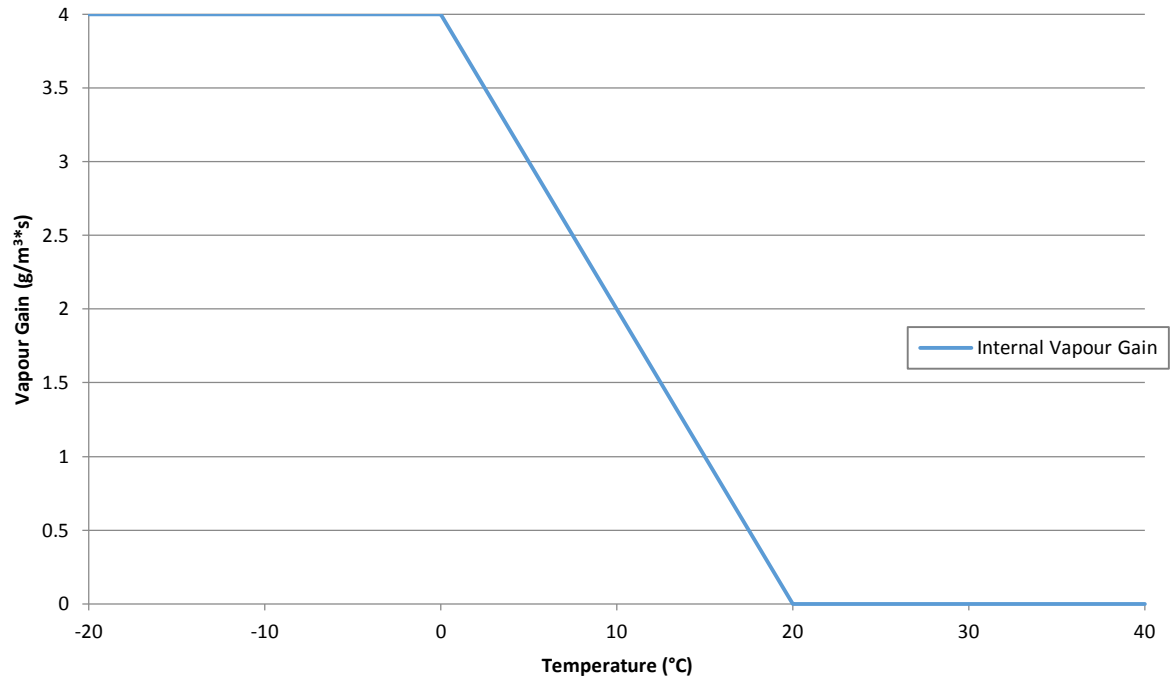

Figure 5.7 Internal vapour gain (g/m^3s) at a given external temperature

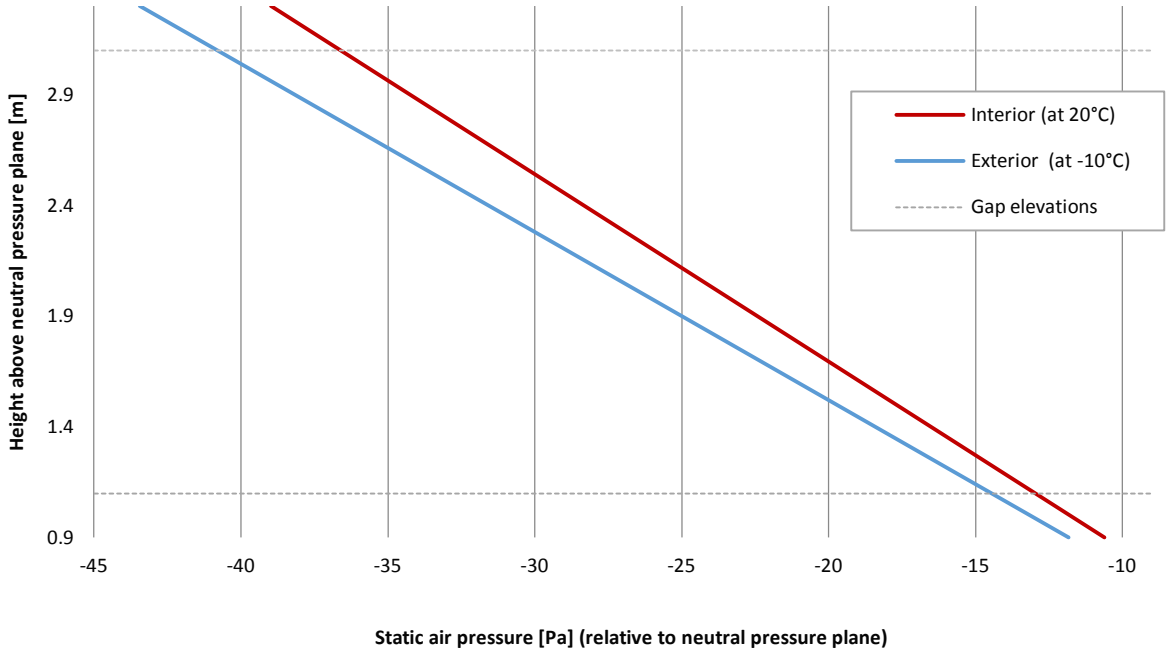

Figure 5.8 Static air pressure at interior and exterior boundaries relative to neutral pressure plane when exterior temperature is -10 °C and the interior temperature is at 20 °C.

5.3.2 Results

The cut line data displayed in Figure 5.10, Figure 5.11 and Figure 5.12 follow the line style format given in Figure 5.9 and the method of denotation given in Table 5.1, with the addition that the data presented from simulation A1 is in black, A2 is in blue and A3 is red. A1 exhibits identical cut line data at all heights therefore only cut line data from the middle of the domain is included. Note that the upper and lower cut lines pass through the centre of the gaps in the interior layer.

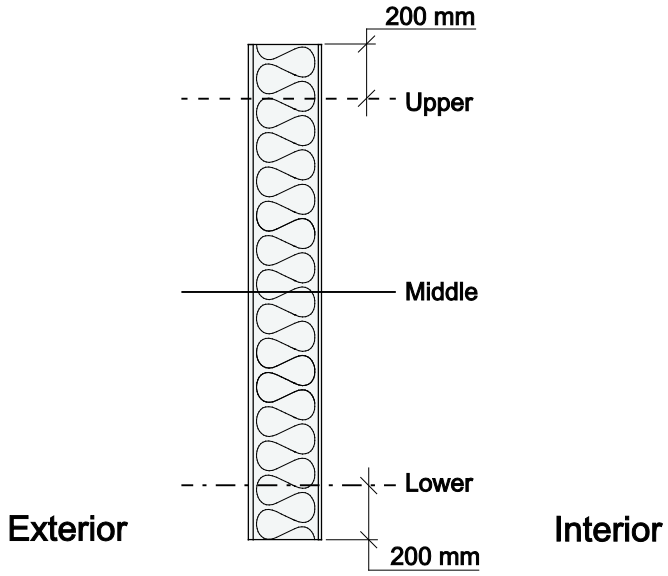

Figure 5.9 *Wall geometry cut-line locations with corresponding graphical line types. Upper (dash), Middle (solid) and Lower (long dash dot).*

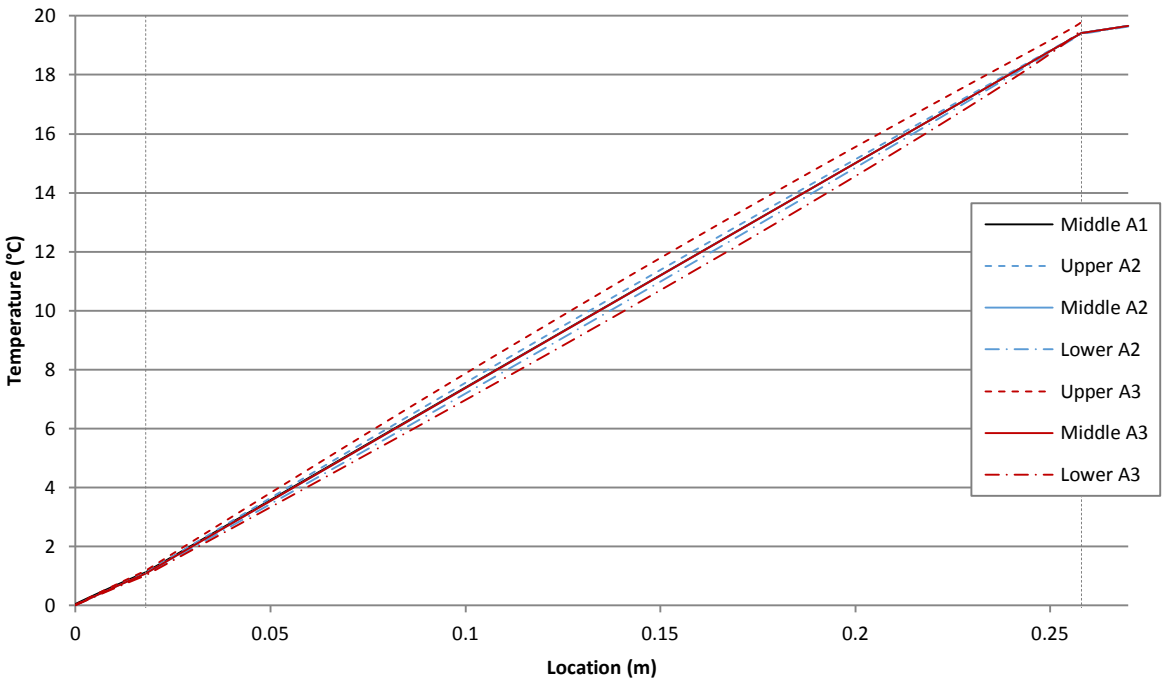

Figure 5.10 *Temperature (°C) over the wall cross section for simulations A1 (black), A2 (blue) and A3 (red) at the upper, middle and lower cut lines in the geometry.*

It can be seen in Figure 5.10 that the induction of natural convection in simulation A2 within the domain creates discrepancies in the temperature at the upper and lower sections of the wall cavity compared to A1, namely a slight increase in temperature at the upper section of the wall and a slight decrease at the lower section of the wall. This behaviour is more apparent in A3 where heat transfer due to increased natural convection (Figure 5.13) is more pronounced.

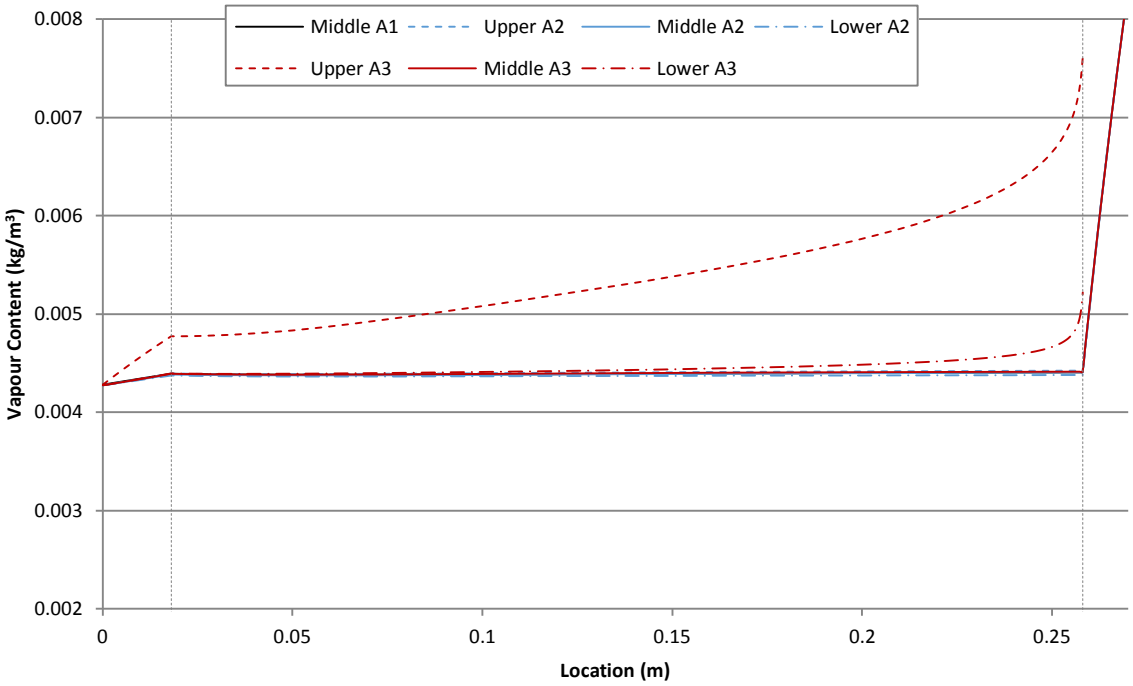

Figure 5.11 Vapour content (kg/m^3) over the wall cross section for simulation A1 (black), A2 (blue) and A3 (red) at the upper, middle and lower cut lines in the geometry.

It is seen in Figure 5.11 that vapour redistribution due to natural convection within the wall cavity is only apparent in A3 at the upper and lower cut lines where there is a gap in the OSB layer. This is due to the fact that the interior boundary condition is tied directly to the mineral wool layer.

Vapour redistribution due to convection is negligible in A2 as at any given time, and at any given point, the vapour content is virtually constant within the wall cavity and at the cavity-side surface of both sheathing layers. This is attributed to the large μ value possessed by the modelled OSB.

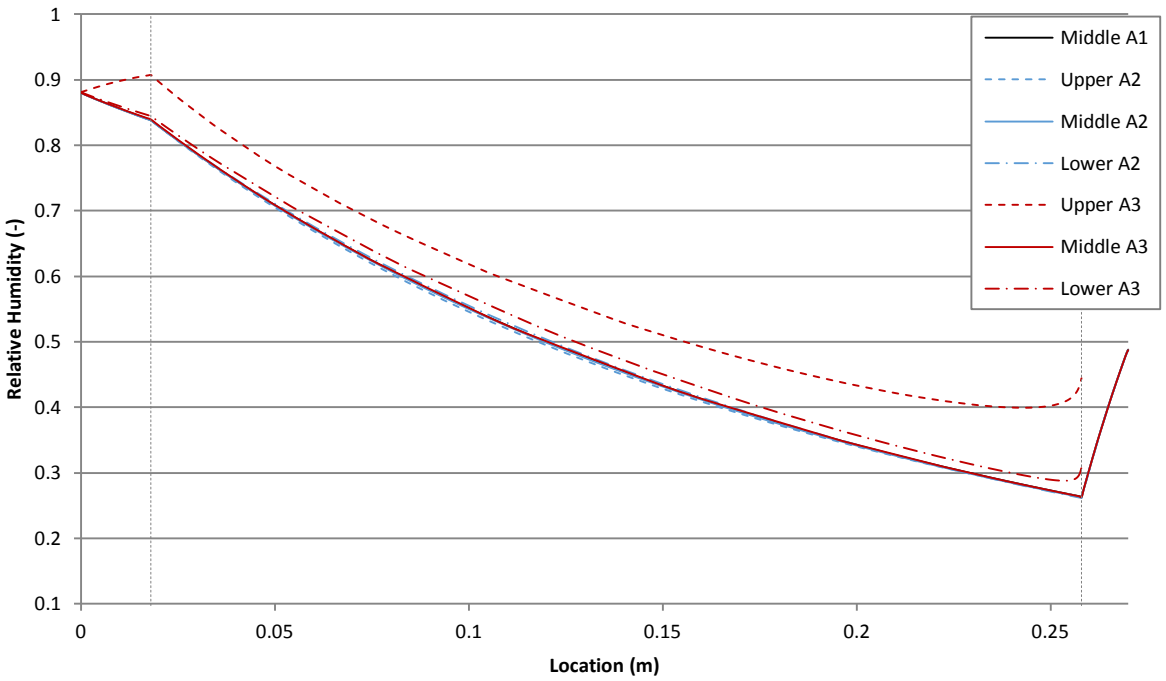

Figure 5.12 Relative humidity (-) over the wall cross section for simulation A1 (black), A2 (blue) and A3 (red) at the upper, middle and lower cut lines in the geometry.

It is noted that behind the fibreboard layer vapour content is highest at the upper cut line for A3. The effect of the increased vapour content at this point is seen in Figure 5.12 where relative humidity is highest for A3 at the upper cutline behind the fibreboard.

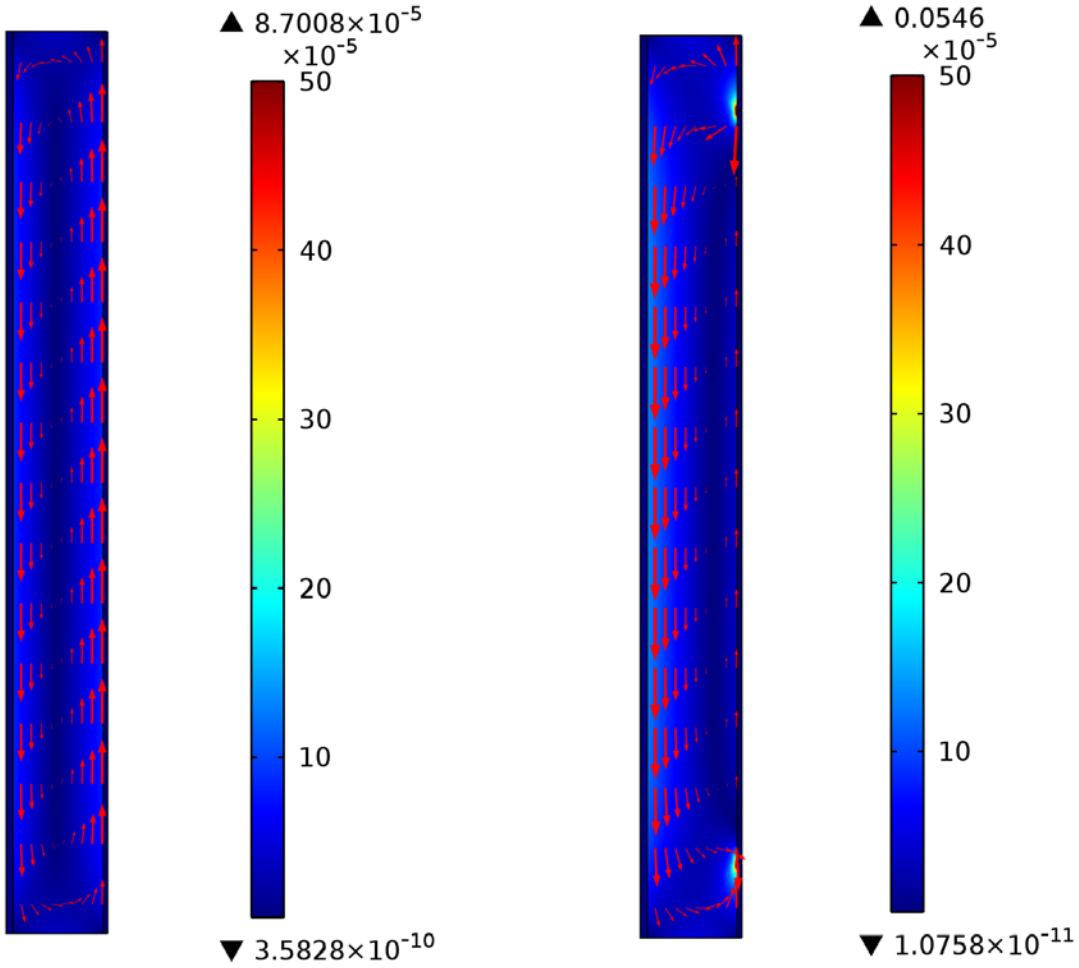

Figure 5.13 Air velocity magnitude (m/s) overlain with general air movement direction for simulations A2 (left) and A3 (right). Minimum and maximum air velocity magnitudes are shown.

Air velocity magnitude and general air movement direction (Figure 5.13) are presented here as two dimensional plots as a comparison between simulations is more intuitive when utilizing this format. Air velocity cut line data is included in chapter Appendix E.

5.3.3 Discussion

The unexpected discrepancy between the vapour content attributed to the interior boundary of the mineral wool layer at both gaps and the interior boundary condition is believed to be because of a two dimensional dispersal phenomena tied to the large difference in vapour resistance between the mineral wool and the OSB as well as the small dimension of the gaps (independent tests were carried out concerning only simple vapour diffusion models with the same results).

The discrepancy between the vapour content attributed to the interior boundary of the mineral wool *at each gap* is because the vapour diffusion flux at the upper gap is supplement by vapour transport through convection from the interior, while at the lower gap convection operates in the opposite direction, from the mineral wool layer to the interior, effectively drying the insulation at this point.

The point, just behind the exterior air barrier at the upper section of the wall with the coordinates 0.019 x 2.2 m (Figure 5.16), is deemed most pertinent in the comparison of mould growth potential between simulations when subject to realistic climatic conditions over one year.

5.4 Climate case

The climate case (denoted B in Figure 5.1) is introduced to evaluate mould growth potential for all three simulation types (denoted by 1, 2 and 3 as in Figure 5.1) when considering commonly occurring exterior and interior climatic conditions in the west of Sweden. Exterior relative humidity and temperature conditions are represented by climate data sourced from Landvetter, Sweden, over a typical reference year. The interior temperature conditions is set constant all year round while the interior relative humidity condition is calculated from an internal vapour gain equation and profile tied to the exterior conditions (see Chapter 5.3).

5.4.1 Boundary conditions

The hourly reference exterior temperature variation over one year is shown in Figure 5.14 while the hourly reference exterior relative humidity variation is shown in Figure 5.15. The hour zero represents the 1st of January.

The interior temperature is constant at a value of 20 °C for the duration of the simulation.

The vapour gain equation and profile outlined in the control case boundary conditions (Figure 5.7) is also applied in this case.

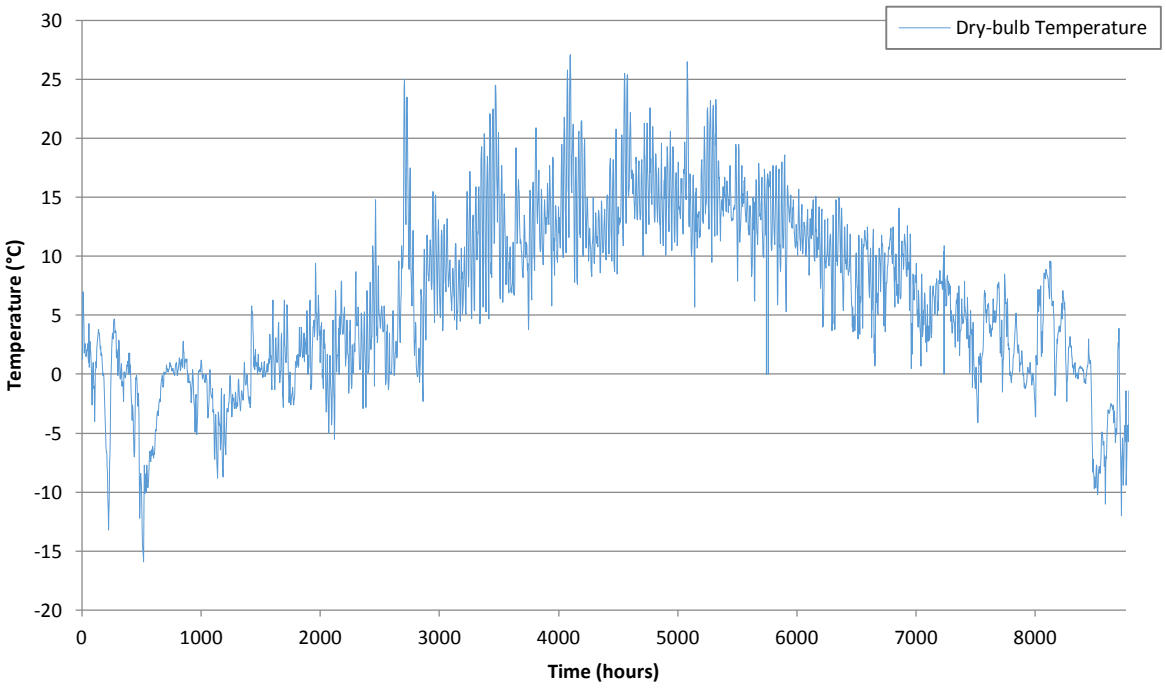

Figure 5.14 Landvetter climate data regarding the hourly variation in temperature (°C) over one year.

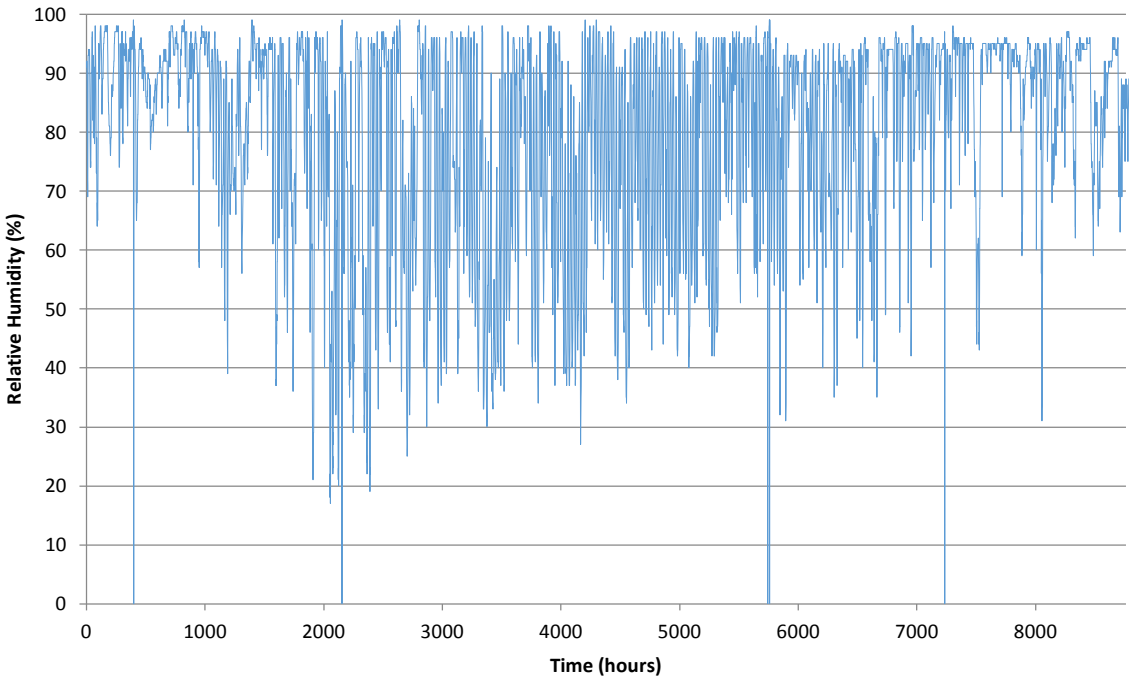

Figure 5.15 Landvetter climate data regarding the hourly variation in relative humidity (%) over one year.

5.4.2 Mould growth potential

To assess the potential risk of degradation to the light-weight timber wall assembly through mould propagation, a critical condition over which mould growth is stimulated and sustained must be established.

This critical condition is found following Johansson's et al. (2012) approximation of the critical moisture levels required in the stimulation of mould growth on selected building materials. Subsequent to the analysis and assessment of mould growth tests on various building material samples Johansson developed material-specific growth limit curves. The data for the growth limit curves was sourced from laboratory tests valid at temperatures of 10°C and 22°C at various relative humidity conditions over a 12 week period. The data was then fit to encompass a wider range of temperatures using the following set of equations:

$$RH = a + c(T^2 - 54T)\ [\%] \tag{5.1}$$

$$c = \frac{RHcr12w_1 - RHcr12w_2}{T_1^2 - T_2^2 - 54(T_1 - T_2)} \tag{5.2}$$

$$a = RHcr12w_1 - c(T_1^2 - 54T_1) \tag{5.3}$$

where T is the temperature in °C, and T_1 and T_2 refer to the tested laboratory temperature conditions, also in °C. RH_{cr12w} refers to the critical relative humidity after 12 weeks incubation.

The parameters a and c (Equations 5.3 and 5.2 respectively) are found using the material-specific RH_{cr12w} data and corresponding test temperature. This data is shown for all materials tested, in Table 5.4.

Table 5.4 Range in which critical moisture level is expected, based on results from 12 weeks incubation. Results are based on both median mould growth (criterion (a)) and Kaplan-Meier estimation (criterion (b)) (Johansson, et al., 2012).

Material	Temperature	
	22°C	10°C
Pine sapwood	$75<RH_{cr12w}\leq 79$	$85<RH_{cr12w}\leq 90$
Plywood	$75<RH_{cr12w}\leq 79$	$75<RH_{cr12w}\leq 85^{*(1)}$
Chipboard	$79<RH_{cr12w}\leq 85$	$90<RH_{cr12w}\leq 93$
Thin hardboard	$85<RH_{cr12w}\leq 89$	$93<RH_{cr12w}\leq 95^{*(2)}$
Wet-room gypsum plaster board	$89<RH_{cr12w}\leq 95$	$95<RH_{cr12w}$
Exterior gypsum plaster board	$89<RH_{cr12w}\leq 95$	$95<RH_{cr12w}$
Asphalt paper	$89<RH_{cr12w}\leq 95$	$95<RH_{cr12w}$
Cement-based board	$95<RH_{cr12w}$	$95<RH_{cr12w}$
Glass fibre	$95<RH_{cr12w}$	$95<RH_{cr12w}$
Expanded polystyrene	$95<RH_{cr12w}$	$95<RH_{cr12w}$

* This is based on the criterion (b). When using the criterion (a) concerning median rating ≥2, the result was (1) $85<RH_{cr12w}\leq 90$ (2) $95<RH_{cr12w}$.

The tested materials in the report were limited to those give in the table above, however, asphalt impregnated cellulose paper was considered significantly similar to bituminous fibreboard in composition that relevant results could be drawn for the latter from the growth limit curve of the former.

One upper bound growth limit curve and one lower bound growth limit curve exists for many of the materials tested. The 'true' critical moisture condition in terms of the stimulation of mould growth, for a given material may lie at any point between the two, or above the former.

For means of comparison with regard to mould growth potential the lower bound growth limit curve is included in the following results section, the upper bound growth curve is omitted.

As mentioned previously, mould growth potential is only considered for the external bituminous fibreboard sheathing. No allowances have been made for the presence of internal timber studs even though these may be the most critical wall assembly elements regarding the potential for mould growth. For example, it can be seen in Table 5.4 that the critical relative humidity pertaining to pine is lower than that of asphalt impregnated paper.

5.4.3 Results

As previously stated the evaluation point chosen for the comparison of the simulations is point 0.019 x 2.2 m, as seen in Figure 5.16, where moisture accumulation seems most pronounced. Simulation B1 is omitted as it is not relevant in the comparison.

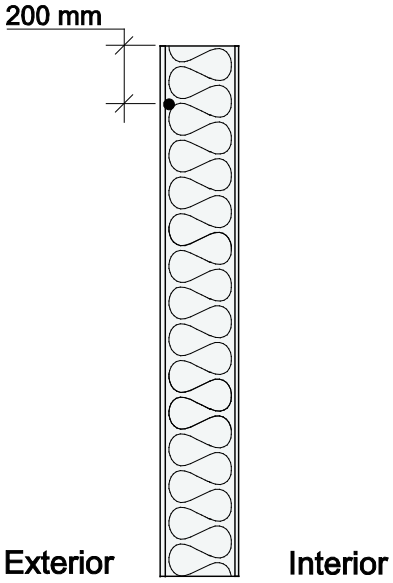

Figure 5.16 Location of evaluation point for data output in climate case (0.019 x 2.2 m).

It should be noted that the temperature profiles at point 0.019 x 2.2 m over the full year were almost identical for both simulations B2 and B3, as such, this was not represented graphically. The critical relative humidity value for the position in question is then representative for both simulation B2 and B3.

Figure 5.17 that B3 exhibits greater values of relative humidity in the winter months than B2 (up to 10% in some instances) while towards the summer months the two simulations become almost indistinguishable. This is further emphasized in Figure 5.18 where comparatively large relative humidity discrepancies between the two simulations are found at low temperatures (between 0 °C and -10 °C) while the two simulations exhibit very similar relative humidity values at temperatures above 10 °C.

The discrepancy in relative humidity values between B2 and B3 at temperatures below 10°C (Figure 5.18) is because during the winter months the driving potential for convection, and so moisture transfer from the interior into the wall cavity, is at its strongest. Additionally the vapour gain at the interior is also at a maximum during the winter months. In the summer where exterior and interior temperatures converge at around 20 °C, both of these factors are diminished leading to similar relative humidity values for both B2 and B3.

This convergence of relative humidity values for both simulations in the summer months also coincides with the lowest, and in this case, most pertinent critical relative humidity values. While during the winter when B3 shows noticeably higher values of relative humidity, the mould growth potential of the material is not significant as the temperature is too low to stimulate any kind of growth.

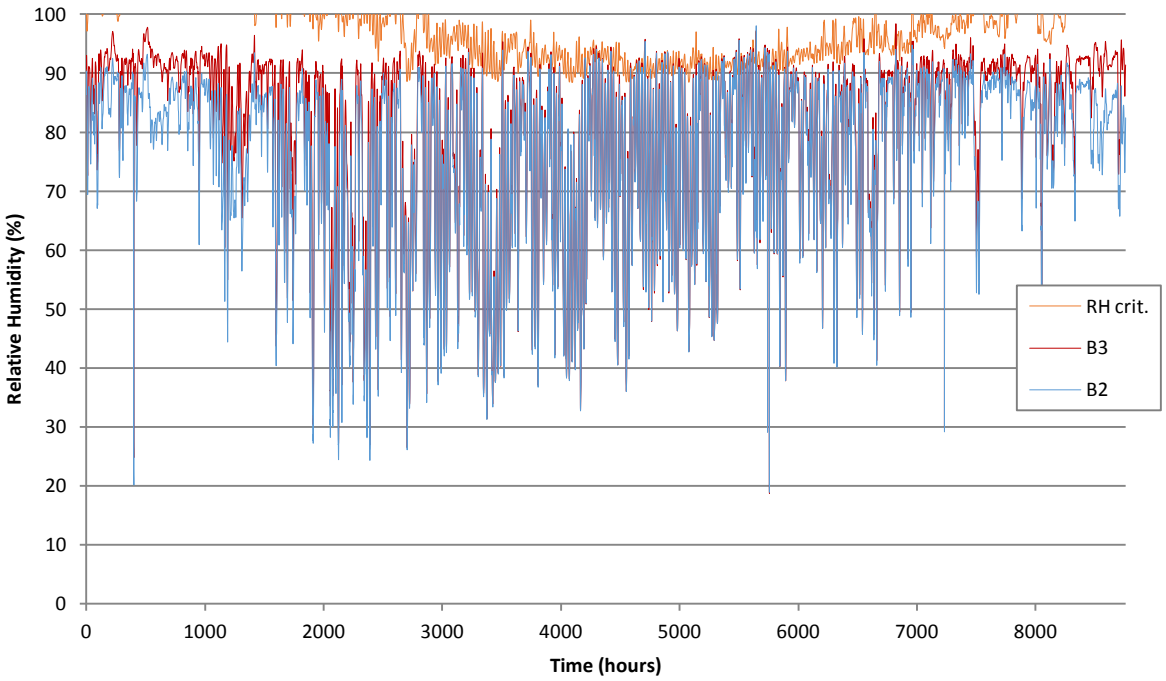

Figure 5.17 *Relative humidity exhibited at point 0.019 x 2.2 m for simulation B2 (blue) and B3 (red) over 8760 hours (365 days). This is plotted with the lower bound critical relative humidity condition for mould growth on asphalt impregnated paper at the corresponding temperature.*

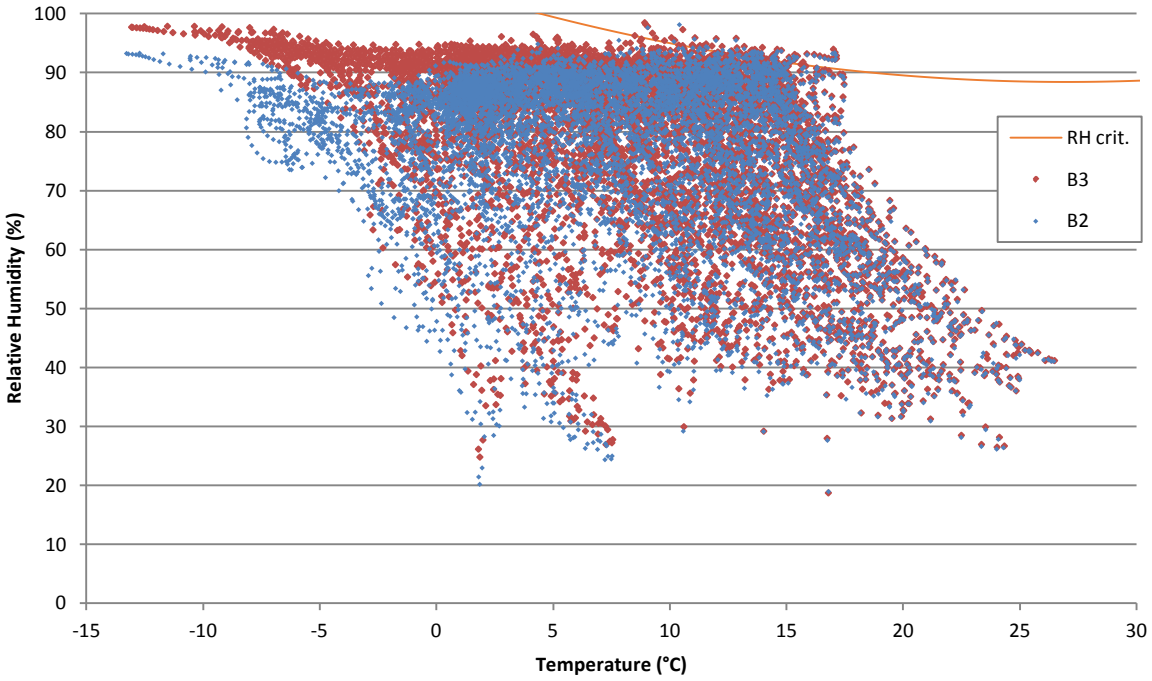

Figure 5.18 *Relative humidity exhibited at point 0.019 x 2.2 m for simulation B2 (blue) and B3 (red) over 8760 hours (365 days) at the corresponding temperature. This is plotted with the lower bound critical relative humidity condition for mould growth on asphalt impregnated paper at the corresponding temperature.*

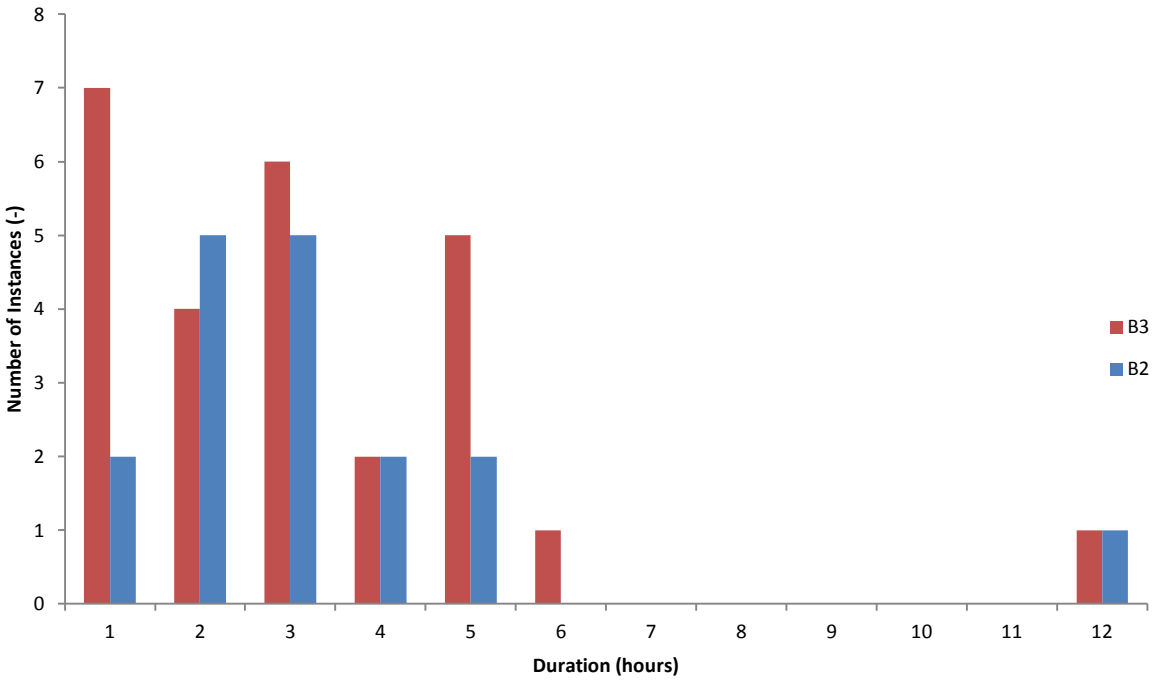

Figure 5.19 Instances of consecutive hours above critical relative humidity condition for asphalt impregnated paper at the corresponding temperature at point 0.019 x 2.2 m for simulation B2 (blue) and B3 (red).

The number of instances each simulation exceeds the critical relative humidity value, along with the duration of each instance, is shown in Figure 5.19. On average it can be seen that B3 exhibits a greater tendency to exceed the critical relative humidity value, and often for a greater period of time. It can then be said that B3 present conditions with the highest potential for mould growth in comparison with B2.

Again it is noted that Figure 5.19 is utilized mainly for a means of comparison between simulation B2 and B3. It presents only an approximation of mould growth potential. The significance of this limited time spent in conditions optimal for mould growth when considering the duration of the full year is an important consideration.

6 Conclusion

A two dimensional numerical HAM model was constructed and verified in COMSOL Multiphysics to evaluate the mould growth potential of a light-weight timber wall system where the air barrier is located at the exterior and an unsealed vapour retarder at the interior. The test simulation wall is subject to climate conditions representative of the Gothenburg region of Sweden over one year. The light-weight timber wall system assessed is comprised of bituminous impregnated soft fibreboard with a treated exterior surface as the exterior air barrier, mineral wool as the cavity insulation and orientated strand board type 3 (OSB/3) as the interior vapour retarder. To quantify the results a second identical reference simulation is assessed but where the internal vapour retarder is sealed.

An unsealed interior vapour retarder is simulated by introducing two gaps of 1 mm in the interior vapour retarder layer geometry at 200 mm from the top and bottom of the wall. An analytical model representing a gap airflow is then applied to the gap boundaries. A sealed interior vapour retarder is modelled as a continuous material layer with no gaps in the layer geometry.

It was concluded that HAM transport mechanisms within the scope of building physics related problems can be accurately modelled in both one and two dimensions using the COMSOL Multiphysics software.

It was found that natural convection plays a role in moisture redistribution within light-weight timber framed wall assemblies. With regard to the previously outlined investigation limitations and simulation types, moisture accumulation due to natural convection over the full year is most pronounced in the upper section of the wall cavity immediately behind the exterior air barrier when the interior vapour retarder is unsealed (gaps present) in comparison to where it is sealed (no gaps). The discrepancy in moisture accumulation at this point is only evident during the winter months when the interior moisture load is highest and driving potential for air convection is strongest. In the summer months both of these factors are diminished and so relative humidity values exhibited in both cases are almost identical.

Therefore, the difference in mould growth potential between walls possessing an unsealed interior vapour retarder (gaps present) and a sealed interior vapour retarder (no gaps) is not considered significant in this case. This is because the critical relatively humidity value is only exceeded in the summer months when relative humidity values exhibited in both simulated wall geometries are almost identical. Where there is a discrepancy in relative humidity values, during the winter, the critical relative humidity value is not applicable as exterior temperatures are sufficiently low to prevent any mould growth regardless of the relative humidity value. Hence, in this case, there is no significant reduction in the risk of mould growth and associated degradation if the internal vapour retarder is sealed (no gaps) than if it is left unsealed (gaps present).

7 Recommendations

This study may be supplemented to incorporate many different exterior/interior climatic conditions, materials properties and wall geometries in two dimensions to increase the scope and reliability of the data set.

Depending on material properties, moisture transfer through liquid transport may also be included in the numerical HAM model.

Intuitively, the next stage in the development of the study would be to model wall assemblies in three dimensions to study the lateral hygrothermal performance of the wall, especially concerning the influence of the walls structural components.

Beyond that, the entire three dimensional light-weight timber framed envelope may be modelled to accurately locate the areas within such a building which are most critical in terms of moisture accumulation and so mould growth.

8 References

Bankvall, C., 2013. *Luftboken.* 1 red. Lund: Studentlitteratur AB.

Blom, P. & Uvsløkk, S., 2012. *Bygg tett – og ventiler rett!*, OSLO: SINTEF Byggforsk.

Boverket, 2009. *The health of our houses - Report on the Swedish governments commissions regarding the technical standard of Swedish buildings,* Karlskrona: The Swedish National Board of Housing, Building and Planning.

Braathen, O. M., 2010. *Hunton Fiber - Racking strengths and stiffness of soft fibreboards impregnated with bitumen,* Trondheim: SINTEF.

COMSOL AB, 2013. *COMSOL Multiphysics 4.3b, User Manual*, Stockholm: COMSOL.

Fraunhofer Institut Bauphysik (IBP), 2010. *Fraunhofer material database as depicted in WUFI 2D Version 3.3,* Holzkirchen: Fraunhofer Institut Bauphysik (IBP).

Glaser, H., 1958. Waermeleitung und Feuchtigkeitsdurchgang durch Kuehlraumisolierungen. *Kaltetecknik,* Volym 3, pp. 86 - 91.

Glaser, H., 1959. Graphisches Verfuhren zur Untersuchung von Diffusionsvorgangen. *Kaltetecknik,* Volym 11, pp. 345 - 355.

Hagentoft, C.-E., 2001. *Introduction to Building Physics.* 1:4 red. Lund: Studentlitteratur AB.

HAMSTAD Group, 2002. *Determination of liquid water transfer properties of porous building materials and development of numerical assessment methods,* Göteborg: Chalmers Univesity of Technology.

Hansen, E. J. d. P., 2010. Timber-Frame Walls: Feasible with a Damaged Vapour Barrier. *ASHRAE,* Issue Buildings XI.

Holme, J., 2008. *Mould growth on board-based wind barrier products*, Trondheim: SINTEF.

Holøs, S. & Relander, T.-O., 2010. *Airtightness Measurements of Wood Frame Low Energy Row Houses, BEST2 Conference proceedings.* Portland, National Institute of Building Sciences.

Janssens, A., 1998. *Reliable Control of Interstitial Condensation in Lightweight Roof Systems.* Leuven: Katholieke Universiteit Leuven.

Johansson, P., Ekstrand-Tobin, A. & Svensson, T., 2012. *Mould growth on building materials under different climatic conditions: determining the critical moisture level,* Lund: Lund University.

Jokisalo, J. & Kurnitski, J., 2002. *Simulation of Energy Consumption in a Typical Finnish Detached House,* Espoo: Helsinki University of Technology.

Kalamees, T. & Kurnitski, J., 2009. *Moisture convection performance of wall and attic floor joint,* Helsinki: Helsinki University of Technology.

Karagiozis, A., 2002. *Building enclosure hygrothermal performance study phase 1,* Oak Ridge: Oak Ridge National Laboratory.

Korsnes, S., 2013. *Moisture risk in prefabricated wooden wall elements (TES-elements) with a vapour retarder of OSB/3.* Göteborg, Passivhus Norden 2013.

Kronvall, J., 1980. *Air Flows in Building Components.* Lund: Lund Institute of Technology.

Langmans, J., Klein, R., De Paepe, M. & Roels, S., 2010. Potential of wind barriers to assure airtightness of wood-frame low energy constructions. *Energy and Buildings,* Issue 42, pp. 2376 - 2385.

Langmans, J., Nicolai, A., Klein, R. & Roels, S., 2012. A Quasi-Steady State Implementation of Air Convection in a Transient Heat and Moisture Building Componentn Model. *Building and Environment,* Issue 58, pp. 201-218.

Langmans, J., Roels, S. & Desta, T. Z., 2011. Experimental data set for validation of heat, air and moisture transport models of building envelopes. *Building and Environment,* Issue 46, pp. 1038-1046.

Maier, T., 2012. *ISO 13788: Hygrothermal calculation procedure of building components (internal surface temperature to avoid critical surface humidity and interstitial condensation),* Munich: European Building Codes.

Mattsson, B., 2004. *Luftläckage i bostäder - litteraturstudier, modellering och mätningar,* Göteborg: Chalmers.

Nield, D. & Bejan, A., 2006. *Convection in Porous Media.* Third red. New York: Springer Science+Business Media, Inc..

Ojanen, T. & Ahonen, J., 2005. *Moisture performance properties of exterior sheathing products made of spruce plywood or OSB,* Espoo: VTT working papers 22.

Quirouette, R., 1985. *The Difference Between a Vapour Barrier and an Air Barrier,* Ottawa: National Research Council Canada.

Relander, T.-O., 2011. *Airtightness of wood-frame houses,* Trondheim: Norwegian University of Science and Technology.

Relander, T.-O., Holos, S. & Thue, J. V., 2011. *Airtigtness estimation - a state of the art review and an en route upper limit evaluation principle to increase the chances that wood-frame houses with a vapour and wind barrier comply with the airtightness requirements,* Trondheim: Norwegian University of Science and Technology.

Roels, S., Langmans, J. & Klein, R., 2012. Hygrothermal risks of using exterior air barrier systems for highly insulated light weight walls: A laboratory investigation. *Building and Environment,* Issue 56, pp. 192-202.

Sandberg, P. I. & Sikander, E., 2004. *Lufttäthetsfrågorna i byggprocessen-Kunskapsinventering, laboratoriemätningar och simuleringar för att kartlägga behov av tekniska lösningar och utbildning,* Borås: SP Sveriges Provnings- och Forskningsinstitut.

Sasic Kalagasidis, A., 2004. *HAM-Tools, An Integrated Simulation Tool for Heat, Air an Moisture Transfer Analyses in Building Physics.* Göteborg: Chalmers Univeristy of Technology.

Sikander, E. & Olsson Jonsson, A., 1997. *Lufttäthet i hus med träregelstomme och utan plastfolie,* Borås: SP Sveriges Provnings- och Forskningsinstitut.

Solvang, M. & Handal Bjelland, A. S., 2011. *Tett Bygg - Lufttetthet i norske nybygg,* Akershus: Universitetet for miljø- og biovitenskap.

Tariku, F., 2008. *Whole Building Heat and Moisture Analysis.* Montreal, Quebec, Canada: Concordia University.

Tariku, F. & Ge, H., 2010. Modeling of Hygrothermal Responses of a Sheating Board in a Prefabricated Wall System and Comparison with Experimental Result.

Tariku, F., Kumaran, K. & Fazio, P., 2009. Transient model for coupled het, air and moisture transfer throgh mulitilayered porous media. *International Journal of Heat and Mass Transfer.*

van Schijndel, J., 2007. *Integrated Heat Air and Moisture Modeling and Simulation.* Eindhoven: Technische Universiteit Eindhoven.

Wahlgren, P., 2010. *Goda exempel på lufttäta konstruktionslösningar,* Borås: SP Technical Research Institute of Sweden.

Wahlgren, P. & Sikander, E., 2010. Methods and Materials for an Airtight Building. *ASHRAE,* Issue Buildings XI.

Williams Portal, N. L., 2011. *Evaluation of Heat and Moisture Induced Stress and Strain of Historic Building Materials and Artefacts.* Göteborg: Chalmers University of Technology.

Zou, Y., 2010. *Classification of buildings with regard to airtighness,* Göteborg: Chalmers University of Technology.

Appendix A - Benchmark 2

Benchmark 2 is a 1D, HM numerical model verification tool initiated by the Israel Insitute of Technology (Technion) for the HAMSTAD project. This benchmark provides an analytical solution which implicitly demonstrations the validility of the tested model.

In this benchmark a homogenous layer is analysed under isothermal conditions. The geometry of the layer is shown in Figure A.1.

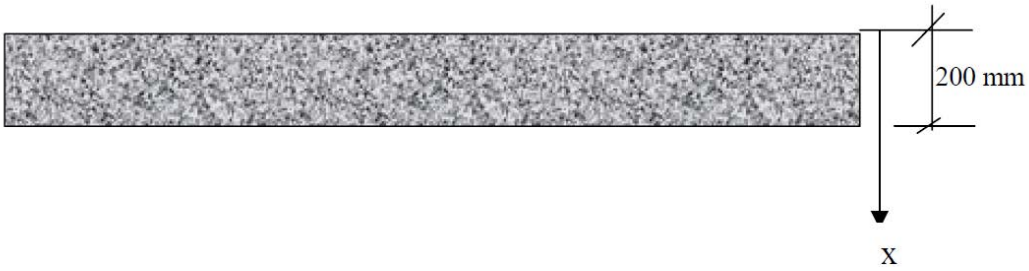

Figure A.1 Geometry of homogenous layer in HAMSTAD benchmark 2, exterior (top side), interior (bottom side).

The layer is considered in a steady-state condition with both boundaries (interior and exterior) exhibiting constant and equal relative humidity values of 95%. This is until at a time zero where there is a step change in relative humidity values at each boundary, to 65% on the interior and 45% on the exterior. Effectively this represents the 'drying-out' of the layer as moisture is re-distributed and released to the interior and exterior. The duration of the simulation, a temperature of 20°C is found constant at both boundaries. Heat and moisture transport mechanisms with respect to air movements are neglected.

Global parameters and material properties

The global parameters applicable to this benchmark are identical to those outlined for benchmark 3 (chapter 4.2.2). The material properties of the layer are represented by numerous equations which are implemented in the numerical model.

Sorption isotherm.

$$w = \frac{116}{\left(1 - \frac{1}{0.118} \cdot \ln(\phi)\right)^{0.869}} \ (\mathrm{kg/m^3}) \tag{0.1}$$

$$\phi = \exp\left(0.118 \cdot \left(1 - \left(\frac{116}{w}\right)^{\frac{1}{0.869}}\right)\right) \ (-) \tag{0.2}$$

Vapour diffusion.

$$\delta_p = 1.0 \cdot 10^{-15} \text{ (s)}$$

Moisture diffusivity.

$$D_w = 6.0 \cdot 10^{-15} \text{ (s)}$$

$$D_w = -K \frac{\partial P_{suc}}{\partial w} + \delta_p p_s \frac{1}{\xi} \tag{0.3}$$

$$\frac{\partial P_{suc}}{\partial w} = -\frac{RT\rho_w}{M_w} \frac{1}{\phi\xi} \tag{0.4}$$

Thermal conductivity.

$$\lambda = 0.15 \text{ (W/(m·K))}$$

Specific heat capacity.

$$c_p = 800 \text{ (J/kg·K)}$$

Density.

$$\rho_0 = 525 \text{ (kg/m}^3\text{)}$$

Boundary and initial conditions

Exterior boundary conditions.

$$RH_{ext} = 45\% \text{ , } T_{ext} = 20℃ \text{ at } t > 0$$
$$\alpha_{ext} = 25 \text{ (W/m}^2\text{·K) , } \beta_{ext} = 1.0 \cdot 10^{-3} \text{ (s/m)}$$

Interior boundary conditions.

$$RH_{int} = 65\% \text{ , } T_{int} = 20℃ \text{ at } t > 0$$
$$\alpha_{int} = 25 \text{ (W/m}^2\text{·K) , } \beta_{int} = 1.0 \cdot 10^{-3} \text{ (s/m)}$$

Initial conditions.

$$RH = 95\% \text{ , } T = 20℃$$

Output requirements

The simulation time for the benchmark is 1,000 hours. Moisture content, $w(x)$, is output at three time steps (100, 300 and 1000 hours) for numerous x-coordinates to form a representative cross section of the layer.

Results

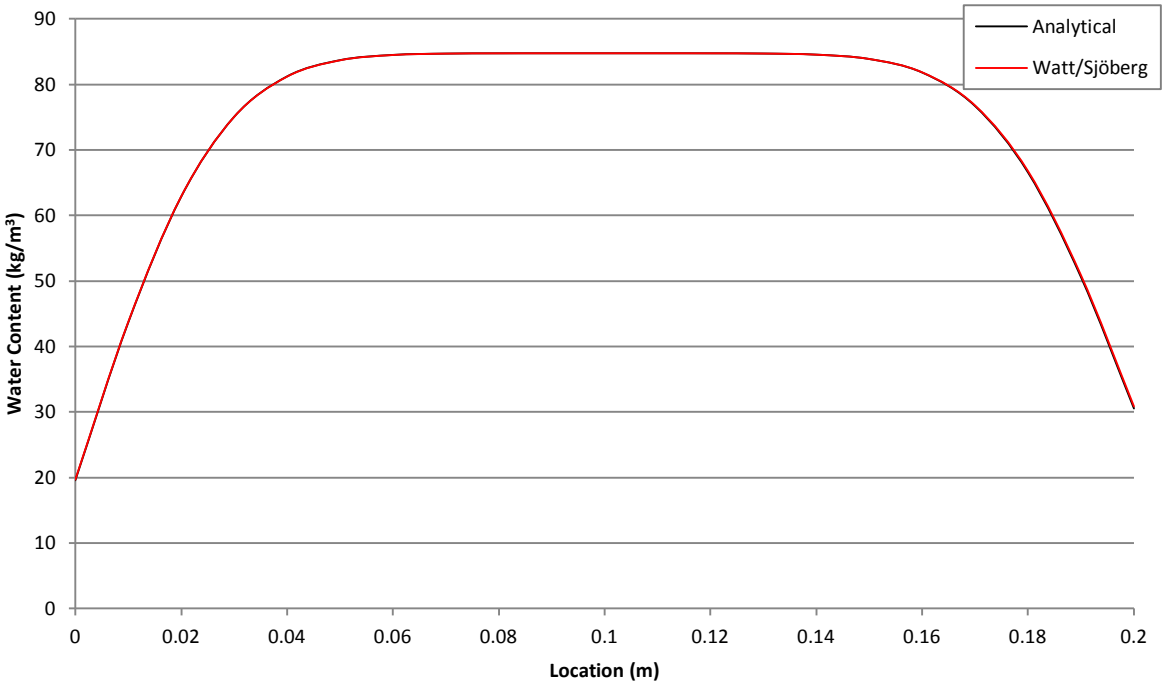

Figure A.2 Benchmark 2: Moisture content over material cross section at 100 hours.

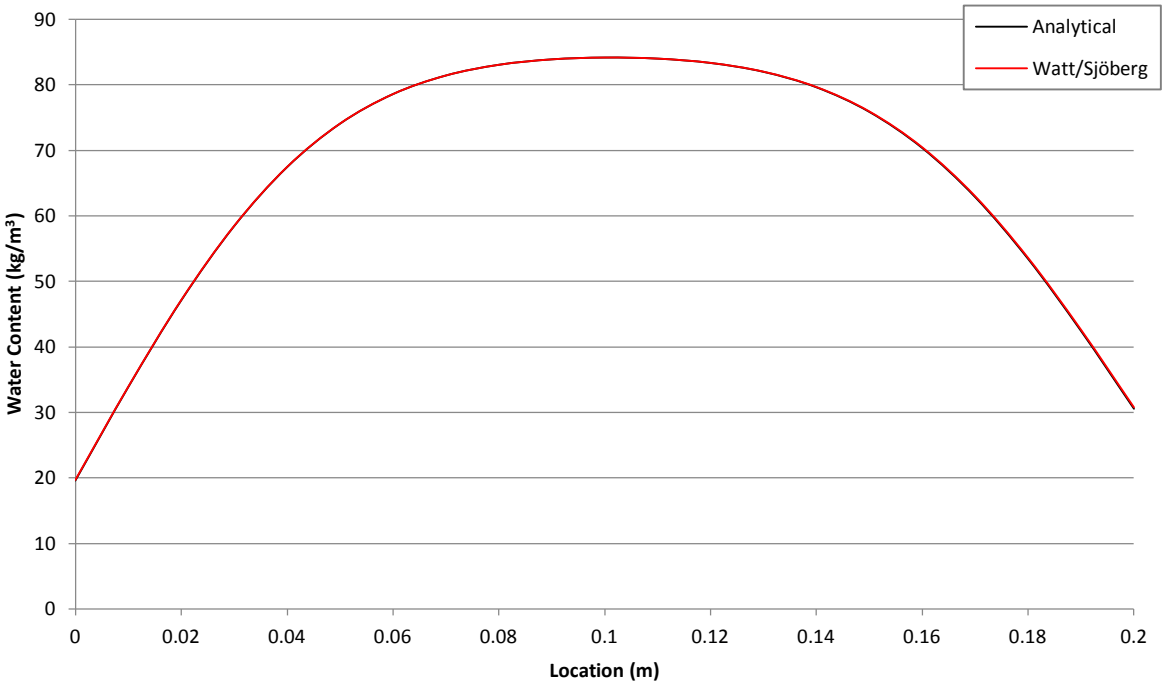

Figure A.3 Benchmark 2: Moisture content over material cross section at 300 hours.

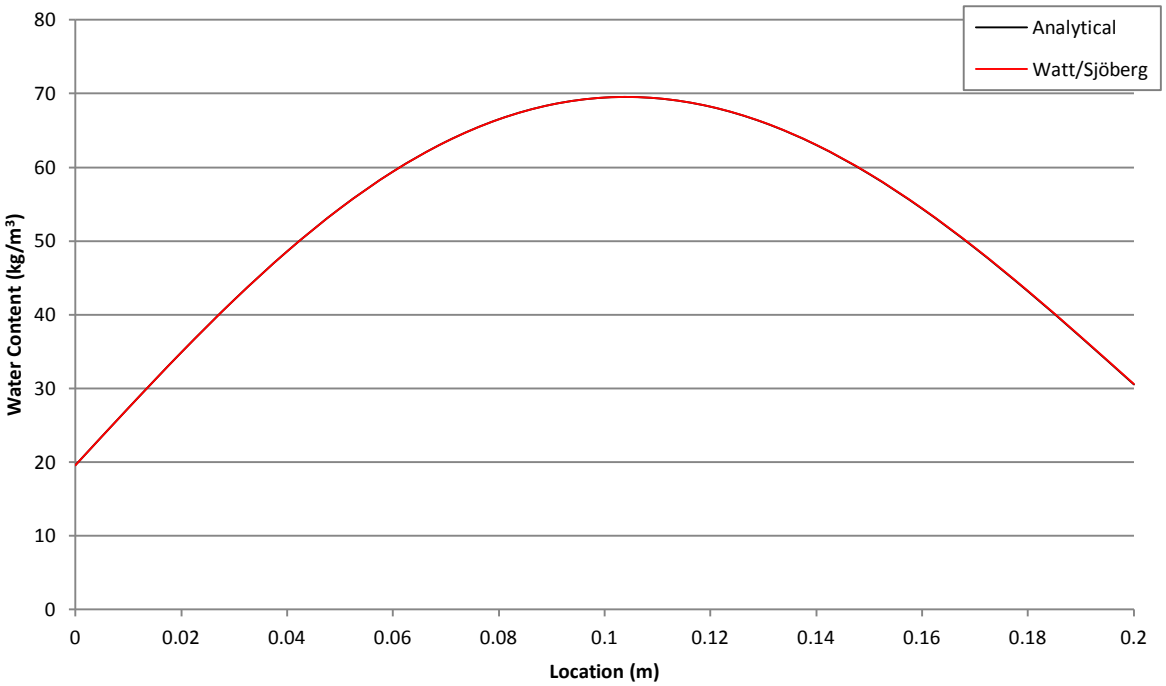

Figure A.4 Benchmark 2: Moisture content over material cross section at 1000 hours.

Appendix B - Benchmark 3

Extended results

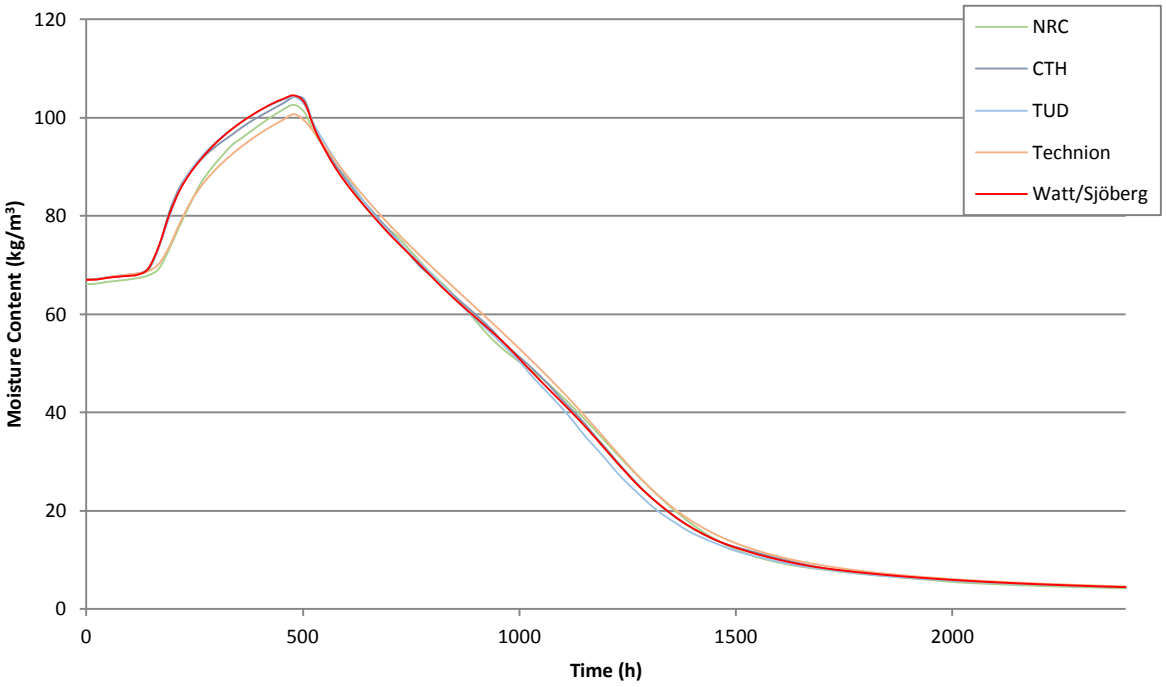

Figure B.1 Benchmark 3: Moisture content at x = 0.05 m over 100 days.

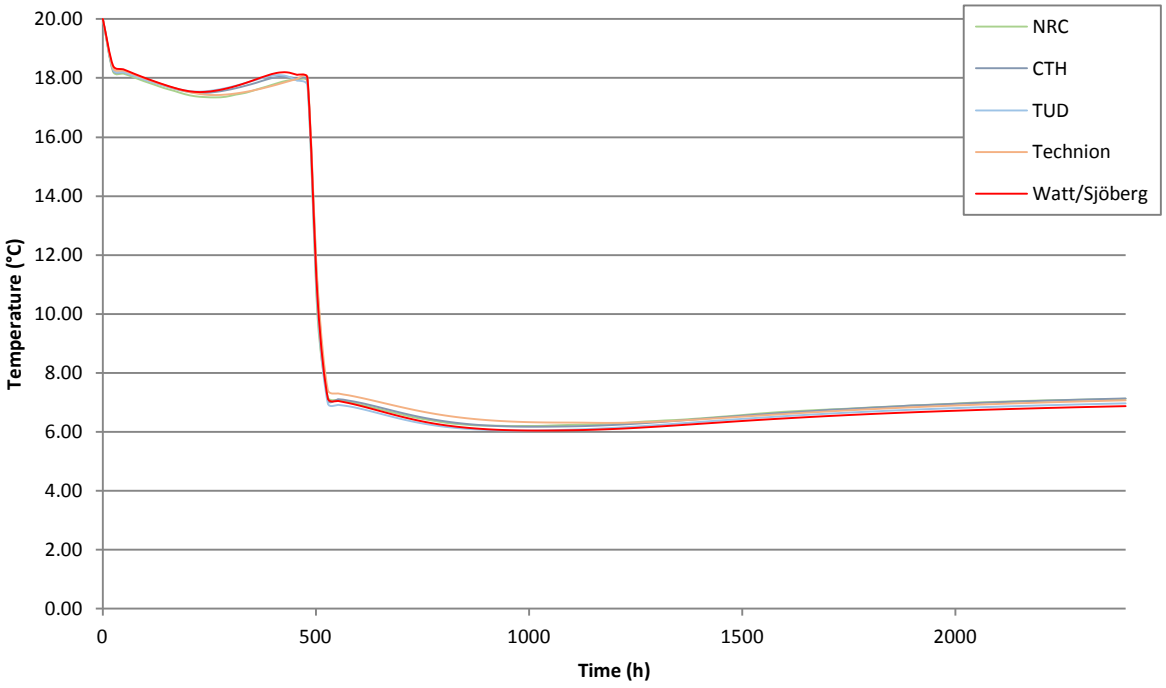

Figure B.2 Benchmark 3: Temperature at x = 0.05 m over 100 days.

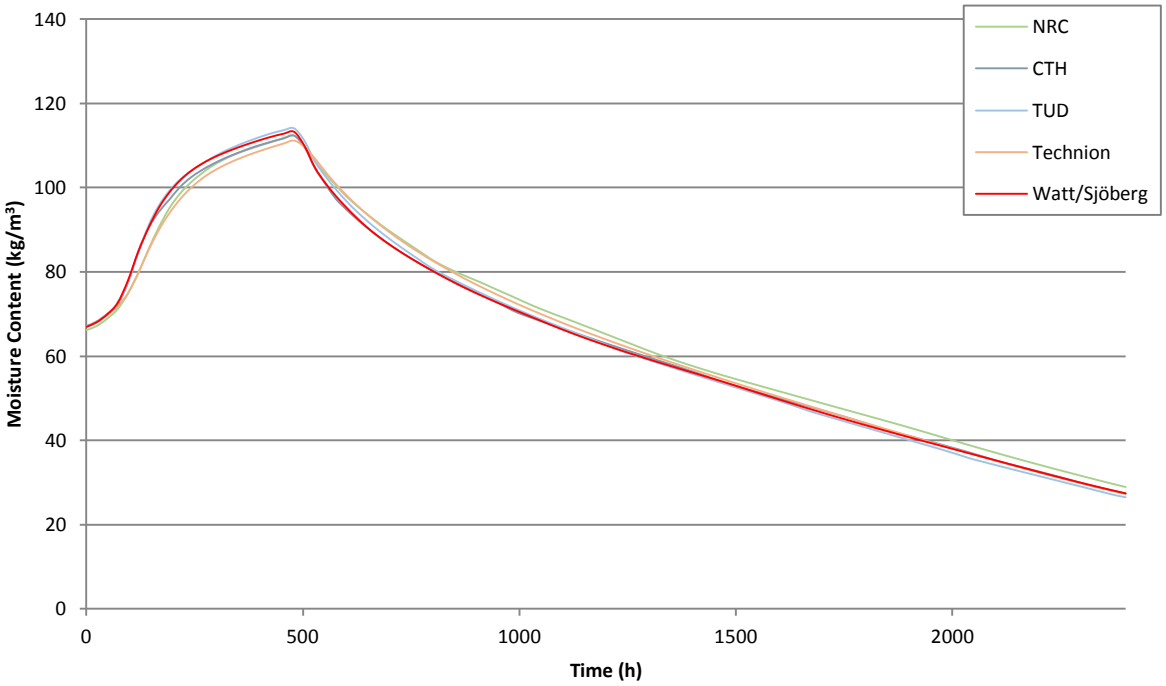

Figure B.3 Benchmark 3: Moisture content at x = 0.1 m over 100 days.

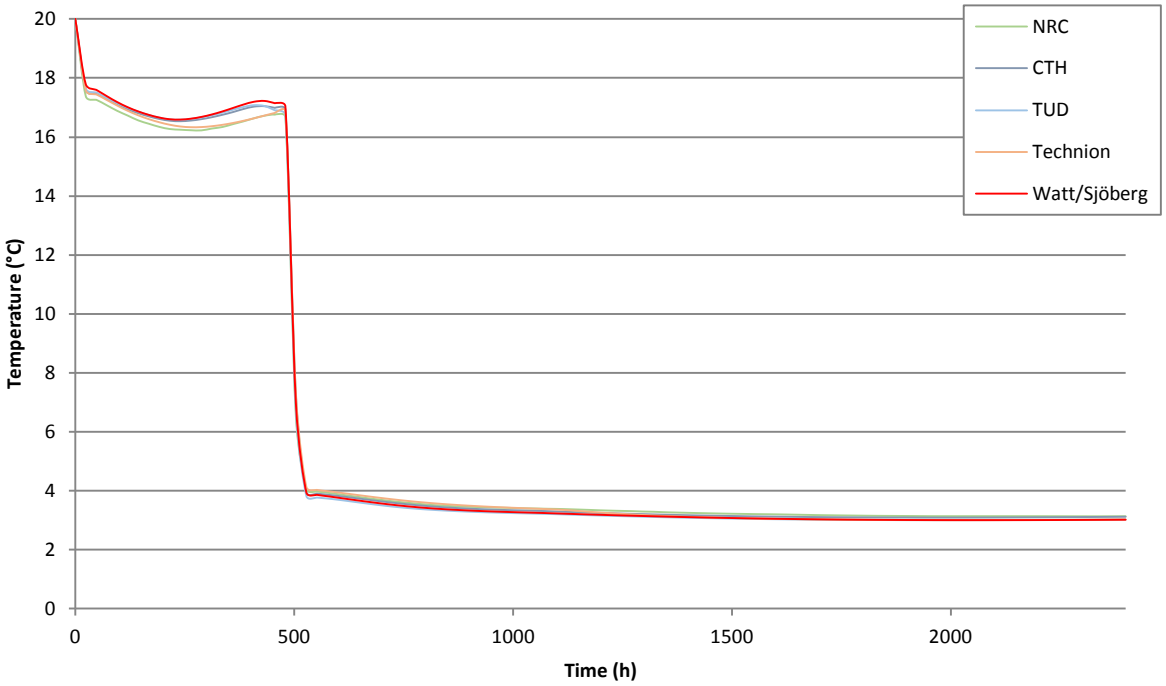

Figure B.4 Benchmark 3: Temperature at x = 0.1 m over 100 days.

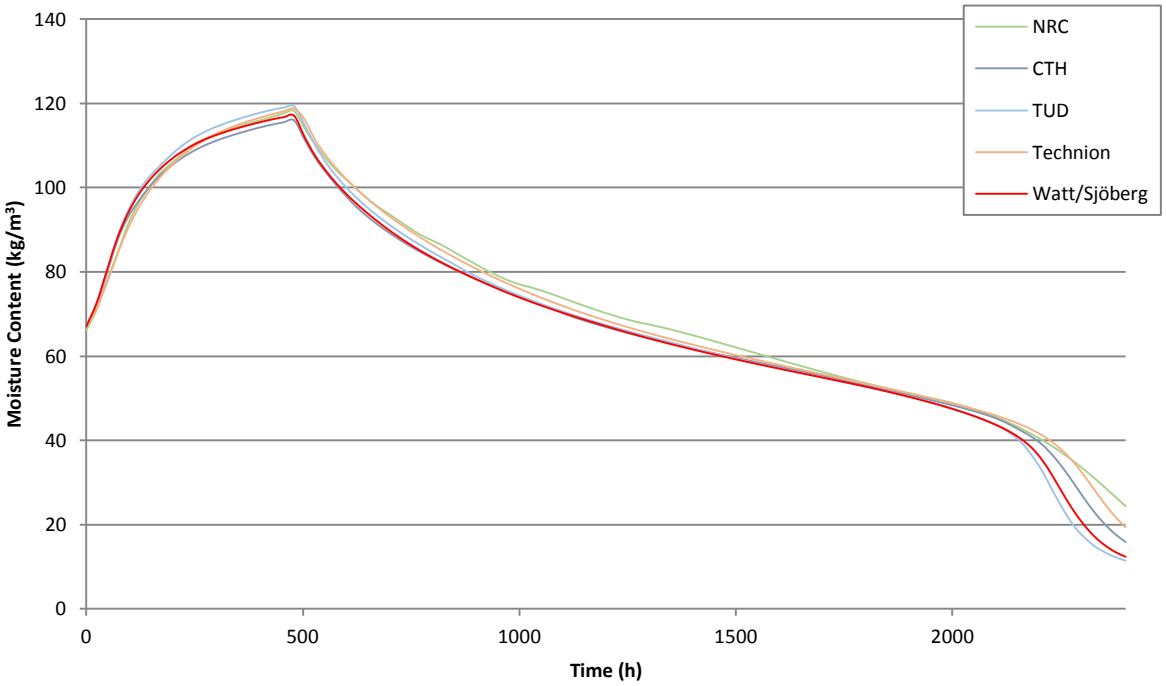

Figure B.5 Benchmark 3: Moisture content at x = 0.15 m over 100 days.

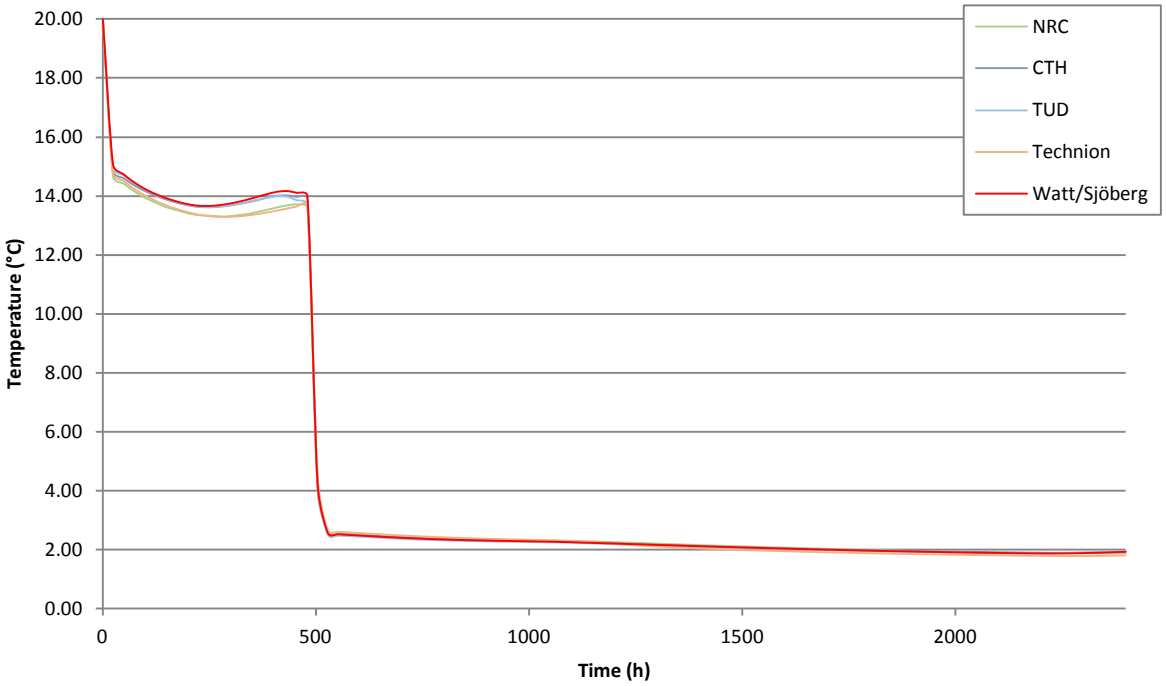

Figure B.6 Benchmark 3: Temperature at x = 0.15 m over 100 days.

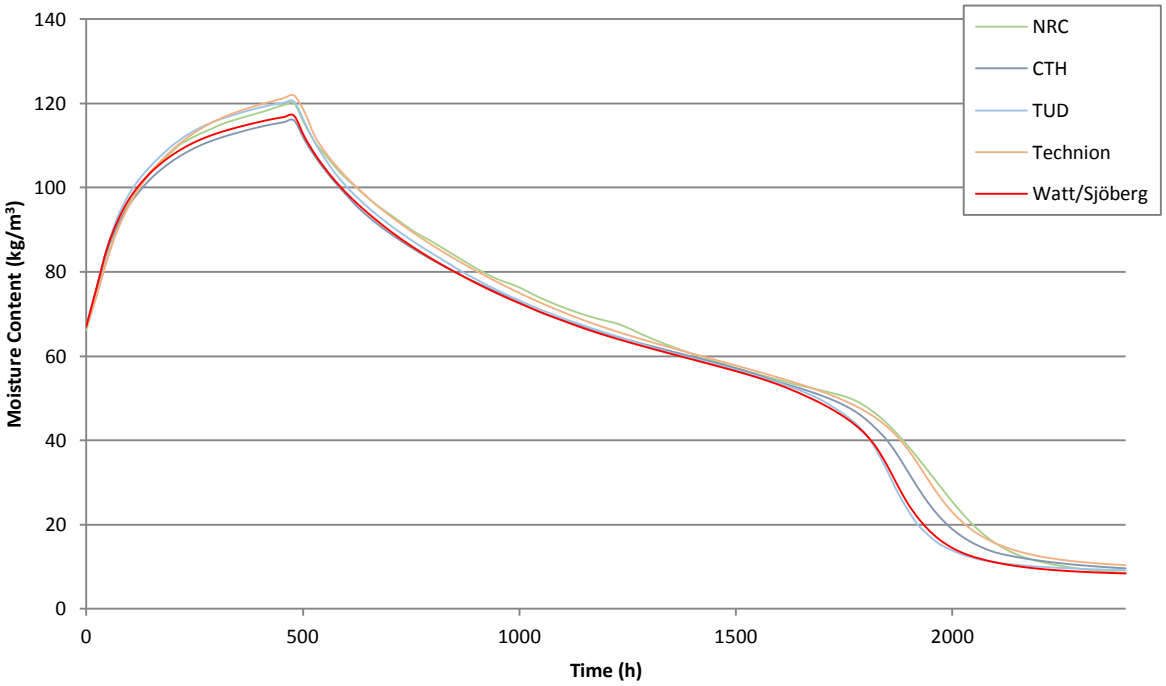

Figure B.7 Benchmark 3: Moisture content at x = 0.17 m over 100 days.

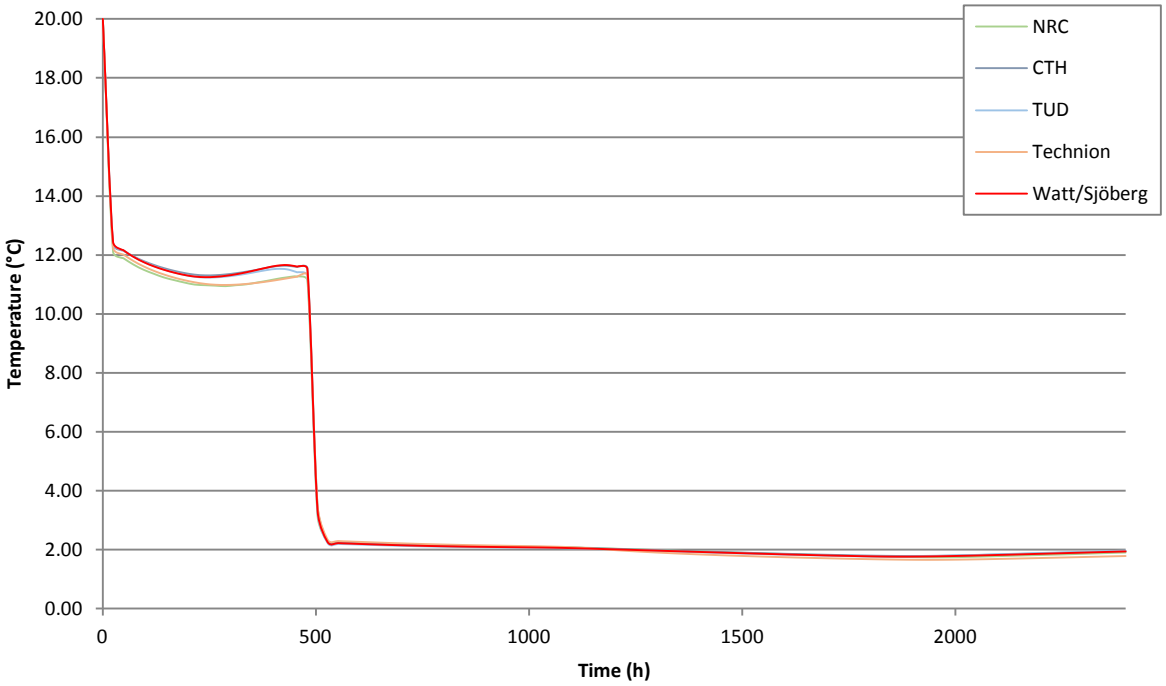

Figure B.8 Benchmark 3: Temperature at x = 0.17 m over 100 days.

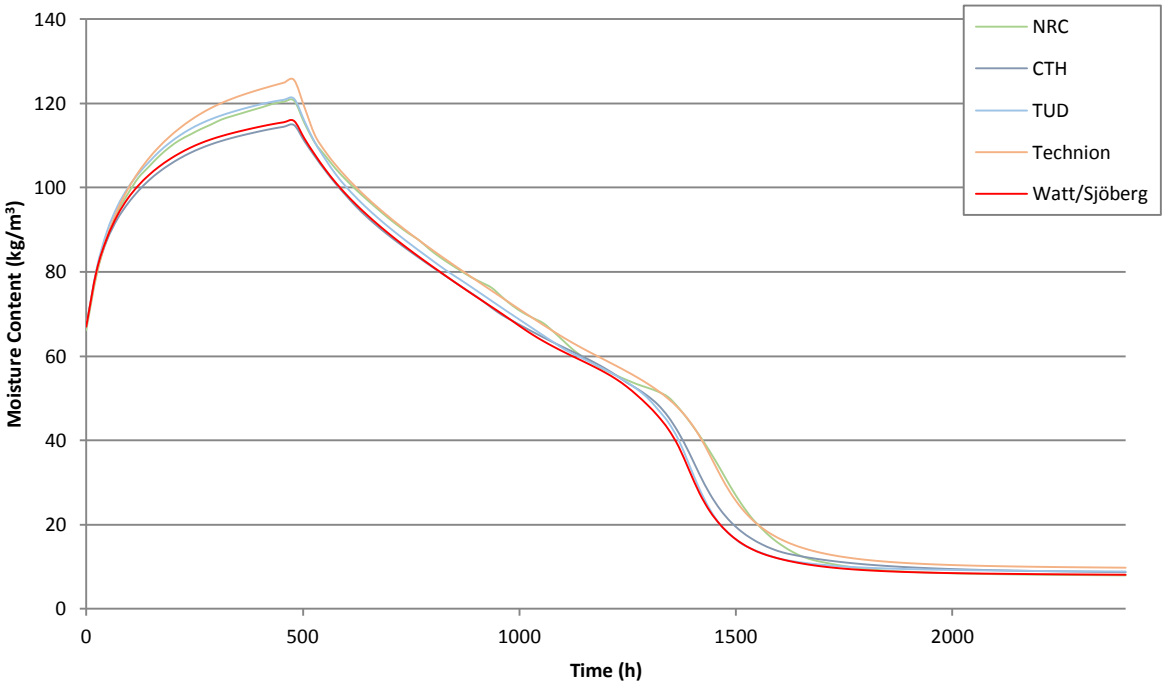

Figure B.9 Benchmark 3: Moisture content at x = 0.19 m over 100 days.

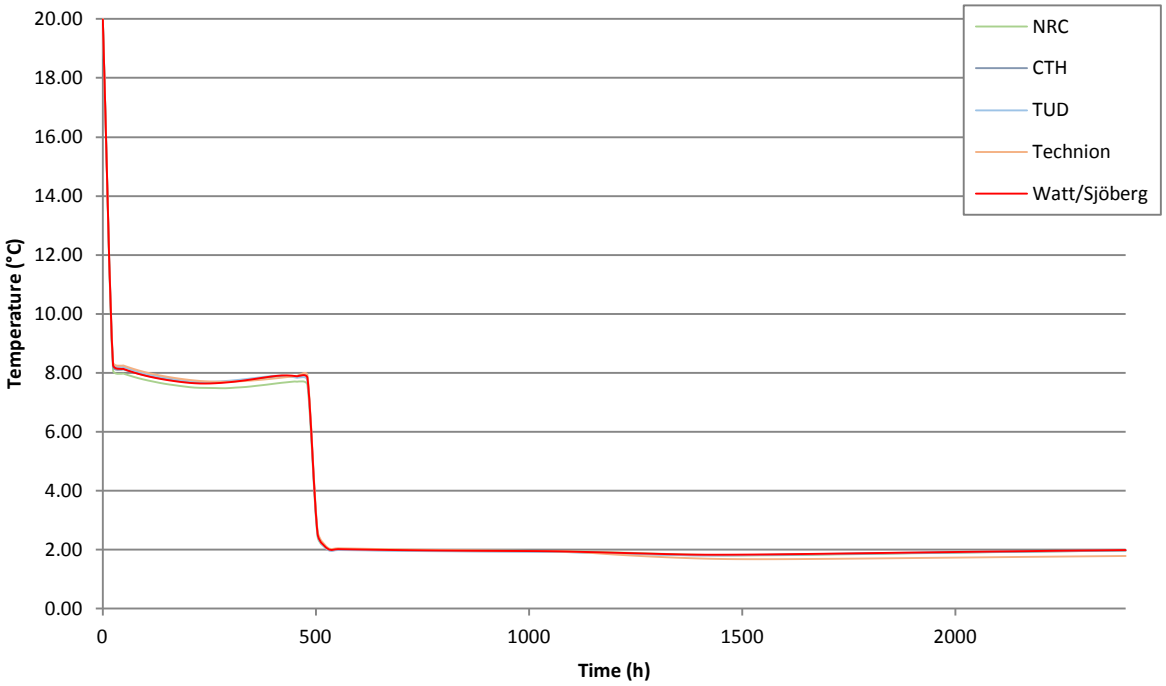

Figure B.10 Benchmark 3: Temperature at x = 0.19 m over 100 days.

Appendix C - Benchmark 5

Benchmark 5 is a 1D, HM numerical model verification tool initiated by the Technical University of Dresden (TUD) for the HAMSTAD project. This benchmark provides comparative solutions from various universities involved in the HAMSTAD project, against which the numerical model can be assessed for conformity and so relative accuracy.

In this benchmark a brick and mortar wall structure with interior insulation is modelled in one dimension. Here the moisture and temperature distribution across three capillary active materials is analysed. The geometry of the layer is shown in Figure C.1.

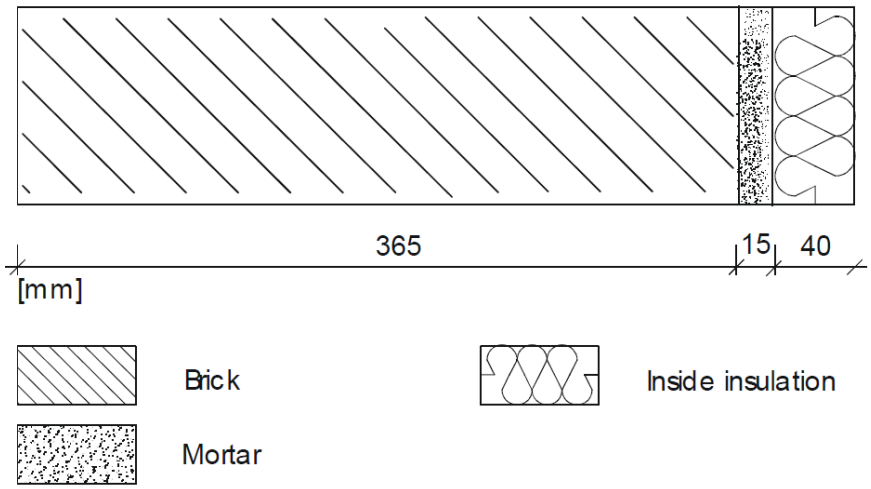

Figure C.1 Geometry of wall structure in HAMSTAD benchmark 5, exterior (left side), interior (right side).

The wall structure is considered in a steady-state condition with both boundaries (interior and exterior) exhibiting constant and equal relative humidity and temperature values of 60% and 25°C. This is until at a time zero when there is a step change in relative humidity and temperature values at each boundary, to 60% and 20°C on the interior and 80% and 0°C on the exterior. Heat and moisture transport mechanisms with respect to air movements are not included.

Global parameters and material properties

The global parameters and equations which describe the properties of the materials for Benchmark 5 are identical to those which are found in the Benchmark 3 description (Chapter 4.2.2).

Table 0.1 Benchmark 5 fitting parameters.

	Brick	Mortar	Insulation
Water retension			
w_{sat} (kg/m^3)	373.5	700	871
k_1 (-)	0.46	0.2	0.41
k_2 (-)	0.54	0.8	0.59
a_1 (-)	0.47	0.5	0.006
a_2 (-)	0.2	0.004	0.012
n_1 (-)	1.5	1.5	2.5
n_2 (-)	3.8	3.8	2.4
Vapour diffusion			
μ_{dry} (-)	7.5	50	5.6
p (-)	0.2	0.2	0.2
Liquid water conductivity			
a_0 (-)	-36.484	-40.425	-46.245
a_1 (-)	461.325	83.319	294.506
a_2 (-)	-5240	-175.961	-1439
a_3 (-)	-2.907e+4	123.863	3249
a_4 (-)	-7.41e+4	0	-3370
a_5 (-)	6.997e+4	0	1305
Thermal conduction			
λ_{dry} (-)	0.682	0.6	0.06
λ_{mst} (-)	0	0.56	0.56
Heat capacity			
ρ_0 (kg/m^3)	1600	230	212
c_0 (kg/m^3)	1000	920	1000

Boundary and initial conditions

Exterior boundary conditions.

$$RH_{ext} = 60\%\,,\ T_{ext} = 0℃ \text{ at } t > 0$$

$$\alpha_{ext} = 25\ (\mathrm{W/m^2{\cdot}K})\,,\ \beta_{ext} = 1.838200 \cdot 10^{-7}\ (\mathrm{s/m})$$

Interior boundary conditions.

$$RH_{int} = 80\%\,,\ T_{int} = 20℃ \text{ at } t > 0$$

$$\alpha_{int} = 8\ (\mathrm{W/m^2{\cdot}K})\,,\ \beta_{int} = 5.8823 \cdot 10^{-8}\ (\mathrm{s/m})$$

Initial conditions.

$$RH = 60\%\,, T = 25℃$$

Output requirements

The simulation time for the benchmark is 60 days. Moisture content, $w(x)$, and relative humidity, ϕ(x), is output at the final time step for numerous x-coordinates to form a representative cross section of the layer. For the load bearing layer the inner and outer centimetre has to be given in 1 mm-steps, a maximum of 5 mm-steps at all other positions.

Results

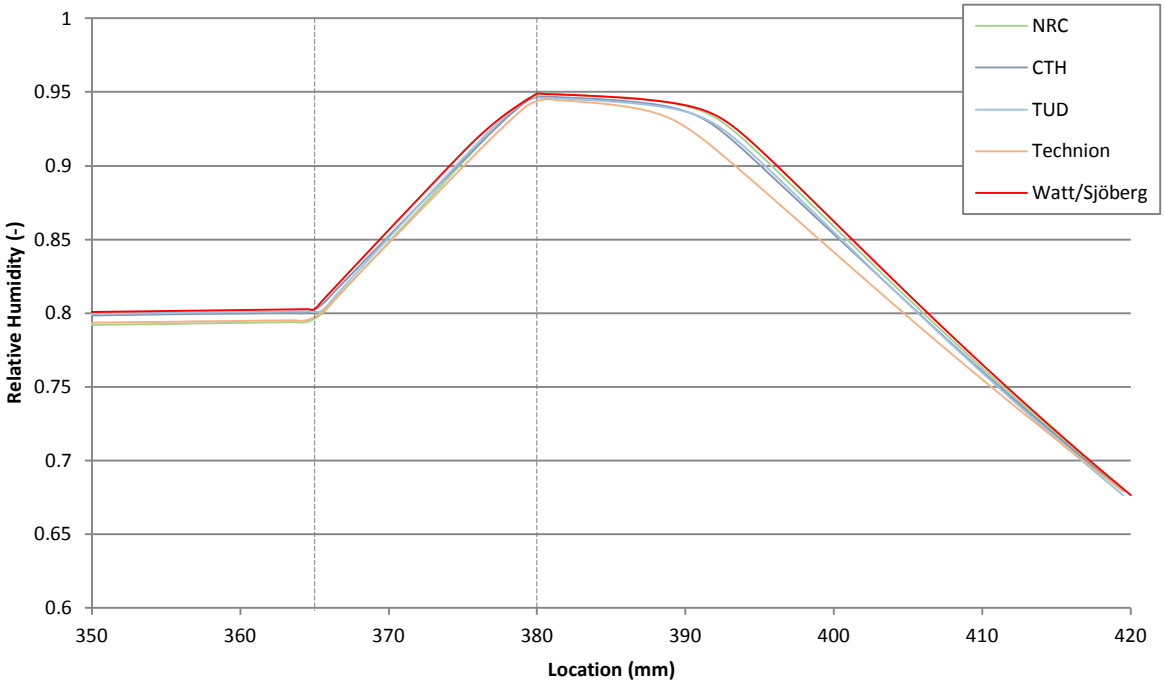

Figure C.2 Benchmark 5: Relative humidity at the transition zone after 60 days.

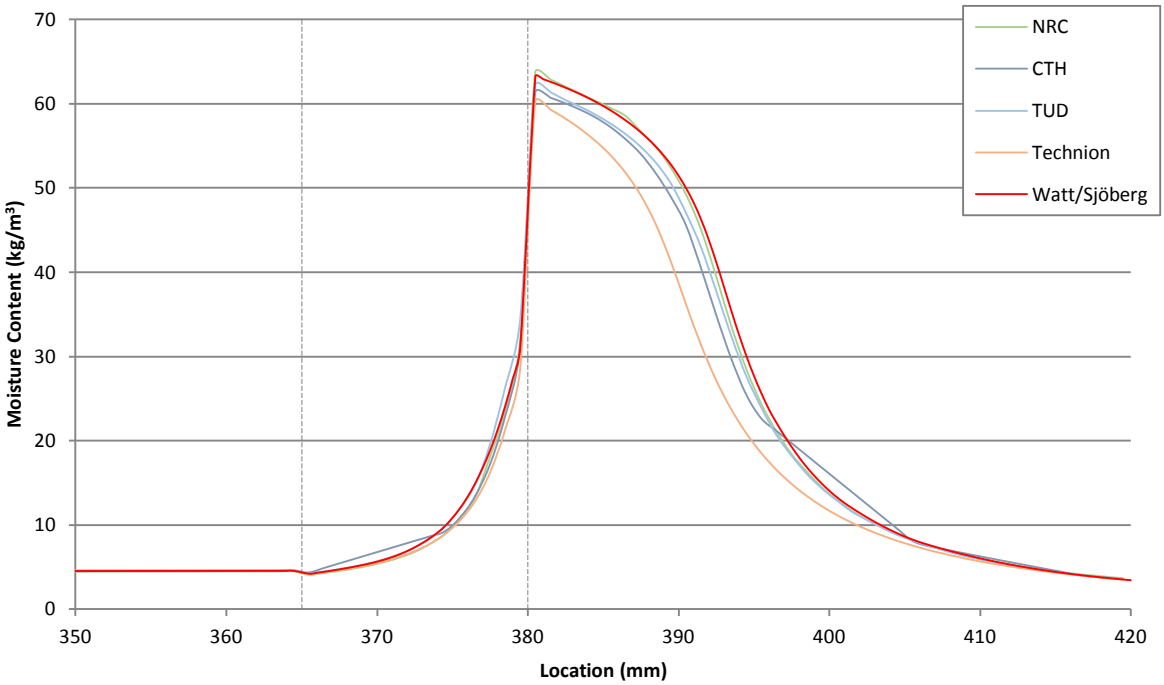

Figure C.3 Benchmark 5: Moisture content at the transition zone after 60 days.

Appendix D - Additional material parameters

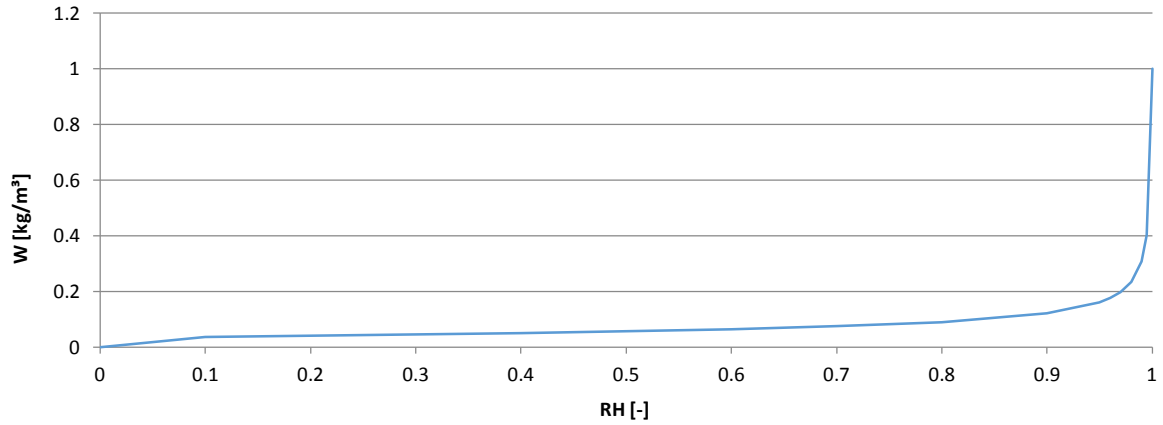

Figure D.1 Fibre board sorption isotherm (w).

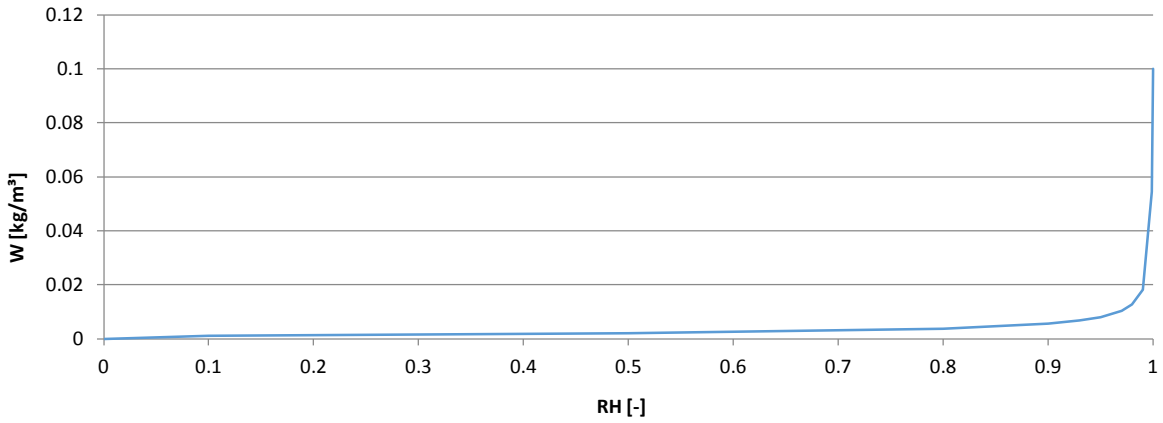

Figure D.2 Mineral wool sorption isotherm (w).

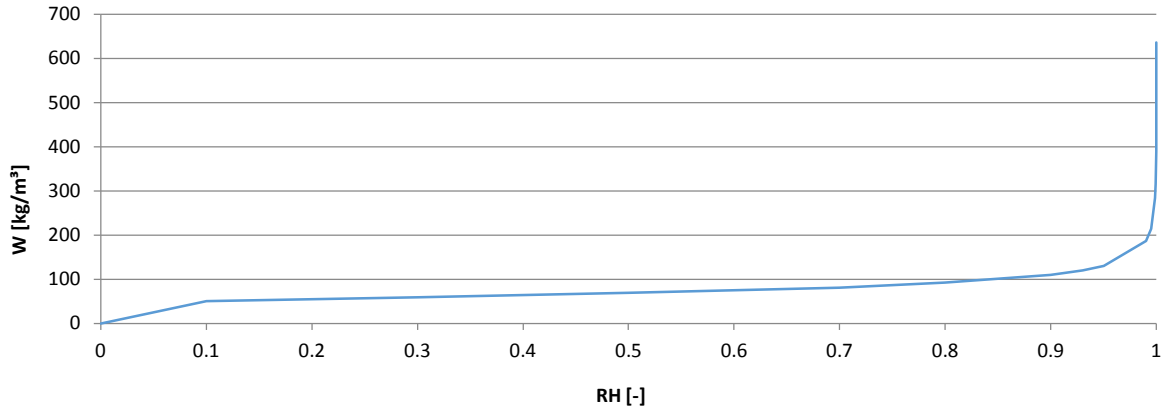

Figure D.3 OSB sorption isotherm (w).

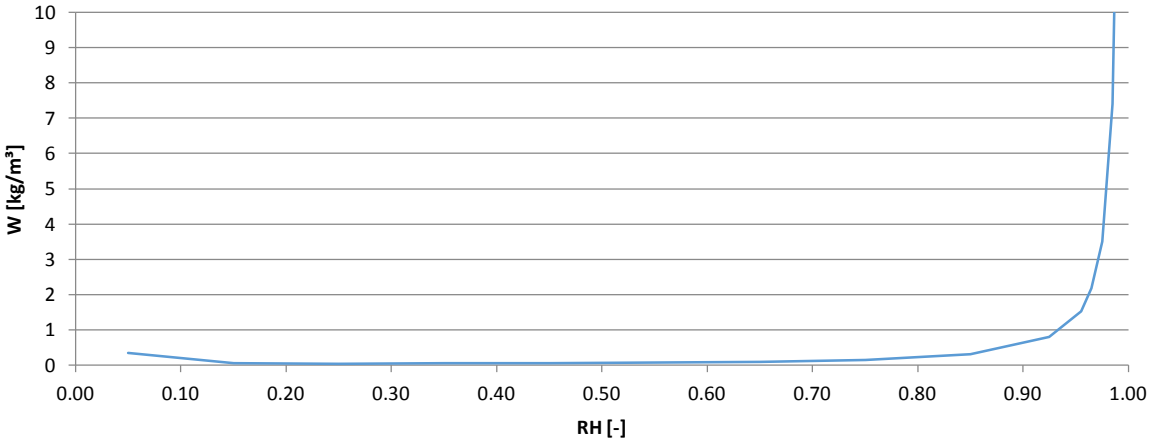

Figure D.4 Fibre board moisture capacity (ξ).

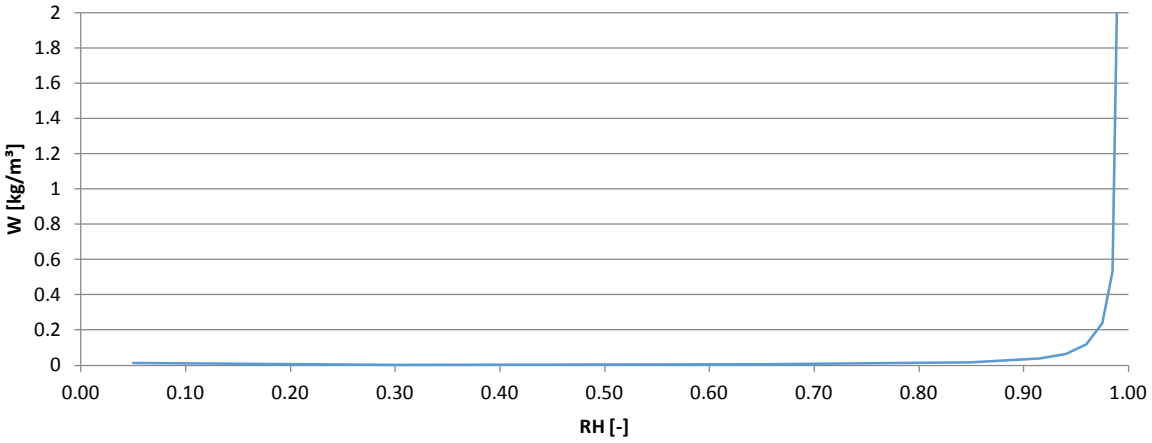

Figure D.5 Mineral wool moisture capacity (ξ).

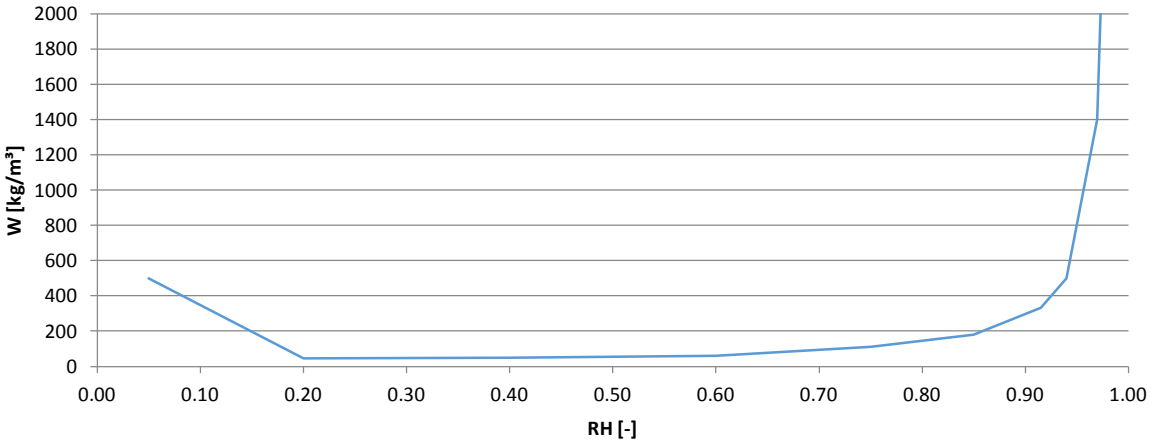

Figure D.6 OSB moisture capacity (ξ).

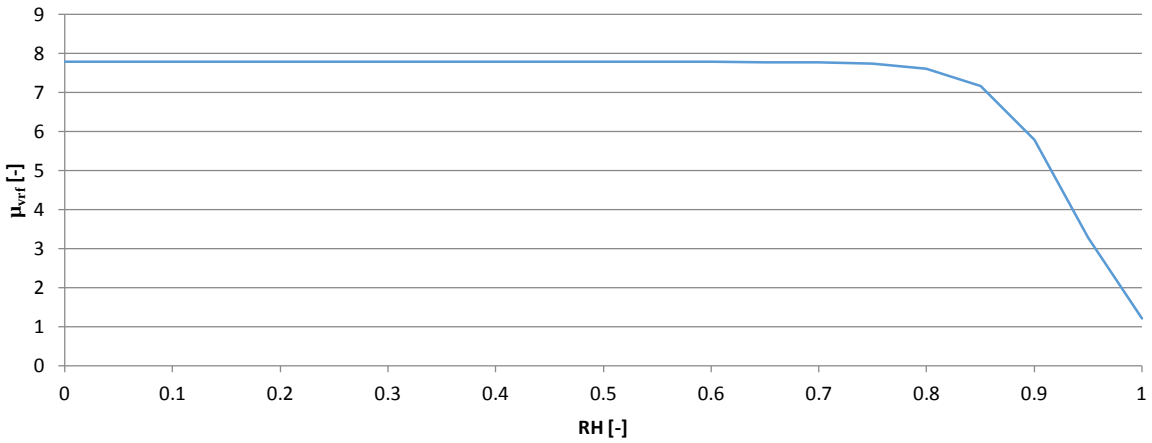

Figure D.7 Fibre board vapour diffusion resistance factor (μ_{vrf}).

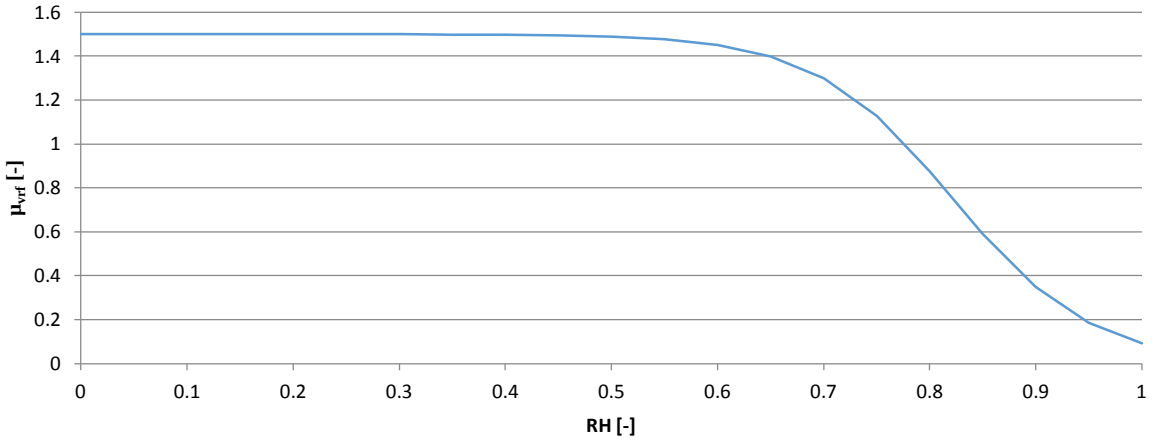

Figure D.8 Mineral wool vapour diffusion resistance factor (μ_{vrf}).

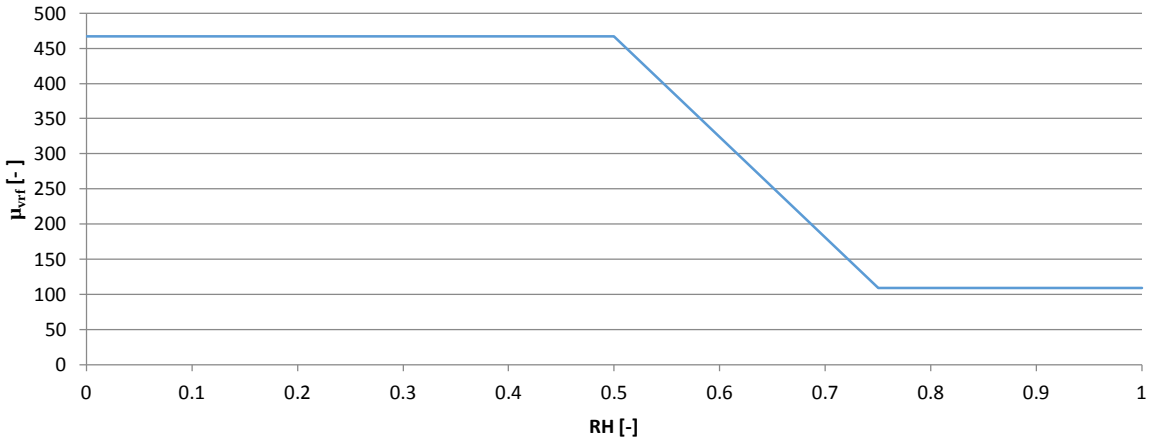

Figure D.9 OSB vapour diffusion resistance factor (μ_{vrf}).

Appendix E - Control case simulation results

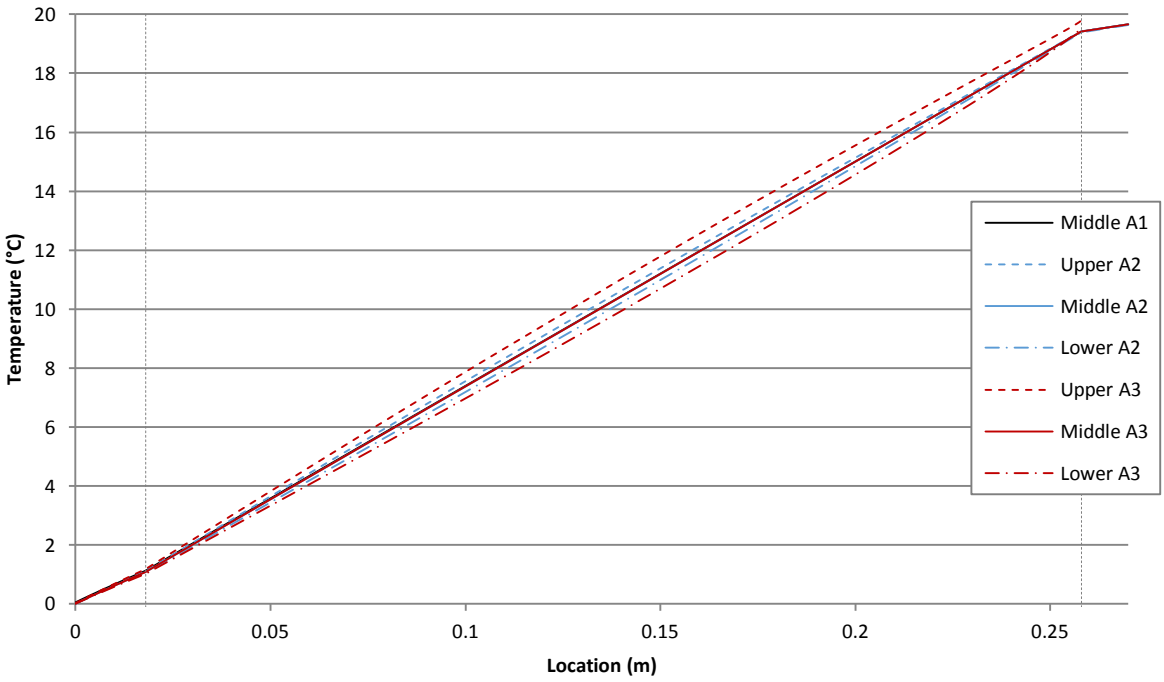

Figure E.1 *Temperature (°C) over the wall cross section for simulation A1 (black), A2 (blue) and A3 (red) at the upper, middle and lower cut lines in the geometry at 60 days.*

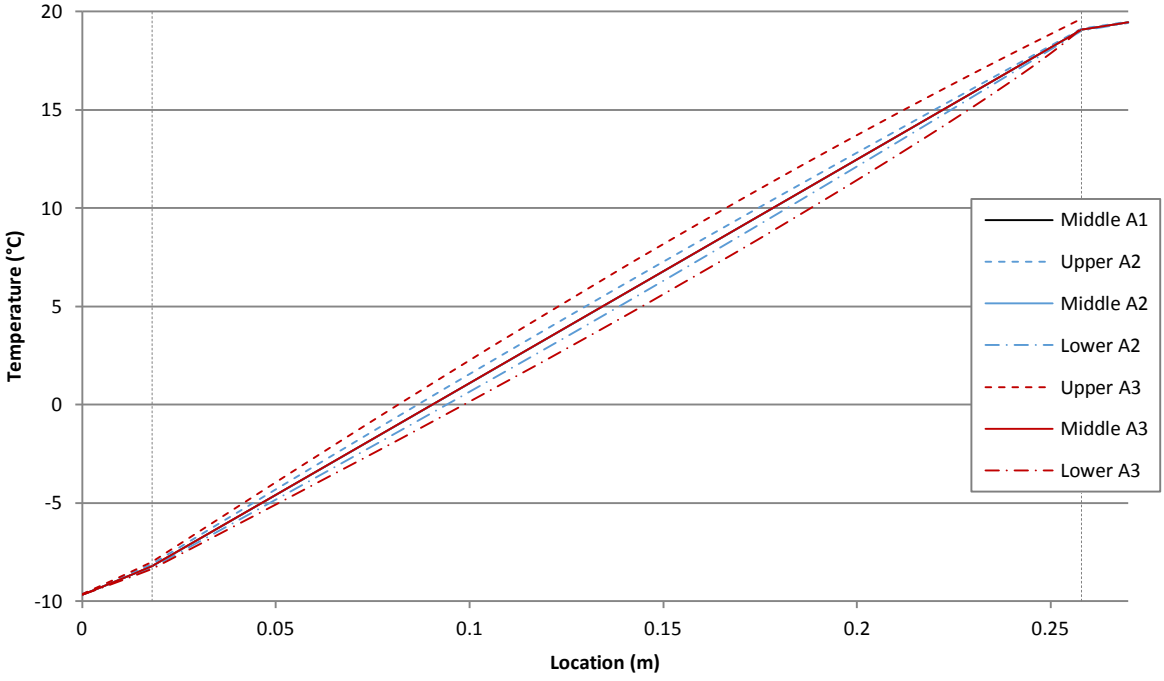

Figure E.2 *Temperature (°C) over the wall cross section for simulation A1 (black), A2 (blue) and A3 (red) at the upper, middle and lower cut lines in the geometry at 31.5 days.*

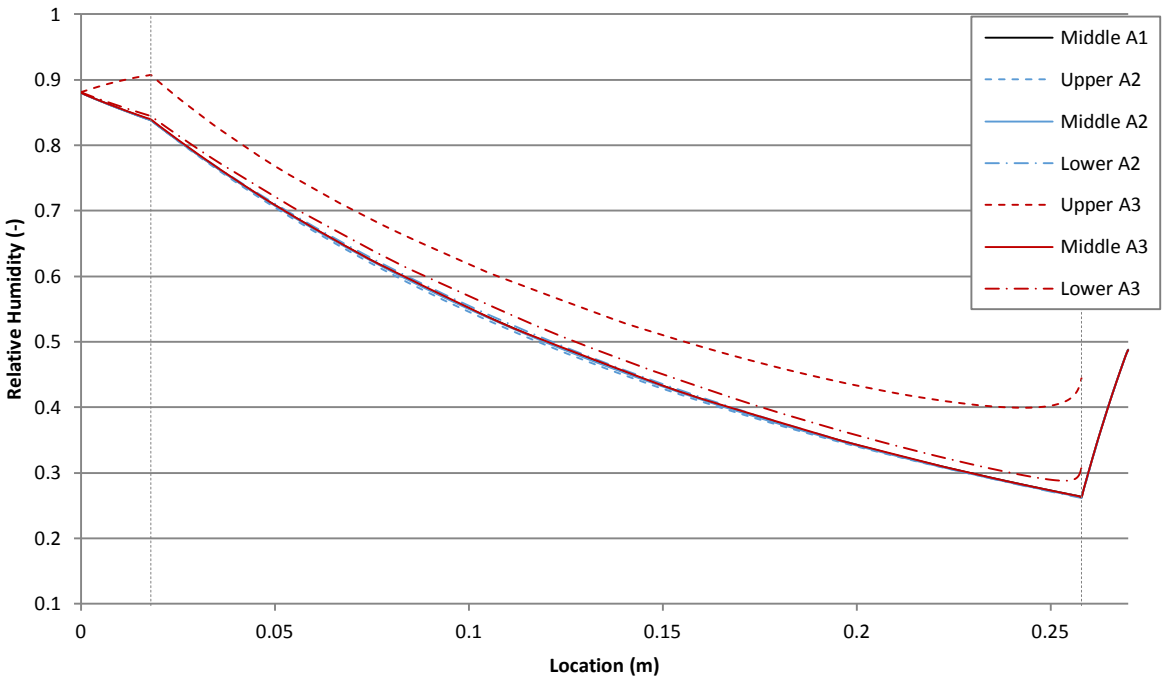

Figure E.3 *Relative humidity (-) over the wall cross section for simulation A1 (black), A2 (blue) and A3 (red) at the upper, middle and lower cut lines in the geometry at 60 days.*

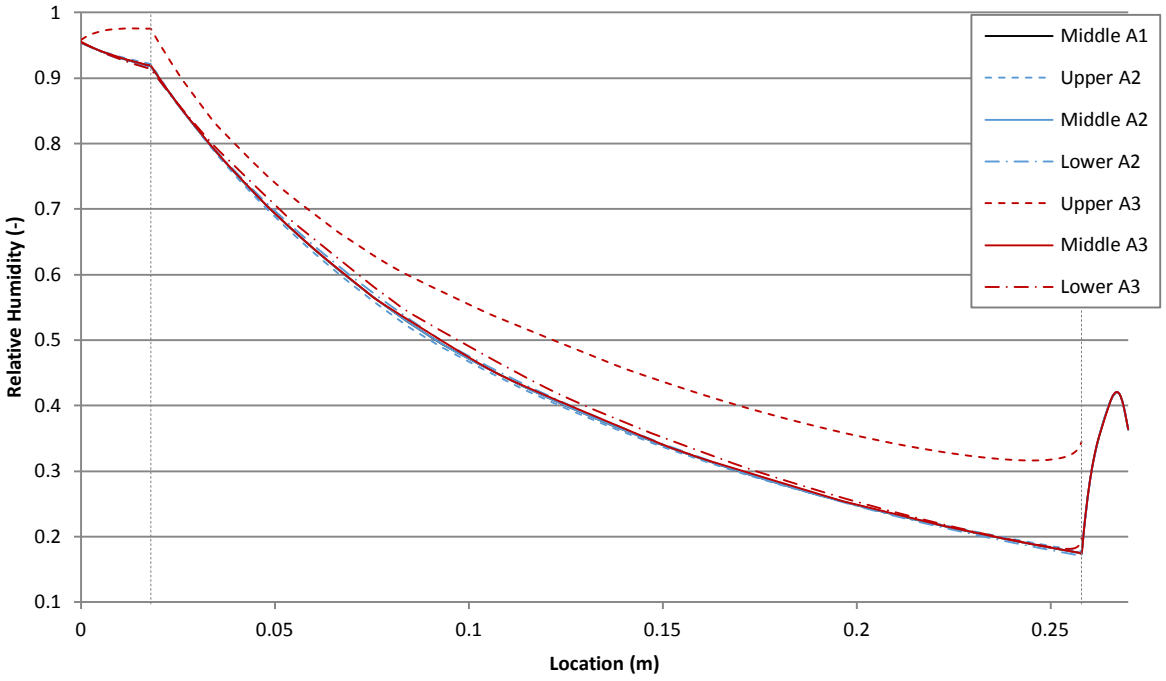

Figure E.4 *Relative humidity (-) over the wall cross section for simulation A1 (black), A2 (blue) and A3 (red) at the upper, middle and lower cut lines in the geometry at 31.5 days.*

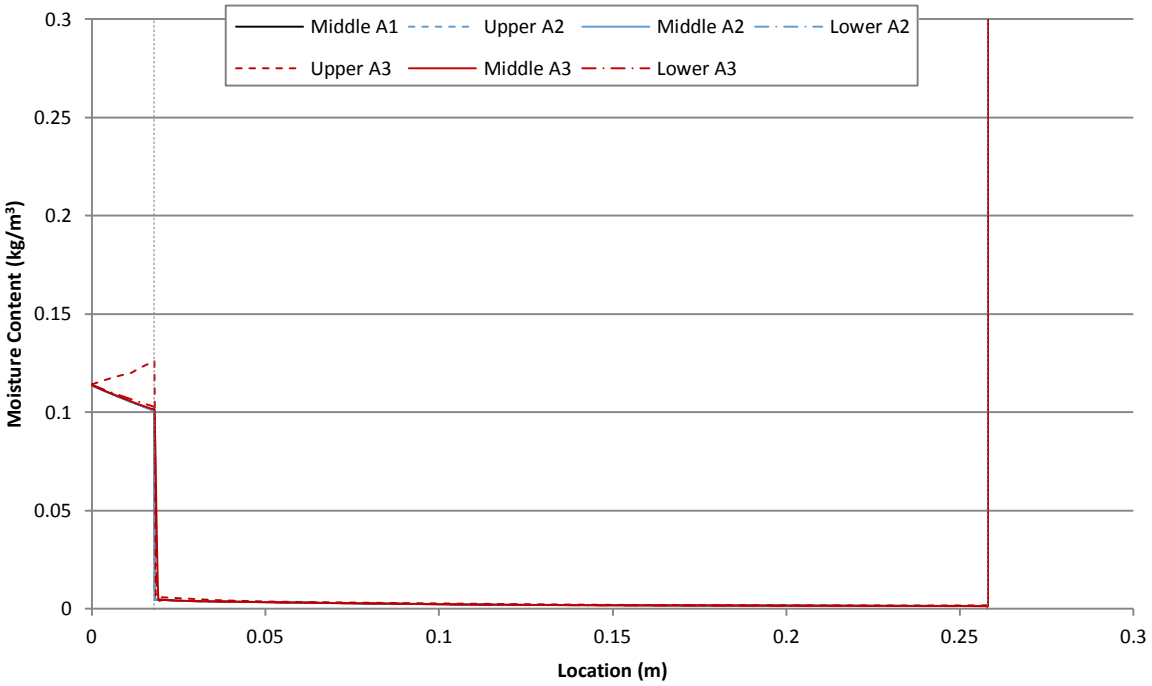

Figure E.5 *Moisture content (kg/m^3) over the wall cross section for simulation A1 (black), A2 (blue) and A3 (red) at the upper, middle and lower cut lines in the geometry at 60 days. Y-axis is limited at 3 kg/m^3.*

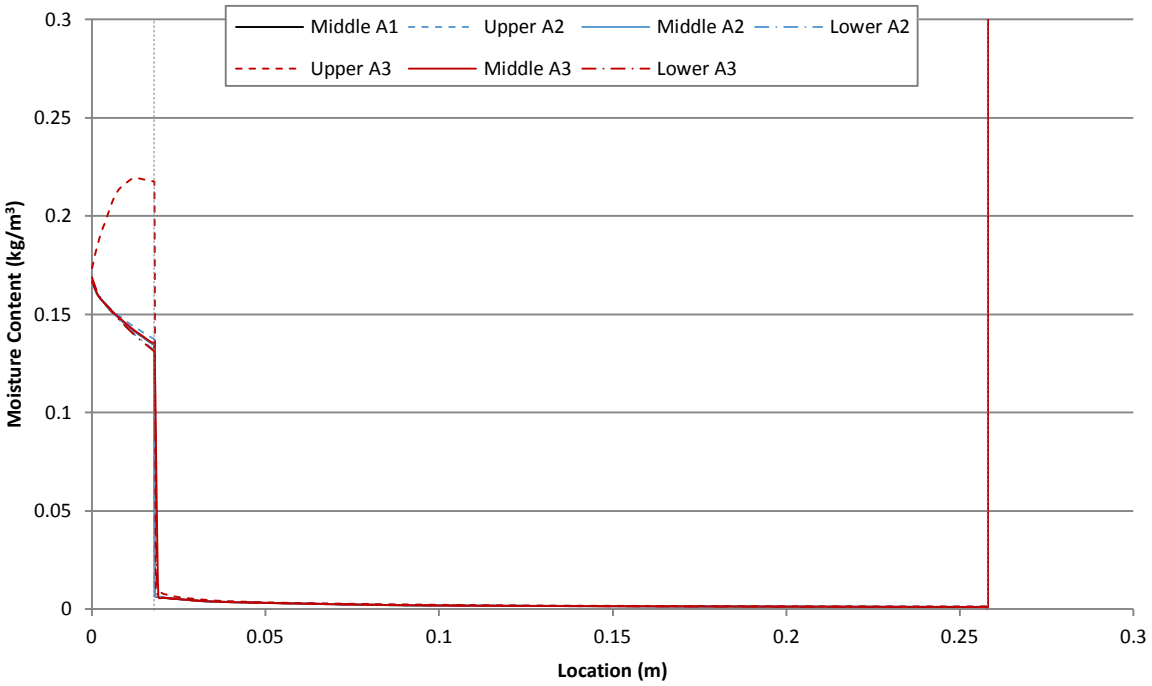

Figure E.6 *Moisture content (kg/m^3) over the wall cross section for simulation A1 (black), A2 (blue) and A3 (red) at the upper, middle and lower cut lines in the geometry at 31.5 days. Y-axis is limited at 3 kg/m^3.*

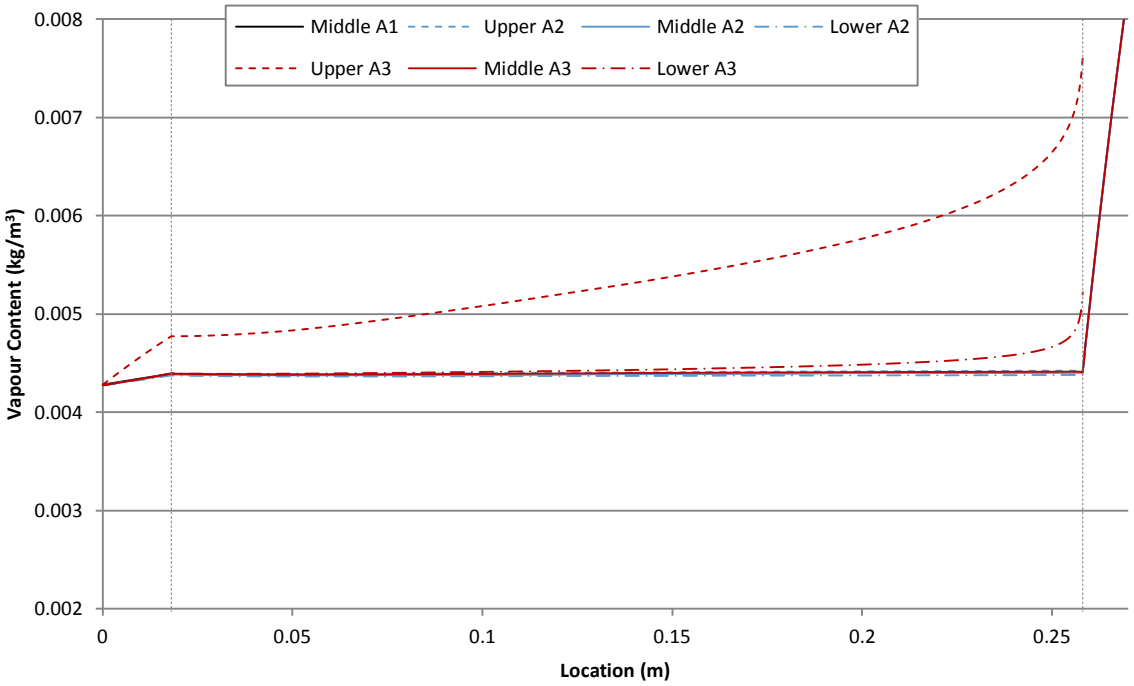

Figure E.7 *Vapour content (kg/m^3) over the wall cross section for simulation A1 (black), A2 (blue) and A3 (red) at the upper, middle and lower cut lines in the geometry at 60 days.*

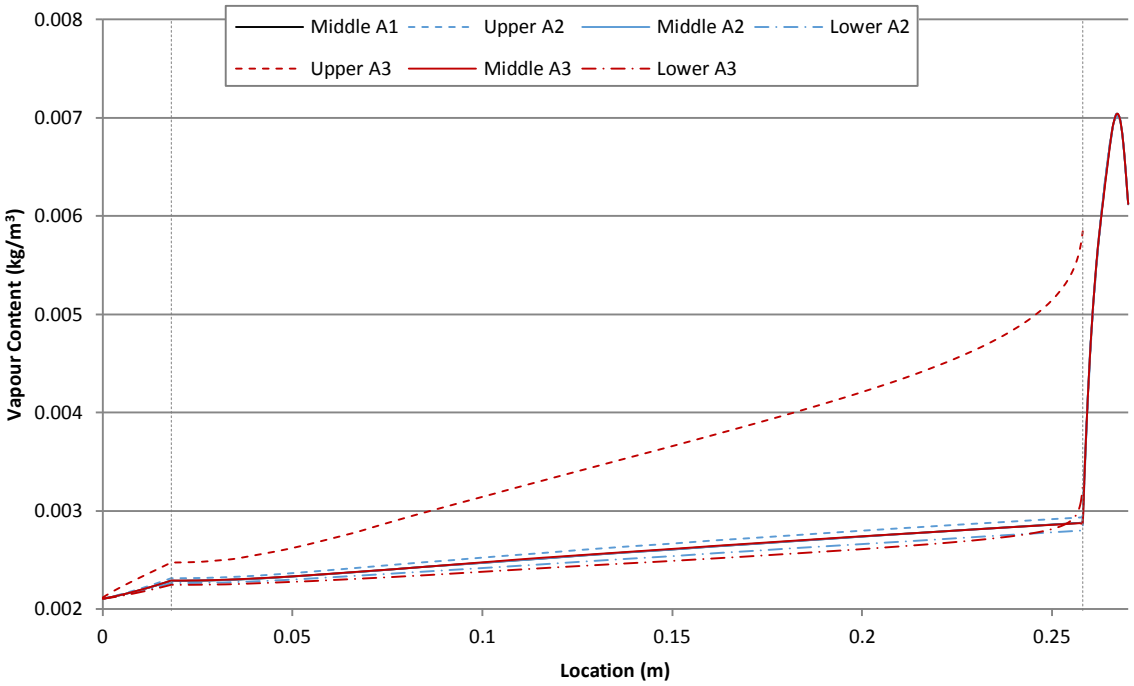

Figure E.8 *Vapour content (kg/m^3) over the wall cross section for simulation A1 (black), A2 (blue) and A3 (red) at the upper, middle and lower cut lines in the geometry at 31.5 days.*

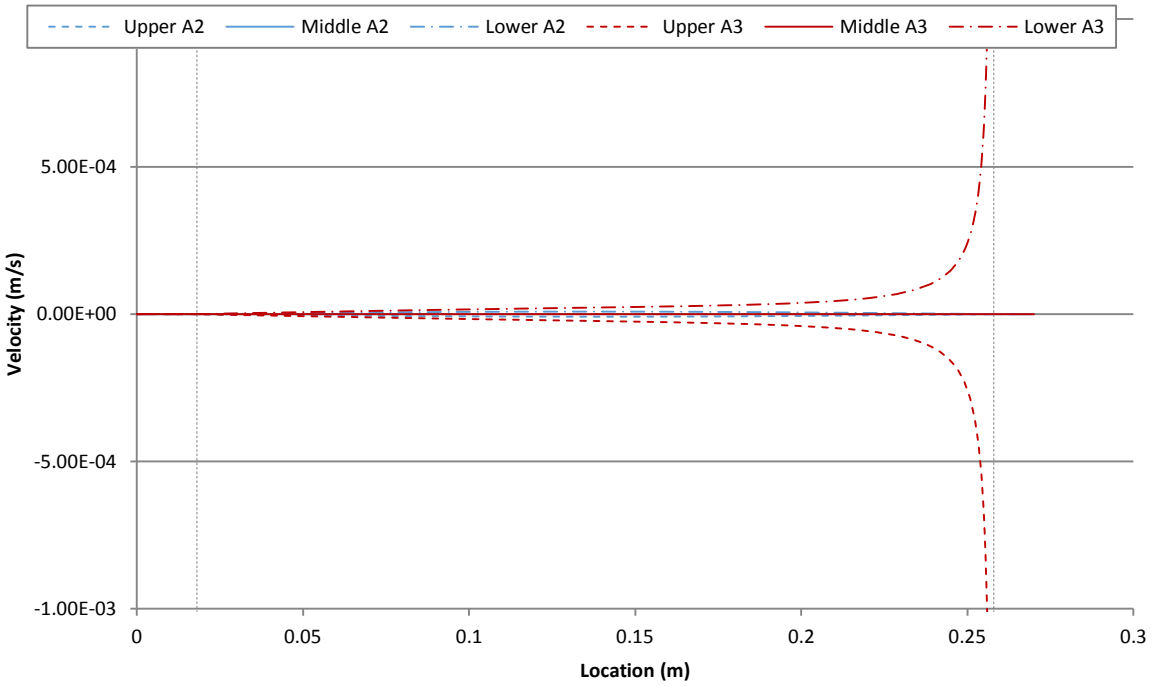

Figure E.9 *Air velocity (m/s) in the horizontal direction over the wall cross section for simulation A2 (blue) and A3 (red) at the upper, middle and lower cut lines in the geometry at 60 days. Flow is negative to the exterior and positive to the interior.*

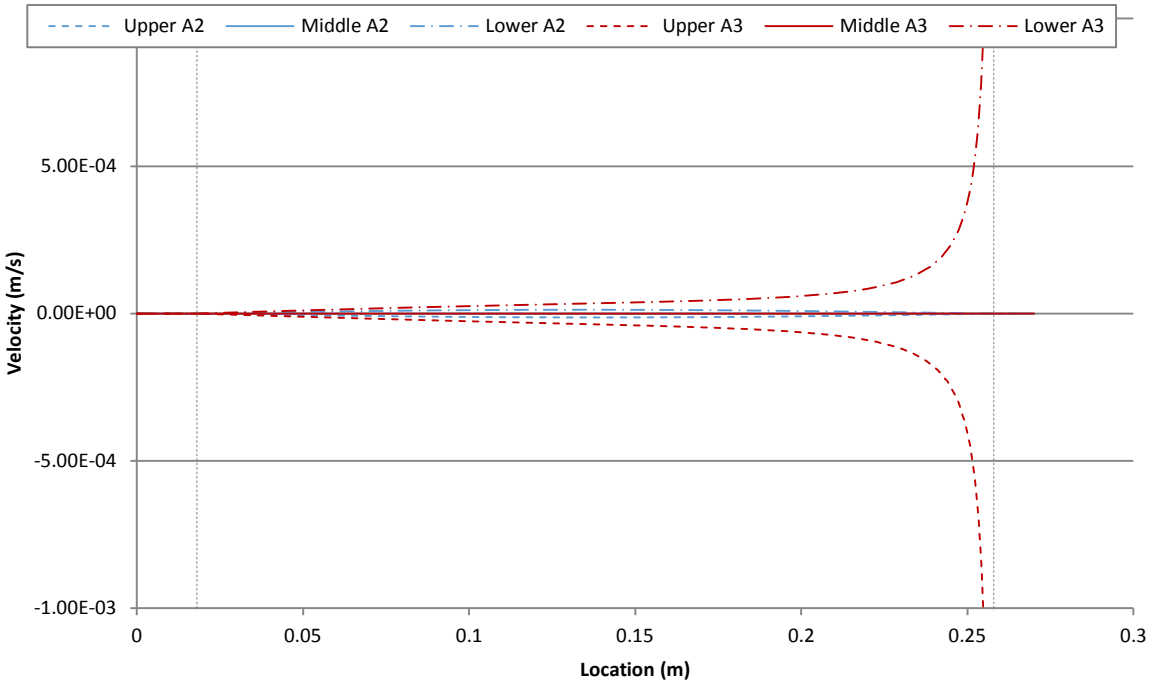

Figure E.10 *Air velocity (m/s) in the horizontal direction over the wall cross section for simulation A2 (blue) and A3 (red) at the upper, middle and lower cut lines in the geometry at 31.5 days. Flow is negative to the exterior and positive to the interior.*

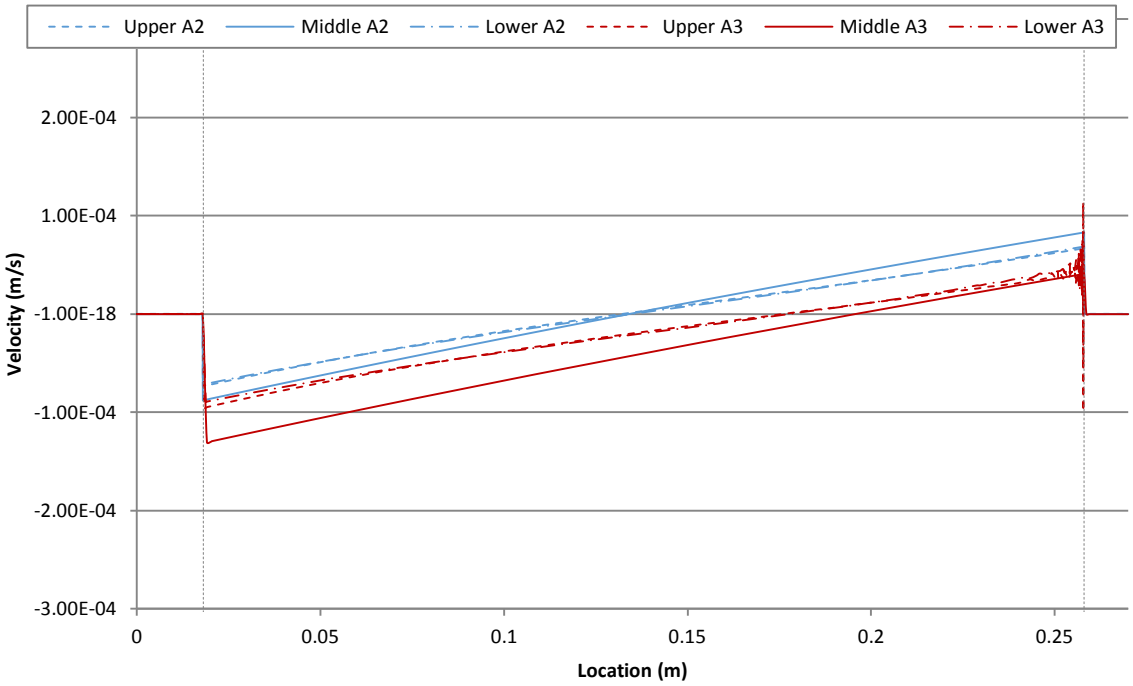

Figure E.11 *Air velocity (m/s) in the vertical direction over the wall cross section for simulation A2 (blue) and A3 (red) at the upper, middle and lower cut lines in the geometry at 60 days Flow is negative to the base of the wall and positive to the top of the wall.*

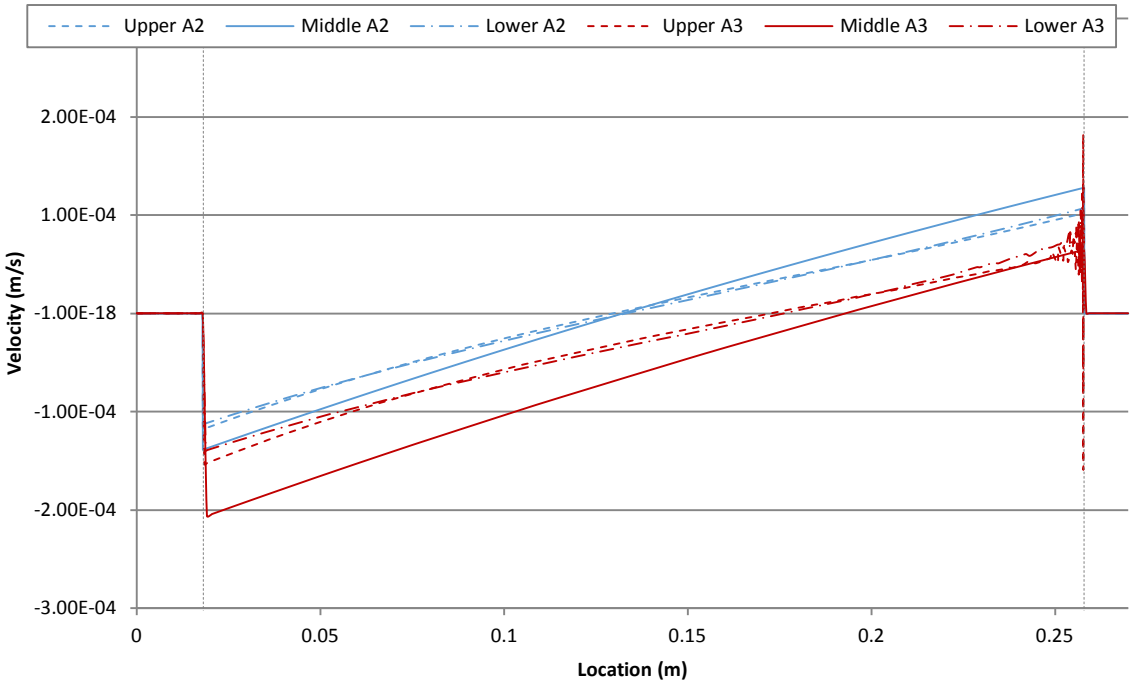

Figure E.12 *Air velocity (m/s) in the vertical direction over the wall cross section for simulation A2 (blue) and A3 (red) at the upper, middle and lower cut lines in the geometry at 31.5 days. Flow is negative to the base of the wall and positive to the top of the wall.*

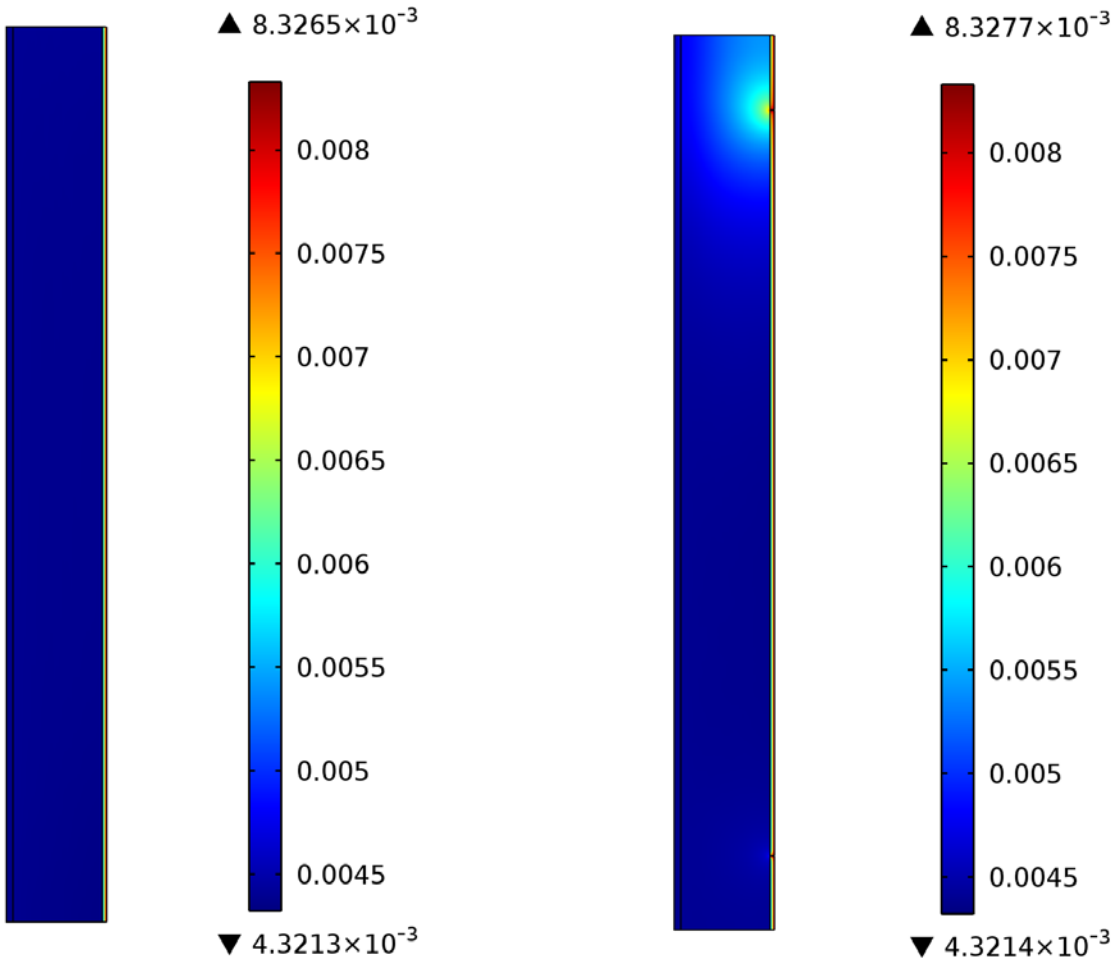

Figure E.13 Vapour content (kg/m^3) for simulation A2 (left) and A3 (right) after 60 days.

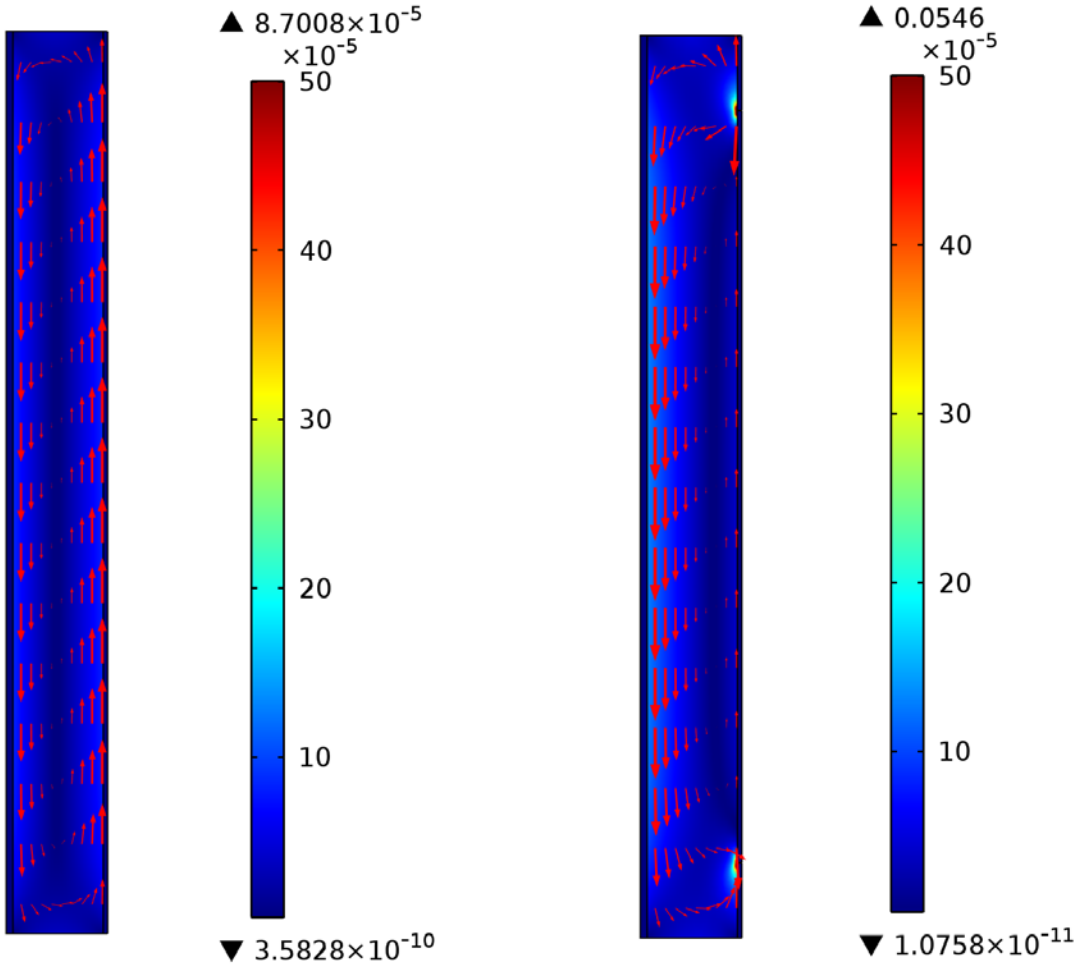

Figure E.14 Air velocity magnitude (m/s) overlain with general air movement direction for simulation A2 (left) and A3 (right) after 60 days. Minimum and maximum air velocity magnitudes are shown.